An-Najah National University
Faculty of Graduate Studies

TECHNICAL AND ECONOMIC FEASIBILITY OF INTEGRATING ENERGY STORAGE SYSTEM INTO GRID CONNECTED PV SYSTEM - CASE STUDY APPROACH

By
Rami Hossam Yaqoub

Supervisor
Dr. Aysar Mahmoud Yasin

This Thesis is Submitted in Partial Fulfillment of the Requirements for the Degree of Master of Clean Energy Engineering and Conservation of Consumption, Faculty of Graduate Studies, An–Najah National University, Nablus, Palestine.
2025

TECHNICAL AND ECONOMIC FEASIBILITY OF INTEGRATING ENERGY STORAGE SYSTEM INTO GRID CONNECTED PV SYSTEM - CASE STUDY APPROACH

By
Rami Hossam Yaqoub

This Thesis was defended successfully on 30/07/2025 and approved by:

Dr. Aysar Mahmoud Yasin Supervisor	Aysar Mahmoud Masoud Yasin Signature
Prof. Samer Al Sadi External Examiner	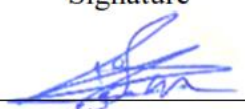 Signature
Dr. Moien Omar Internal Examiner	 Signature

Dedication

The researcher may dedicate his work to relatives, friends and family members.

Acknowledgements

The Researcher may thank people, institutions and different parties who helped him in accomplishing his work.

Declaration

I, the undersigned, declare that I submitted the thesis entitled:

TECHNICAL AND ECONOMIC FEASIBILITY OF INTEGRATING ENERGY STORAGE SYSTEM INTO GRID CONNECTED PV SYSTEM - CASE STUDY APPROACH

I declare that the work provided in this thesis, unless otherwise referenced, is the researcher's own work, and has not been submitted elsewhere for any other degree or qualification.

Student's Name	Rami Hossam Yaqoub
Signature:	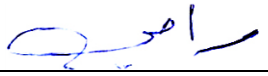
Date:	30/07/2025

List of Contents

List of Figures

List of Tables

List of Appendices

ASSESSING THE TECHNICAL FEASIBILITY AND ECONOMIC BENEFITS OF INTEGRATING ENERGY STORAGE SYSTEM INTO GRID CONNECTED PV SYSTEM - CASE STUDY APPROACH

By
Rami Hossam Yaqoub
Supervisor
Dr. Aysar Mahmoud Yasin

Abstract

This study investigates the technical and economic impacts of integrating energy storage systems into grid-connected PV systems using the electrical network of Jenin's Arraba village as a case study. Four different configurations of PV and sizes of energy storage systems are compared to assessing their impact on the most critical grid performance parameters, including voltage regulation, energy loss reduction, and dynamic load control. Utilizing ETAP for simulation, the study also analyzes actual grid behavior under real conditions, harmonic distortion due to the PV inverter, and reverse power flow when there is high PV penetration. Harmonic distortion was found to be moderate in Case 0 and increases notably in Cases 1 and 3, with the highest distortion observed at low-voltage buses in Case 3. Reverse power flow was observed in Case 3 with negligible export to the upstream grid, highlighting the importance of control mechanisms at high penetration levels.

Economic efficiency is assessed considering the System Advisor Model with high focus on main indicators like payback period, net present value, and levelized cost of energy. Among the four cases, Case 1 is the most efficient cost-saving setting with the smallest levelized cost of energy of 17.4 cents/kWh and a payback period of 8.2 years. While having superior technical performance in Case 2 and Case 3, their increased investment cost reduces their economic efficiency. The conclusion is that Case 1 has the optimal trade-off between technical effectiveness and economic viability, and it is an acceptable solution for grid stability, power quality management, and peak-shaving in small- to medium-size applications. The report wraps up by recommending longer-term investigation of hybrid energy storage technology, predictive algorithms, and long-term service reliability of energy storage under the conditions of diverse grids.

Keywords: Energy Storage System, Grid-Connected Photovoltaic System, Technical Feasibility, Economic Benefits, Voltage Regulation.

Chapter One
Introduction and Theoretical Background

1.1 Introduction

Palestinian territories suffer from high shortage of conventional energy, and it imports all its needs of petroleum and about 90% of electrical energy needs from Israeli energy companies. This corresponds to high-energy prices with drastic fluctuation. The tendency to exploit renewable energy is one of the robust solutions to mitigate the dilemma of energy crisis as Palestine has been granted with high potential of solar energy.

The exploitation of the solar energy in Palestinian Territories for electricity generation mainly using PV grid-connection mode is growing up and spread widely and for this purpose further investigations on performance analysis is important and necessary.

Most of the Palestinian electricity is imported from Israel Electric Corporation. There is only one generation station located in Gaza, but it is insufficient to meet the demand in that area. Palestine depends on importing all the energy requirements, since it has no conventional energy sources like petroleum ang gas. Because of that the energy prices in Palestine are considered the highest in compare with near countries [1].

Palestine has an average solar radiation intensity of 5.4 kWh/m² per day and around 3000 hours of sunshine annually, which is considered a high potential for solar energy generation. These conditions make the use of photovoltaic systems a sustainable option. Solar radiation levels often exceed 8 kWh/m² per day in summer, while the lowest average is recorded in winter at approximately 3.01 kWh/m² per day. The average solar radiation values the Jordan Valley region is shown in Figure 1 [3].

Micro-grid solar PV systems offer a promising solution for delivering electricity to rural areas, supporting both electrification and local development. As the cost of PV panels continues to decline, these systems are becoming increasingly affordable and practical. Their adoption in rural communities contributes to enhanced social infrastructure, improved water access, better agricultural productivity, and the expansion of other income-generating activities. Additionally, the use of solar PV can help these regions transition toward more environmentally sustainable practices [4].

Figure 1

The Monthly Average Solar Radiation in Jordan Valley

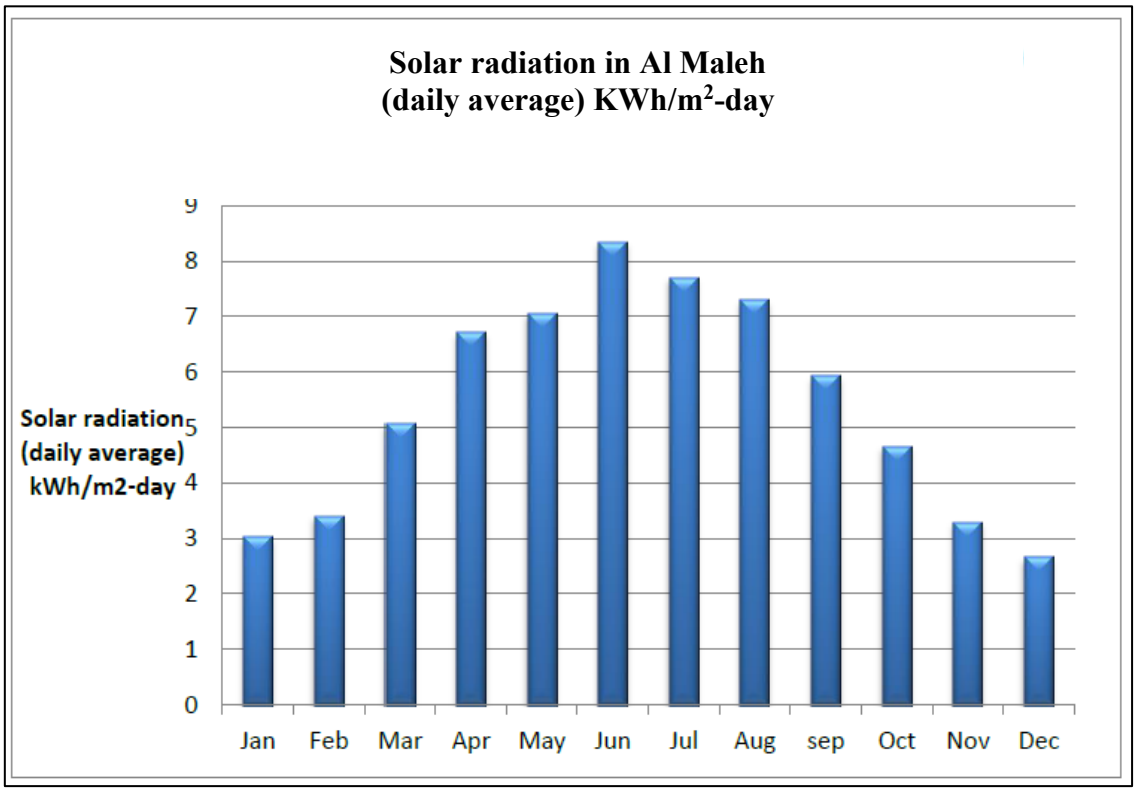

In recent years, the installation of grid-connected PV systems on the rooftops of residential buildings has become increasingly common in Palestine. This growth is largely driven by the declining cost of PV technology and the introduction of government policies that promote the adoption of renewable energy. In addition to homes, several schools, municipal facilities, and private companies have also implemented similar solar PV systems [1].

The majority of energy consumed in Palestine is delivered from Israel. However, due to political factors, the Israeli authorities regulate and limit the supply of electricity available to Palestinians. That resulted in frequent power shortages across Palestinian regions. In response, many Palestinians have turned to grid-connected PV systems as a way to reduce dependency and address the energy gap. Despite this shift, limited technical expertise and weak regulatory frameworks have posed challenges, leading to inefficiencies and strain on the Palestinian distribution network [2].

1.2 Problem Statement

In the last few years, there has been significant growth in the deployment of large and small PV systems in Palestinian cities. While as much as possible of this transition to renewable energy is appreciated, the intermittent nature of solar power has introduced some issues of its own in the form of fluctuations and periodic outages of power. These instabilities are a risk to power reliability and quality provided to consumers.

To meet these challenges, the implementation of Energy Storage System (ESS) has been proposed as an effective solution. ESS technologies can store energy generated in excess during peak sun hours and dispense it during low generation or high demand times, essentially delivering a shot of adrenaline to grid stability and reliability. To be economical and effective, these systems must be optimized to the specific characteristics and constraints of the host electrical grid.

This research addresses this gap with a comprehensive techno-economic analysis of ESS integration in the model Palestinian village electricity grid. The study aims to find out the best type and size of storage technology based on technical performance parameters. Meanwhile, the study will also address economic factors in terms of initial capital outlay, operational and maintenance expenditures, and the potential for cost savings or generation of revenues in the long run.

The end goal is to derive actionable results and policy recommendations for stakeholders on the cost-effective integration of energy storage systems. By doing so, the research enables informed decision-making processes and supports the overall mission of creating resilient and sustainable local energy systems.

1.3 Study Hypothesis

The integration of an ESS in an electrical grid at village-scale is anticipated to offer a safe and inexpensive answer to overcome the volatility of renewable sources of energy and enhance the overall efficiency of the grid as a whole. The hypotheses are formed based on the problem statement:

- A properly sized ESS should be able to effectively reduce peak power loads on the village grid and hence reduce the likelihood of power shortages during peak demand.

- By holding excess energy generated during high solar generation times and releasing this when generation falls, the ESS can aid significantly in leveraging renewable energy resources.
- Although capital and operational cost of deploying the ESS initially may be expensive, these will be recoverable through potential earnings from grid support services such as frequency regulation, peak shaving, harmonic distortion, and demand management.
- The optimum selection of ESS system size and ESS technology would be to rely on the actual operating characteristics of the local grid, i.e., the degree of peak loads, profile, and capacity for renewable generation.

1.4 Importance of the study

The suggested techno-economic analysis of ESS integration in a village-level electrical grid is of the highest priority due to a number of technical, economic, and policy-level considerations:

- With increasing electricity demand, particularly in rural and semi-urban areas, the use of renewable energy sources has been an increasing necessity. However, the intermittence of solar and wind power often causes power fluctuations and momentary outages. Integration with an ESS can minimize these issues significantly by supplying a stable and continuous power output to satisfy local demands.
- The storage plants can also be utilized to enhance the utilization of renewable energy by storing the excess energy produced during the high-generation hours and releasing it when the generation is low. Apart from making the supply-demand profile more predictable, this also reduces the reliance on conventional fossil-fuel-based backup facilities, promoting the utilization of cleaner energy.
- One of the key benefits for improving grid reliability is the integration of ESS. Through the provision of instantaneous backup power during peak demand hours, disturbances, or outages, ESS provides power quality and reduces the economic cost of supply outages to the local communities.
- While ESS solutions are typically capital-intensive, a techno-economic study in detail ensures the most cost-effective installation. This includes the determination of the optimal size, type, and operating policy of the ESS and thereby ensuring

improved system performance at the lowest possible investment and maintenance cost.

- The research findings can give important comments to policy and regulatory measures required to promote the integration of ESS at the village level grid. These can vary from recommendations on financial incentives, subsidy policies, and regulatory reform that favor investment in energy storage plants.

1.5 Research Objectives

After the problem statement and research hypothesis, the following specific objectives are stated:

- To analyze and ascertain the precise requirements and operational constraints of the village electricity system, e.g., peak power demand, energy usage pattern, and viable renewable power generation.
- To compare various energy storage systems in their technical properties and to identify the optimum technology and system size to utilize for the village grid.
- To examine the economic viability of ESS deployment by reviewing primary financial performance factors such as initial investment, running and maintenance cost, and potential revenue in the form of value-added grid services such as harmonic distortion, peak shaving, and demand response.
- To assess the composite impact of ESS integration upon grid performance by peak load reductions, improved reliability, and ratio of renewable energy source utilization.

1.6 Literature review

Some scholars investigated the implementation of photovoltaic (PV) systems linked to the electrical grid and the energy storage systems. Transient stability assessment of hybrid grid-connected battery-PV configurations were conducted within the Baubau power system. Based on the findings of the assessment regarding the influence of PV on-grid integration with the PLN electricity infrastructure in the Baubau system, it can be deduced that:

1. The implementation of 10 MWac photovoltaic systems in conjunction with 4 MWh energy storage solutions within the Baubau framework did not adversely affect the

overall stability of the system; this has been evidenced by the outcomes of power flow simulations and 80% lean down simulations.

2. The operation of the 10 MWac PV on the electricity network in the Baubau area will increase the power capacity and installed power of the plant.
3. The reduced operating hours of the 30 MW Gas Power will reduce fuel consumption and will reduce the f generating electricity in the Baubau system.
4. The electric energy mix from renewable energy especially in the Baubau system will increase by up to 20% [5].

The connection of PV system to the electrical grid was studied from a technical point of view. The integration of PV systems into electrical grids presents various operational challenges, primarily due to the intermittent and variable nature of solar energy. These challenges affect critical aspects of grid performance, including system stability, protection mechanisms, and overall network management. The complexity of these impacts is significantly heightened in weak or islanded grids, where system resilience is already limited. To effectively determine suitable PV penetration levels and understand the influence of distributed solar generation on the distribution network, a comprehensive understanding of the associated technical constraints is essential. This also enables the identification of both technical and economic opportunities associated with PV deployment. This study provides a detailed analysis of the effects that PV system integration can have on grid performance, focusing on phenomena such as voltage and frequency fluctuations, as well as voltage imbalance. In response to these issues, the paper explores a range of mitigation strategies, including advanced control techniques, enhanced protection systems, and the incorporation of energy storage solutions. These approaches aim to minimize adverse effects, enhance the ancillary services provided by PV systems, and ensure the continued stability and reliability of the electrical grid [6].

A study on the distributed generating was performed. This study investigated how small-scale electricity producers affect power loss and voltage behavior in low-voltage distribution networks. Using a combination of simulation work in Python and practical data analysis, it became clear that having PV systems on the network can help lower distribution losses and improve voltage consistency, at least up to a point. Specifically, when PV capacity stays between 1 and 3 kWp, the system seems to benefit the most.

However, going beyond 3 kWp starts to increase losses, in some cases even more than what a regular grid without PV would produce. It's worth noting that these conclusions are based on a few assumptions, like constant solar input, unlimited grid support, normal transformer tap positions, and fixed load profiles. The more technical effects, like transformer characteristics or line capacitance, weren't factored in. Even so, the presence of prosumers—anywhere from 1 to 6 kWp—didn't push voltage levels beyond accepted limits, whether measured against NEC's ±5%, Europe's EN 50160 standard, or Ghana's own ±5% threshold. That's an important finding for energy planners, especially in markets where utility companies and private energy producers often have conflicting interests. This research gives those managing the grid a reason to consider residential and small commercial solar power as part of the solution to energy losses. That said, one key limitation remains: when the main grid goes offline, these PV systems can't supply power on their own. So, future studies should definitely explore how to make local PV generation useful during outages too [7].

The use of batteries with on-grid PV system was analyzed. The study focuses on finding a practical and affordable energy solution for a household in Larkana, Pakistan, where power outages are a regular challenge. Using HOMER Pro© software, researchers explored different system setups to identify one that balances cost and reliability. They considered several real-life factors in the modeling process, including both scheduled and unscheduled blackouts, fluctuations in ambient temperature, and the effect of PV panel tilt angle on energy output. The household's electricity needs were estimated at around 13.2 kWh per day for regular use, with an additional 0.52 kWh/day of deferrable load and a peak demand of 0.6 kW. Results showed that relying on the unreliable grid combined with battery storage alone is roughly 48% more expensive per unit of energy than using a system that pairs solar power with the grid. Overall, the hybrid setup was found to be not only more economical but also more environmentally sound than the standalone grid-and-battery option [8].

The feasibility of installing a 1 MWp grid-connected PV system on a university campus in Malaysia was analayzed. The findings, based on simulation results, offer several key insights. The annual energy output of the proposed PV system was estimated at approximately 1,390 MWh. Interestingly, when comparing results from PVGIS and PVWatts, the outputs were nearly identical, differing by only about 2–3%. It was also

determined that a 20 MW solar farm, occupying just 12 hectares of land, would be sufficient to meet the entire energy demand of the UMP-Pekan campus—surpassing the global benchmark of 1 MW per 2 hectares in terms of land-use efficiency. Investing in solar infrastructure would allow the university to make meaningful progress toward its sustainability goals, including a reduction in greenhouse gas emissions and its overall carbon footprint. Financially, the project is projected to cover around 5% of the campus's daytime energy needs and could generate annual savings of approximately RM 700,699. Over its lifetime, the PV plant is expected to offset around 173,318 tons of CO_2 emissions—an impressive figure when compared to conventional fossil-fuel-based generation. The comparative analysis also suggests that both UMP-Pekan and UMP-Gambang campuses are well-suited for solar PV installations, given the high predicted energy yields. However, the study emphasizes the need for future work to validate the simulation results with real-world performance data and to explore the potential for scaling up the system to meet the entirety of the university's energy demand. [9].

In a conference presentation, the role of battery energy storage in grid-connected PV systems was explored, supported by experimental results from a small-scale prototype. The study introduced and tested a novel approach, where batteries are integrated in parallel with selected modular components of the PV array—whether at the level of individual strings, modules, or even cells. When strategically placed and appropriately sized in terms of voltage and capacity, these batteries can effectively track the maximum power point (MPP) of each component. This configuration not only enhances energy capture but also helps mitigate the effects of mismatch losses. The approach is proposed as a promising alternative to conventional designs that rely on multiple DC-DC converters connected to each module. In addition to improving energy harvesting, the inclusion of an ESS adds several practical benefits to grid-connected PV plants. These include increased grid support through better power availability, peak load shaving, reduced reliance on UPS, and simplified integration with other renewable energy sources—features that are not typically present in traditional PV grid systems. [10].

The challenge of determining the optimal battery size for grid-connected PV systems was addressed. In their study, they proposed both lower and upper bounds for the required storage capacity and developed an efficient algorithm to calculate suitable battery sizing. The primary roles of the batteries in this context include power arbitrage and peak

shaving. The authors also noted an emerging scenario in which PV generation reaches grid parity, where the cost of solar energy matches or falls below that of conventional grid electricity. In such cases, the system may experience demand peaks and elevated electricity prices at night, while daytime prices remain low due to excess solar production. To handle this, the study explored the use of batteries for energy shifting, storing excess energy generated during the day for use when demand exceeds solar output, typically in the evening. In their modeling, the efficiency of both the PV system's DC-to-AC converter and the battery's DC-AC and AC-DC conversion processes was treated as constant. However, the authors recognized that this simplification does not fully reflect real-world behavior, as converter efficiency typically varies nonlinearly with input power [11].

A year-long comparative study of various discharge strategies aimed at improving self-consumption in residential grid-connected PV systems equipped with BESS was conducted. The study examined three distinct discharge approaches: a baseline scenario, an adaptive algorithm, and a remote-controlled strategy tailored to energy market dynamics. All strategies adhered to the existing regulatory limits on residential load reduction via BESS. Importantly, the simulations were based on real-world measurement data to ensure practical relevance. The adaptive, grid-friendly algorithm employed a combination of global optimization techniques and a moving average model to enhance self-consumption during periods of high grid load. In contrast, the remote-controlled strategy focused on optimizing self-consumption by discharging the battery during times of peak intraday electricity prices, whenever conditions allowed. To support system sizing and strategy selection, the researchers used a feedforward neural network with a hidden layer to generate predictive equations for optimization purposes. These equations were then integrated into a user-friendly, web-based application designed to simplify the economic optimization of BESS sizing and to facilitate comparisons between different manufacturers' storage systems [12].

An in-depth analysis of the configuration, design, and operational behavior of multi-megawatt grid-connected solar PV systems was conducted, using practical insights drawn from a 10 MW field deployment. To enhance the system's capacity factor, the PV array is operated at its maximum power point during periods of low solar irradiance, while output is capped at a predefined rated level under high irradiance conditions to prevent

overgeneration. A key feature of the proposed system is the integration of a utility-scale BESS, connected to the grid through a dedicated inverter. The design builds on operational experience from a previously deployed 1 MW / 2 MWh battery demonstrator. The BESS contributes significantly to power smoothing and frequency regulation, as demonstrated through both theoretical modeling and experimental validation. System performance was assessed using a modified IEEE 14-bus network implemented in PSCAD™/EMTDC™, a simulation environment widely adopted in industrial and utility applications. Results from the simulations confirm the combined PV-BESS system's improved transient response, particularly in scenarios involving sudden PV shading. In addition to supporting grid stability, the BESS can perform ancillary services such as frequency control by dynamically absorbing or injecting power as needed to maintain nominal grid frequency. Experimental data from the 1 MW / 2 MWh prototype showed strong alignment with simulation results. The study also presents a methodology for sizing large-scale energy storage systems to enable dispatchable output from multi-MW PV plants. While the required energy capacities are substantial and current battery technologies may not yet be economically viable for such applications, the study suggests that alternative storage solutions—such as pumped hydro—could offer a promising path forward [13].

Researchers tackled two critical questions in their study: what constitutes an optimal storage size for integrating large-scale PV plants into the grid, and which energy storage technologies are best suited to support this integration. To address these questions, the authors introduced a metric called the "Usefulness Index," which helps identify PV-storage combinations that enable high levels of grid penetration without requiring unnecessarily oversized storage systems. This index is designed to be adaptable to varying levels of grid flexibility. The study also explores how sensitive the calculated optimal storage size is to changes in underlying assumptions. While the analysis is numerically focused on the Israeli electricity grid, the proposed framework is intended to be applicable in a broader context. The authors argue that the "appropriate storage size" identified using this approach offers a strong foundation for more advanced optimization studies. On the technological side, the review finds that no single energy storage solution currently meets all the performance requirements necessary for large-scale PV-grid integration. However, the study suggests that hybrid configurations may provide a viable pathway toward

achieving reliable and efficient integration of massive PV installations into the power grid [14].

The role of energy storage in grid-connected PV systems was investigated, particularly as a solution to the challenges faced in low-voltage distribution networks. Their analysis of grid quality revealed that many distribution systems around the world already exhibit vulnerabilities, which are likely to worsen as electricity demand continues to rise. While decentralized energy generation can help alleviate some of the strain on these networks, the study found that peaks in PV production do not consistently align with periods of peak electricity demand. As a result, energy storage becomes essential for shifting excess PV generation to times when it is more needed by the grid. Additionally, the study pointed out that PV systems can negatively affect the quality of low-voltage networks, and conversely, poor network quality can reduce a PV system's performance ratio by up to 40%. Integrating storage can help mitigate these effects, reducing the PV system's impact on the grid while also improving its efficiency and reliability. Over the long term, incorporating energy storage allows utilities to better manage grid operations, ensuring that PV-generated electricity is injected during periods of high demand. Based on data from Spain, the researchers calculated that a system rated at 2.2 kWp with a 1.5 kW inverter could reliably contribute energy to the grid for approximately 3 to 9.5 hours per day, specifically during times when demand exceeds the daily average by at least 15% [15].

A comprehensive study on the design and small-signal analysis of a grid-connected residential PV system integrated with a hybrid energy storage solution consisting of both batteries and supercapacitors was presented. The focus of their work was on conducting a detailed small-signal AC analysis to support the design of current controllers for two bidirectional DC–DC converters. A key distinction of this study, compared to similar research, lies in its consideration of both boost and buck operating modes during stability analysis. This dual-mode evaluation allows for more precise controller tuning and improved overall system performance. Additionally, the control strategy involved regulating the DC-bus voltage to derive a reference for the inverter's output current. To ensure that the injected current remains in phase with the grid voltage a phase-locked loop was implemented. This approach enables the system to meet grid interconnection standards while enhancing power quality. [16].

The role of battery storage in residential solar energy systems, particularly under scenarios of high renewable energy penetration was examined. Their research highlights the importance of accurately understanding battery behavior under dynamic operating conditions, as this is crucial for both the technical performance and economic viability of such systems. The study focused on key aspects of battery management for batteries integrated into grid-connected, solar-powered buildings. Three distinct battery modeling approaches were proposed, each differing in how they account for battery aging, internal states, and control strategies. These models included methods for estimating voltage-current characteristics, capacity degradation, remaining useful life, and various internal states such as state of charge, state of health, and state of power. To simulate and optimize system performance, the authors employed a criteria-based operational strategy combined with the Non-Dominated Sorting Genetic Algorithm II, aiming to achieve a balance between two main objectives: maximizing the system's self-sufficiency ratio and minimizing the battery life-cycle cost. These objectives are directly influenced by degradation rates and the effective lifetime of the battery. Over the project lifetime, the study also assessed annual battery degradation costs and the self-consumption ratio [17].

To summarize, many studies concentrate on adding storage system to PV on-grid systems in different countries all over the world with different benefits according to the countries location and their regulations. I our research will focus on the economic and technical consideration of adding the storage system within palatine grid.

1.7 Methodology

This research uses a holistic techno-economic assessment methodology in examining the incorporation of ESS in a grid-connected PV system, with the electrical grid of Arraba village located in the Jenin governorate of Palestine serving as a case study. The research approach aims to verify both the technical viability and economic feasibility of ESS deployment with specific focus on technical considerations such as voltage regulation, reduction of energy losses, and peak-load shaving.

Analysis begins with the definition of existing electrical infrastructure including demand profiles, PV generation potential, and distribution system operating limits. Inputs provide baseline conditions for simulation modeling as well as relative comparison between differing system configurations.

Four cases are defined and analyzed to consider the impacts of various capacities of ESS and PV. Case 0 is the base case, in which we have a 1 MW PV system without any energy storage. Case 1 is comprised of the same 1 MW PV system with an ESS of 17% penetration level. Case 2 considers a 3 MW PV system with 50% ESS penetration, and Case 3 has a 6 MW PV system with 100% ESS penetration.

Technical simulations are carried out with the help of ETAP software to carry out both steady-state load flow analysis and dynamic time-domain analysis. The load flow analysis assesses voltage profiles and active/reactive power losses during normal operating conditions. Conversely, the dynamic analysis simulates real-time grid performance with special attention to the performance of ESS in peak demand reduction, load shifting, and mitigating network stress at times of high demand.

A lithium-ion battery technology has been chosen for all designs after a critical review of currently available storage technologies in the literature. The rationale for this choice lies in the positive characteristics of the technology, which comprise high energy density, long cycle life, operating efficiency, and reducing cost trends, and hence making it fit for distributed grid application in developing conditions.

The financial aspect of the study is analyzed through the use of the System Advisor Model (SAM). Critical financial parameters are utilized to quantify the cost-effectiveness of each design. These parameters enable a comparison of the trade-offs that occur between technical performance and capital costs. Lastly, the methodology blends both simulation outputs and economic indicators to arrive at the most optimal ESS configuration. The results are consolidated into a set of recommendations that may be utilized for future planning in rural electrification, renewable penetration, and distributed energy resource management.

Chapter Two
Energy Storage Systems

2.1 Introduction

With the revolution of renewable energy, it is important to store it, so the storage systems are getting advances. ESSs vary and have been developed over the years. There are three main categories for these systems: Electrical, Mechanical, and Thermal [18].

2.2 Flywheel system

A flywheel is a type of mechanical energy storage system that has been in use for thousands of years. It operates based on the principle of inertia, storing energy in the form of rotational kinetic energy [19].

Flywheel energy storage systems (FESS) can play a significant role in supporting power systems that rely on variable renewable energy sources like solar and wind. Due to their rapid response capabilities, flywheels contribute to grid stability and help regulate frequency fluctuations. FESS can be effectively integrated with solar systems to mitigate the power oscillations caused by intermittent solar irradiance. During periods of high solar or wind availability, excess energy can be stored in flywheels and later released to smooth out fluctuations, enhancing overall system reliability. Additionally, flywheels can be used in combination with batteries to boost the consistency and quality of power output from solar installations. In wind applications, flywheels can independently compensate for short-term oscillations, thereby contributing to improved frequency control and grid balance.

The Flywheel Energy Storage System (FESS) offers several advantages, including low maintenance requirements, a long life cycle, and the highest depth of discharge. Additionally, FESS has no environmental hazards, provides a fast power response, and has potentially high specific density, making it suitable for various applications. It also offers short discharge times, efficient energy storage capabilities, and rapid short-term responses, with an efficiency of approximately 90%. However, there are some disadvantages associated with FESS, such as complex durability issues, low-loss bearings, mechanical stress, and relatively higher costs compared to other storage systems. In summary, although the system is more expensive, its unique characteristics

make it potentially more suitable for applications like wind power plants where rapid power response and efficient energy storage are crucial [19].

2.3 Compressed air energy storage (CAES)

Compressed Air Energy Storage (CAES) systems store energy by compressing air and releasing it when energy demand increases. This technology allows excess electricity—often generated by renewable sources during periods of low demand—to be stored and later used to balance supply and demand. While CAES is considered an efficient method for storing surplus energy, especially at grid scale, it faces challenges related to thermal losses. During the compression process, a significant amount of heat is generated. To manage this, the system employs air expansion techniques to dissipate the heat, but this can reduce overall system efficiency in large-scale applications.

CAES system presents several advantages. It provides ramping, intermediate, and peaking power during the day, which helps meet fluctuating energy demands. Additionally, it can store energy generated at night, particularly from wind energy systems, and release it during peak demand periods when electricity prices are higher. CAES offers better frequency control compared to load-based power plants and can operate continuously in synchronous condenser mode. Furthermore, compressed air storage systems have quick startup times, enhancing their responsiveness in meeting energy demands. However, the system also has its disadvantages. A significant challenge lies in the underground geology storage, as the presence of hydrocarbons complicates storage. Site selection is another issue, as suitable locations must have mines, caverns, or specific geological formations for effective storage. Additionally, certain unavoidable losses reduce the amount of energy that eventually reaches the grid, and the need for additional heating during expansion further complicates the system's efficiency [20]

2.4 Batteries

2.4.1 Flow batteries

Flow batteries are emerging as a promising alternative to conventional solid-state batteries, utilizing two liquid electrolytes instead of solid active materials. This design allows for greater flexibility and scalability in energy storage. Unlike traditional batteries, which are limited by the fixed capacity of solid compounds, flow batteries store energy in external tanks, enabling much higher energy capacities with storage efficiencies around

75%. A variety of electrolyte chemistries have been developed, including zinc-bromine (ZnBr), sodium-bromine (NaBr), and vanadium-based systems, with recent innovations incorporating sodium polysulfide. Flow batteries offer several advantages, such as rapid recharging, long operational lifespans (up to 10 years), the ability to fully discharge without damage, and the use of non-toxic, environmentally friendly materials. They also operate effectively at relatively low temperatures. However, one key drawback lies in the complexity and mechanical movement of system components, which poses challenges for widespread commercial deployment and increases maintenance requirements [21].

2.4.2 Lithium ion Batteries

Lithium-ion batteries were first commercially introduced by Sony in the early 1990s and have since evolved into one of the most widely adopted and influential battery technologies in the global energy storage market [22].

A typical lithium-ion battery consists of a cathode made from lithium metal oxides, such as lithium cobalt oxide or lithium transition metal oxides, and an anode composed of graphitic carbon. The electrolyte is usually a non-aqueous organic solvent containing dissolved lithium salts, such as lithium perchlorate. Li-ion batteries are particularly well-suited for applications where fast response times, compact size, and lightweight design are critical. They offer rapid response in the millisecond range and exhibit high power and energy densities, ranging from approximately 1500 to 10,000 W/L for power density, 75 to 200 Wh/kg for energy density, and 150 to 2000 W/kg for specific power. Additionally, they boast high cycle efficiency, reaching up to 97%. However, there are notable limitations. The depth of discharge (DoD) significantly influences battery lifespan, and Li-ion battery systems typically require an integrated battery management system to monitor and control operation, which adds complexity and increases the overall system cost.

Li-ion battery energy storage systems have seen growing use in large-scale energy applications by several global companies. In the U.S., AES Energy Storage has deployed Li-ion systems for frequency regulation and to support wind power projects. In the UK, a major trial is underway to assess the economic benefits of using a 6 MW / 10 MWh Li-ion system as part of the country's strategy for low-carbon energy. The project is expected to reduce infrastructure costs and support renewable energy integration. Similarly,

Toshiba launched a 40 MW / 20 MWh Li-ion project in Japan to help stabilize renewable inputs into the grid. Li-ion batteries are also widely used in hybrid and electric vehicles, with capacities ranging from 15 kWh to 50 kWh, depending on the vehicle type [23].

Significance of Lithium-Ion Batteries in Energy Storage

The demand for lithium-ion batteries is experiencing rapid growth, particularly due to the increasing demand for electric-powered vehicles [24]. Grid-scale electrical ESSs serve a vital role in supporting various applications, including power generation, transmission, and the operation of large electronic devices. These systems effectively store excess electrical energy produced during periods of high-power generation in stationary applications. The stored energy is later used during periods of high demand, helping to stabilize electric power systems by using load leveling and peak shaving techniques [25]. Furthermore, the ESS contributes to stabilizing the grid's load and power by swiftly charging and discharging, ensuring a consistent and regulated power supply to the grid. Its rapid response time is instrumental in maintaining grid stability. Additionally, the ESS facilitates the establishment of a sustainable and environmentally friendly electric grid by efficiently utilizing intermittent renewable energy sources. Beyond its role in ensuring power reliability, the power grid system, functioning as a monitoring network, possesses the capability to anticipate and diagnose potential failures, thereby identifying irregularities or weaknesses in a timely manner.

Lithium-ion batteries, also known as Li-ion batteries, have become a prominent technology for storing energy due to their superior energy density, extended lifespan, and effectiveness in storing and discharging electrical energy. These batteries present a hopeful resolution for energy storage applications at both small-scale and grid-level. Their ability to adjust, react quickly, and expand in size makes them a favored option for enhancing the integration of renewable energy and reducing variations in supply [26].

The ESS at the grid level plays a crucial role in managing electricity usage, catering to diverse large-scale applications. Electrical power demand exhibits daily, seasonal, and unforeseen fluctuations, often displaying significant differences between peak and off-peak periods. Hence, the storage of generated power becomes essential, providing surplus power during peak loads through load leveling and peak shaving. Furthermore, renewable energy sources are subject to geographic, seasonal, and temporal variations, resulting in

unpredictable power output fluctuations that might not directly meet the grid's demands. Consequently, the power grid system aims to stabilize the intermittent output power generated by sources like wind and solar energy, reducing the resultant fluctuations by adjusting their output profiles [27].

Lithium-ion batteries have various functions in the integration of power grids. They enable the optimal utilization of sustainable energy sources such as solar and wind by storing surplus energy produced during periods of low demand and delivering it when demand surpasses supply. Peak shaving is a process that helps to balance the grid and alleviate strain during periods of high demand.

Grid Stability and Reliability

Lithium-ion batteries improve grid stability by offering rapid-response capabilities to mitigate abrupt variations in power generation. They function as agile resources that mitigate fluctuations in energy supply and demand, thus ensuring consistent voltage and frequency levels within the grid. Grid ESSs require significant power and energy to maintain their stability.

Effectively managing the wide range of devices integrated into the power grid requires a substantial number of power sources. This diversity and scale introduce major challenges in achieving both autonomous and coordinated operation across the network. One of the key challenges is developing a power management system that ensures long-term system stability, operational reliability, safe energy storage, and economic efficiency. In systems where multiple batteries are connected in a stack, the power management system must regulate and balance electrical parameters—such as voltage and current—for each individual battery. This system plays a critical role in determining how well the battery stack performs in large-scale energy storage applications, directly influencing its safety, efficiency, and overall cost [28].

While Lithium-ion batteries have a high energy density, a single cell is inadequate for fulfilling the requirements of the power grid. Assembling batteries in parallel to increase current capability or in series to raise voltage presents considerable difficulties concerning stability, operational voltage, safety, and cycle life. By connecting a small number of cells in series, the charge current and voltage are evenly distributed among them. Nevertheless, the process of generating a high voltage necessitates the use of multiple cells arranged in

series, resulting in an uneven distribution of voltage across these cells. This leads to an uneven distribution of charge among the cells, with some cells being fully charged while others are excessively charged. Lithium-ion batteries have constraints when it comes to excessive charging, which can lead to safety hazards and reduce the overall lifespan of the system. Therefore, it is crucial to incorporate a system monitor to avoid excessive charging of cells and ensure the batteries are evenly charged, thus enhancing the overall performance of the system.

To guarantee safety, Lithium-ion batteries monitors must adhere to the following guidelines: They must maintain circuit balance to prevent any cell's voltage or current from exceeding the limit by stopping the charging current. This is a critical precautionary measure to address safety concerns and ensure the stability of the system. They must also monitor temperature levels to prevent any cell from surpassing the limit, which would result in the system shutting down and cooling off [29].

Renewable Energy Integration

Renewable sources have become widely accessible and are now considered highly cost-effective for power generation in many regions. The substantial growth of variable renewable sources in recent years has driven the need for more flexible electrical ESSs. BESSs provide an effective method for storing electricity produced by renewable sources, thus improving the stability and dependability of the grid system. As a result, this progress promotes the increased use of renewable energy sources [30].

These batteries facilitate the smooth incorporation of renewable energy sources into the power grid. They accumulate excess energy produced during favorable circumstances and distribute it during times of high demand or when renewable sources are not actively generating electricity.

Integrated lithium-ion batteries can greatly enhance the performance of solar photovoltaic power farms by storing electrical energy and stabilizing output power. This helps to address the issue of intermittence that occurs during night-time or when sunlight is obstructed. This combination creates a resilient operational system that can effectively handle unexpected increases in power and fulfill consistent power requirements. The incorporation of batteries in solar photovoltaic systems has shown enhanced stability in

power output, particularly when confronted with partial shading or fluctuations in solar radiation [31].

Peak Load Management

Lithium-ion batteries are essential for managing peak loads by supplying additional power during periods of high demand, thereby alleviating the burden on conventional power generation systems. The majority of projects that offer frequency regulation services have reported a nominal power that is greater than 1 MW, with an approximate power-to-energy ratio of 1:1 [32]. Battery technologies face a challenge in meeting the requirements of frequency regulation, which include the need for quick response times, high performance, and strong power capabilities. Ensuring consistent and dependable electricity supply is of utmost importance in extensive implementation and remote setups, with a specific emphasis on maintaining stable voltage and frequency. ESSs maintain voltage and frequency stability in situations where there is a difference between power generation and consumption. They are used for both short-term and long-term purposes. Due to their high round-trip efficiency and energy density, lithium-ion batteries have great potential for a wide range of applications [33].

Challenges and Future Prospects

Although lithium-ion batteries possess various benefits, they also present certain challenges, including high costs, safety issues, and a scarcity of raw materials. Scientists are currently investigating innovations in battery technology to tackle these difficulties, with the goal of enhancing energy density, longevity, and recyclability. ESSs for the electricity grid represent a significant change in flexibility, solving the long-standing problem of aligning electricity generation with consumption. This limitation imposes a significant financial burden, necessitating the development of grid infrastructure to accommodate peak demand, which is almost double the average demand, in the absence of storage. The increasing presence of renewable energy sources such as wind and solar highlights the need for storage due to their inherent variability, which can potentially jeopardize grid stability and reliability on a larger scale. The integration of storage with wind and solar power makes these variable sources dispatchable, guaranteeing their immediate availability to meet changing demands. Storage not only reduces the carbon footprint by replacing old, inefficient, high emission "Peaker" plants, but it also utilizes

low-cost, cleaner electricity to charge batteries during off-peak hours for discharge during peak demand, thereby improving the environmental sustainability of the grid [34]. The main obstacle encountered by grid storage is its competition with more economically viable forms of energy generation, particularly gas turbines, which offer electricity at a cost that is roughly one-fifth of the price of the currently accessible batteries. From a purely economic standpoint, it is more favorable to produce electricity using gas turbines as needed, rather than charging batteries during low-demand periods and then discharging them during high-demand periods. In order to compete with gas turbines, the cost of grid batteries must decrease by approximately fivefold [35].

Although there have been significant advancements in energy density and cost reductions for lithium-ion batteries, it is currently impossible to achieve further five-fold improvements. Theoretical constraints on the performance of active components in lithium-ion batteries restrict improvements to approximately 50-100%. It is crucial to make groundbreaking progress in technologies that go beyond lithium-ion in order to completely transform transportation and the electricity grid [36].

Ultimately, lithium-ion batteries are leading the way in energy storage technology. They enable the efficient integration of renewable energy sources into the grid, thereby making a substantial contribution to a more sustainable and dependable energy system. In the future, ongoing research and development efforts will enhance the performance of ESSs, making them a crucial element in their development.

2.4.3 Lead-acid batteries

Lead–acid batteries remain the most widely used type of rechargeable battery, valued for their simplicity and affordability. In a typical configuration, the cathode is composed of lead dioxide (PbO_2), the anode is metallic lead (Pb), and the electrolyte consists of sulfuric acid. These batteries offer fast response times, low daily self-discharge rates, and moderate cycle efficiencies ranging from 63% to 90%. One of their most appealing features is their relatively low capital cost, estimated between $50 and $600 per kWh. Lead–acid batteries are commonly used in stationary applications such as backup power for data centers and telecommunication infrastructure, as well as for general energy management purposes. They have also been adapted for use in hybrid and fully electric vehicles. Despite their widespread use, lead–acid batteries have seen limited deployment

in utility-scale energy storage systems. This is primarily due to limitations such as low cycle life, modest energy density, and low specific energy. Additionally, their performance tends to decline in low-temperature environments, necessitating the use of thermal management systems which is considered as an added cost that further hinders their suitability for large-scale grid applications [37].

2.4.4 Ultra-Capacitor

An ultra-capacitor is an energy storage device characterized by very high capacitance but a relatively low voltage range. It combines features of electrolytic capacitors and secondary batteries, storing 10 to 100 times more energy per volume than typical capacitors and delivering or accepting charge much faster while enduring many more charge-discharge cycles than batteries. Unlike traditional capacitors that use a solid dielectric, UCs utilize an electrolyte and an insulating membrane, replacing metal plates with porous materials. This design creates an electric double layer (EDL) and electrochemical pseudo capacitance, both contributing to the total capacitance.

There are three main types of ultra-capacitors: electric double-layer capacitors (EDLCs), pseudo capacitors, and hybrid capacitors (HCs). EDLCs store energy through electrostatic charge separation at the electrode-electrolyte interface, which allows for very long cycle life due to the physical nature of charge storage. EP capacitors, on the other hand, store charge via faradaic redox reactions involving high-energy electrode materials, resulting in higher energy density but shorter lifespan and slower charge/discharge rates compared to EDLCs. Hybrid capacitors combine these mechanisms, seeking a balance between energy density, power density, and durability.

Ultra-capacitors excel at providing short bursts of high power due to their high power-to-energy density ratio and very low internal resistance, enabling rapid charge and discharge. They are ideal for applications with intermittent high-power demands but are less suitable for continuous power supply needs. UCs also have an almost unlimited number of cycles and exhibit slow self-discharge; however, they tend to be more expensive than conventional batteries.

EDLCs rely on highly porous, conductive carbon-based electrodes, offering excellent cyclic stability and minimal degradation since their charge storage is non-faradaic. EP capacitors deliver higher energy density but suffer from lower power density and fewer

cycles due to electrochemical reactions. Hybrid capacitors use combinations of polarized and non-polarized electrodes, achieving improved cycle life and a cost-effective compromise between energy and power performance [38].

Chapter Three
Current Network Analysis

3.1 Introduction

The electrical network of Arraba village, located in the Jenin district of Palestine, currently operates with a total installed capacity of 1 MW of PV panels. This network represents a typical rural electrical system in Palestinian territories, facing challenges related to energy shortages, high dependency on imported electricity, and integration of renewable energy sources. The integration of PV systems in the village is a step toward reducing energy dependency, but several technical and operational challenges persist, particularly in terms of grid stability, energy management, and maximizing renewable energy utilization [39-40].

In this chapter, a comprehensive analysis of the current operation of the electrical distribution network of Arraba village, which is currently tied with a 1 MW grid-connected PV system, is presented. The main aim is to assess the performance of the system in its current configuration in terms of its efficiency, voltage stability, and energy loss characteristics.

The location of the solar power plant in the town of Arabeh was determined due to technical and logistical considerations related to the characteristics of the local electricity grid in the town. Although the official documents in the agreement signed between the relevant parties focus on the general objectives of the project, an analysis of the technical context indicates that the site is distinguished by its proximity to medium-voltage lines, which reduces transmission losses and grid connection costs. Furthermore, the availability of municipal-owned land facilitates legal aspects and reduces development costs. The site also enjoys high solar radiation levels and suitable geographical conditions for installing and maintaining panels. It also contributes to enhancing energy independence and supporting the local economy through land use returns and infrastructure improvements [39-40].

The examination starts with an investigation of the levels of voltage on different buses of the power grid. This study is crucial in establishing any differences or drops in voltage that could undermine system stability or the quality of service. These variations are

important in establishing the strength of the grid and its ability to ensure adequate voltage levels during normal loading and generation conditions.

To further assess system performance, a load flow study is conducted. The simulation provides an understanding of the manner in which electrical energy is being supplied from the PV system to the end-users in the village. It enables the determination of the areas of high power losses, specifically those related to transmission inefficiencies and reactive power flows. The study also provides for how effectively the current PV system meets local demand and ensures grid reliability.

In conclusion, this chapter presents a comprehensive explanation of the existing condition of the electrical network in Arraba village. It identifies operational inefficiencies and constraints in the system and establishes a foundation for quantifying the benefits of prospective improvements..

3.2 Overview of the Current Network

The current electrical network in Arraba is primarily composed of conventional energy sources complemented by the 1 MW PV panel system. The load flow analysis of the network, as presented in the Time Domain Load Flow (TDLF) Results, provides insights into how the network performs under different conditions, especially with the integration of PV panels.

3.2.1 Electrical Load Distribution

The one-line diagram from the TDLF results provides a clear representation of the layout and distribution of loads across various buses in the system. Appendix A illustrates the network's components, detailing the arrangement of transformers, cables, and buses. The diagram reveals that the village is supported by a series of transformers with capacities ranging from 400 kVA to 630 kVA, which are responsible for feeding multiple loads. Each bus in the network is connected to a specific transformer, with power distribution monitored at various nodes. These nodes offer detailed insights into voltage levels, active power in megawatts (MW), and reactive power in megavars (Mvar) across the network. While the voltage levels at the buses generally remain stable and close to 100%, minor voltage drops are observed at the farthest buses, such as Bus 37 and Bus 30, which suggests that these areas may experience slightly reduced power quality.

3.2.2 Performance of the PV System

The integration of 1 MW of PV panels into the network has been beneficial in reducing the reliance on imported electricity, especially during daylight hours. However, the intermittent nature of solar energy poses challenges to grid stability, particularly during periods of low irradiance or at night. **Figure 2** shows the contribution of the PV system to the overall power supply in 19/1/2023 where the power demand was at its maximum level, which peaks during the midday hours but drops significantly in the evening.

3.3 Challenges in the Current Network

The current configuration of the Arraba village electrical network faces several challenges, despite the benefits provided by the PV system. These challenges include:

1. **Intermittent PV Generation**: Solar energy is variable, and without proper storage solutions, the grid cannot fully utilize the energy generated during peak sunshine hours. This intermittency causes fluctuations in power supply, especially during periods of low solar irradiance.
2. **Voltage Fluctuations**: Although voltage levels remain generally stable, some buses experience voltage drops, particularly during peak demand periods. These drops, if not addressed, can lead to reduced power quality and potential outages in the long term.
3. **Power Losses**: The network experiences noticeable power losses, particularly in reactive power, due to long transmission distances and the lack of reactive power compensation. These losses reduce the overall efficiency of the system and increase the cost of energy supply.
4. **Lack of Energy Storage**: Without an ESS, the grid cannot store excess energy generated by the PV panels during the day for use during peak demand periods in the evening. This results in the utilization of renewable energy and continued reliance on imported electricity during critical hours

Figure 2

PV Generation Output

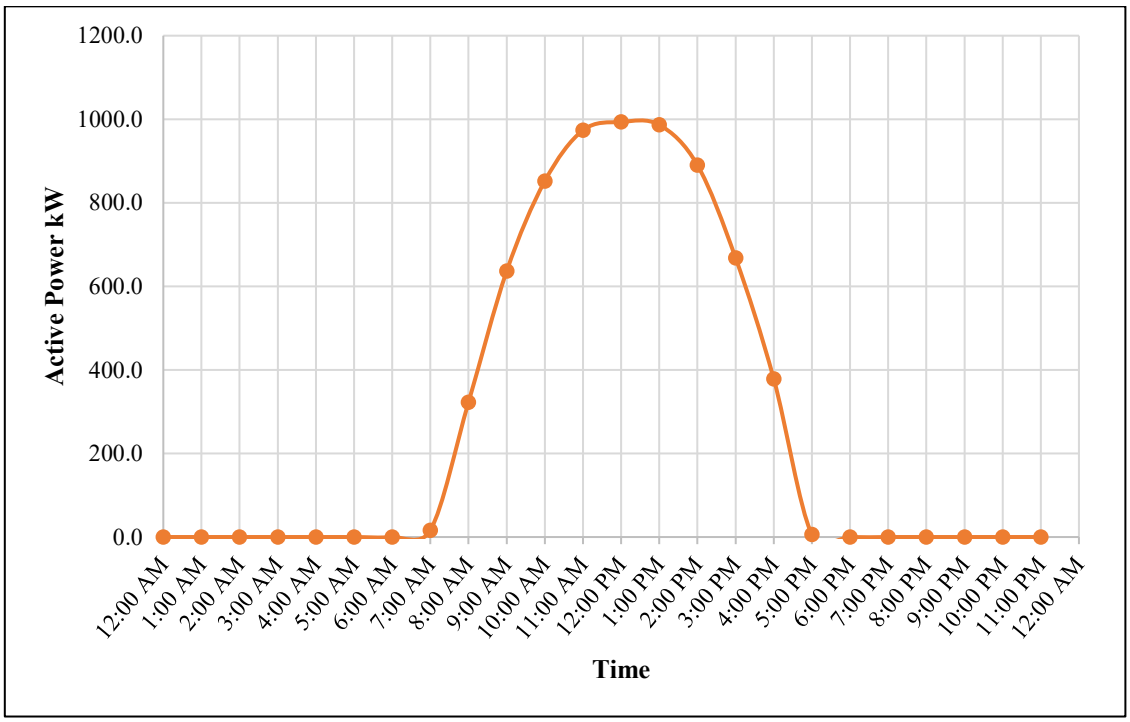

3.4 Scope of the Thesis

This thesis aims to address the challenges by proposing a comprehensive techno-economic study for the implementation of an ESS in the Arraba village electrical grid. The primary focus will be on optimizing the use of renewable energy, improving grid stability, and reducing the reliance on imported electricity. The following sections outline the key components of the thesis:

3.4.1 Grid Performance with ESS

Simulations are run to analyze the effect of adding an ESS on the overall performance of the grid. This study concentrates on various technical and economic metrics that indicate the system's efficiency and reliability enhancement as a result of storage integration.

One of the primary subjects that are examined is voltage regulation, where the role of the ESS is examined according to its ability to stabilize voltage levels within the network. Particular emphasis is given to buses that have been noted to experience voltage drops under normal loading conditions, as the ESS will need to provide or take up power according to real-time voltage excursions, thereby enhancing voltage stability.

Apart from voltage performance, the study investigates the reduction of energy loss, specifically reactive power loss reduction, which can be mitigated by optimized energy dispatch and load balancing facilitated by the ESS. With power flow smoothing and peak to off-peak load shifting, the ESS is anticipated to improve overall energy efficiency and decrease transmission and distribution losses.

Besides, the financial performance of the ESS setups is analyzed in a dedicated financial analysis. This includes a study of such indicators as capital investment requirements, operating costs, and long-term financial returns. The aim is to determine the cost-effectiveness and financial feasibility of each ESS scenario so that technical improvements are supported by economic justification.

3.4.2 Optimization of Renewable Energy Utilization

The ESS will also be evaluated in terms of its ability to maximize the use of renewable energy by storing excess solar power during peak generation periods. This will help reduce the reliance on imported electricity, especially during high-demand periods in the evening and winter months when solar generation is low.

3.5 Single line diagram of the network

The electrical network in Arraba village, located in the Jenin district of Palestine, operates as a grid-connected system with an integrated 1 MW PV system. This solar integration offers substantial potential for meeting the village's electricity needs but introduces challenges related to energy loss and power quality. These issues are explored in detail throughout this thesis, focusing on ways to enhance system efficiency. Figure 3 shows the results of ETAP simulation at maximum load point. A significant issue identified in the current network is the energy loss amounting to 0.629 MWh, representing around 17% of the total system generation. This high energy loss is primarily caused by the lack of an ESS and reverse power flows from the PV system to the grid during periods of low demand. This will be an essential focus for future system improvements. Appindex A visually represents this loss, clearly indicating the inefficiency in the current system that will be targeted with the introduction of the ESS.

As highlighted in the Time Domain Load Flow System Summary, the total daily energy demand of Arraba village is approximately 40.0556 MWh. The PV system contributes

around 6.72 MWh of this demand, while the remainder, approximately 33.96 MWh, is supplied by external alternating current (AC) sources. This reliance on external sources reflects the limitations of the current PV contribution.

Figure 3

Energy Loss Profile in the Network

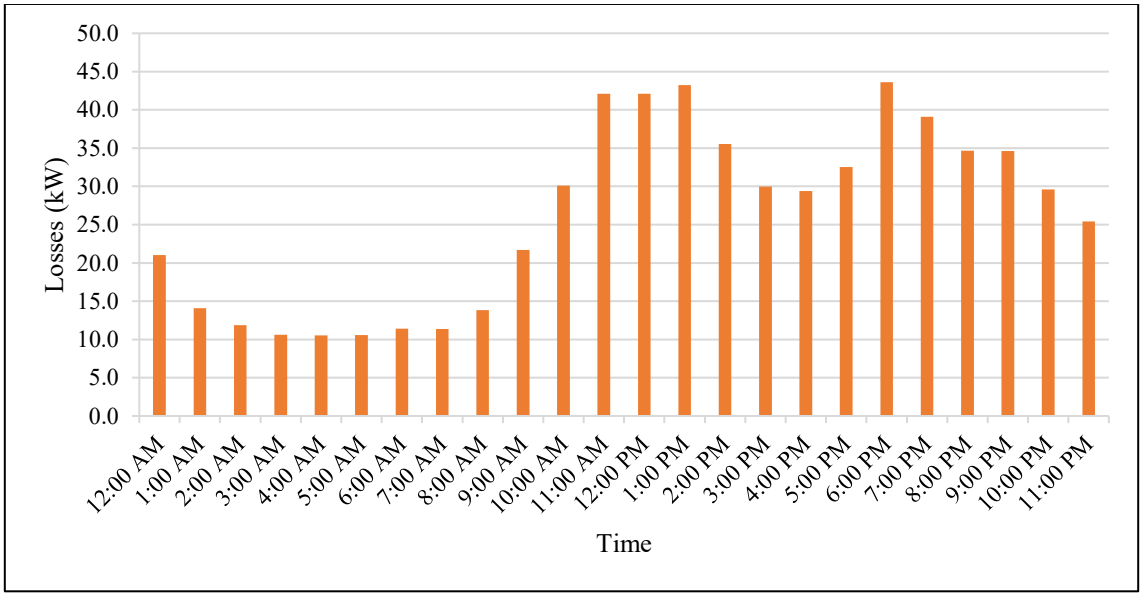

The electrical infrastructure of Arraba village is complex, comprising key elements such as transformers, buses, and cables that distribute power across various areas. Figure 13 illustrates the one-line diagram of the village's distribution network, detailing transformer capacities ranging from 400 kVA to 630 kVA. These transformers facilitate the efficient transfer of energy from the central grid to individual network nodes.

A focused load flow analysis was performed on the current network configuration, to analyze only the current situation without considering variations in load (minimum, maximum, or intermediate). This analysis utilized ETAP software to simulate the electrical network's behavior under existing conditions, helping identify voltage drops, power losses, and potential points of instability, for more detailed information, refer to Appendix A.

Each bus within the network serves a specific load point, with voltage levels across different buses generally stable, albeit with minor drops at buses farthest from the primary power source. Buses 37 and 30, for instance, exhibit slight voltage reductions, which

could impact stability under high load. These voltage distributions are depicted in Figure 4, where minor deviations from ideal voltage levels are noted.

Figure 4

Voltage Profile Comparison Across Network Buses

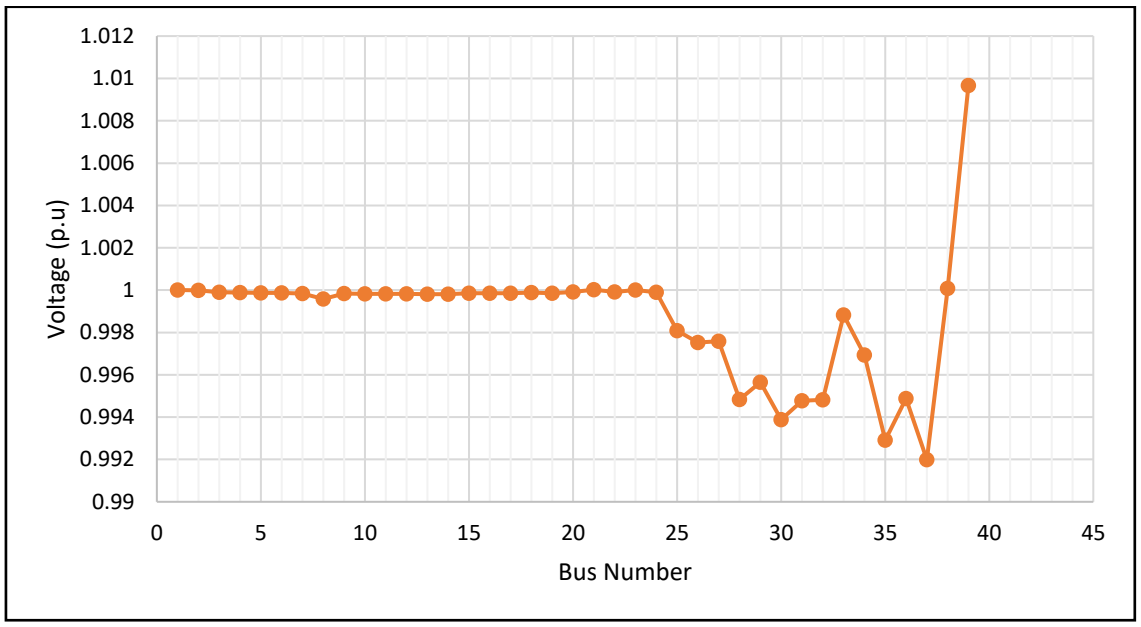

The PV system can reach peak outputs of approximately 993.5 kW, while the maximum external AC generation capacity is 2657.1 kW. Figure 5 demonstrates the active power distribution from PV, grid, and net sources over a 24-hour period, highlighting the intermittent nature of solar generation and the critical role of the AC grid in balancing the village's energy requirements. The net power levels illustrate the reliance on external sources and underscore the potential benefits of an ESS to bridge the energy gap, particularly during peak solar production times.

Figure 5

Active Power Distribution Across Solar, Grid, and P-net Sources Over a 24-Hour Period

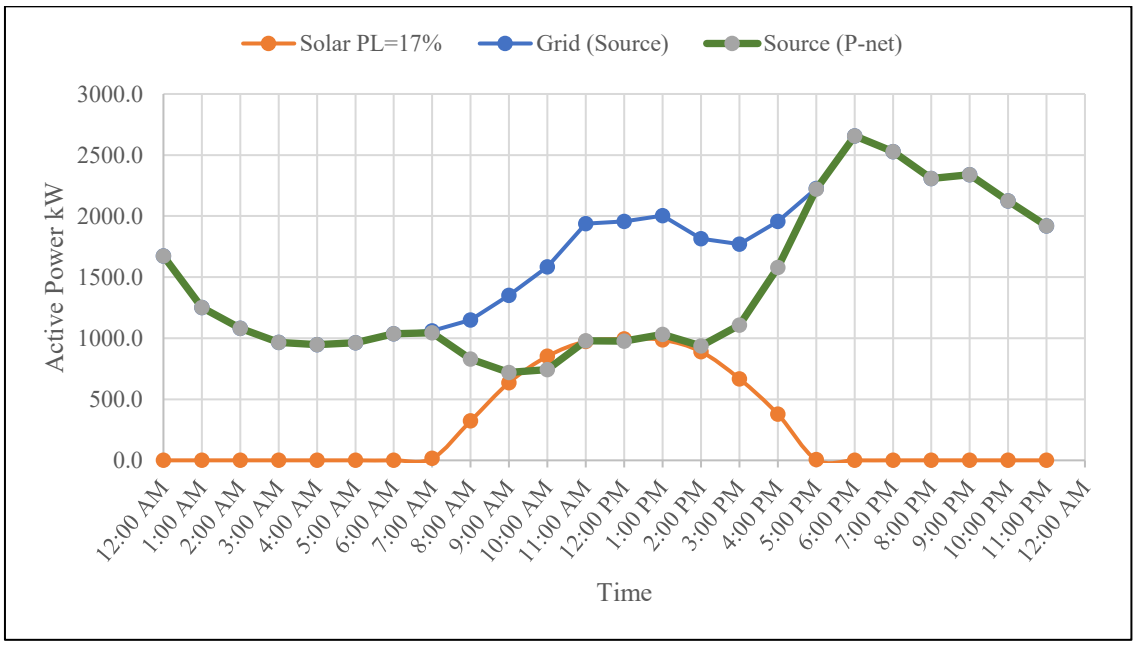

Chapter Four

Results and Discussion

4.1 Introduction

This chapter presents the simulation results for the Arraba village electrical network under four scenarios, analyzing key performance indicators such as voltage stability, power losses, load distribution, and renewable energy utilization:

- Case 0: Current network configuration with 1 MW PV system and no energy storage.
- Case 1: 1 MW PV system with a 17% penetration level and integrated ESS.
- Case 2: 3 MW PV system with a 50% penetration level and integrated ESS.
- Case 3: 6 MW PV system with a 100% penetration level and integrated ESS.

Each case is analyzed for key performance indicators, including voltage stability, power losses, load distribution, and renewable energy utilization

4.2 Load flow analysis

This chapter presents a simulation-based analysis of the present performance of the electrical network of Arraba village through the ETAP (Electrical Transient Analyzer Program). The study is concerned with the operational effects of the presently operational 1 MW grid-connected solar photovoltaic system. Through the simulation of the network under normal operating conditions, the study seeks to evaluate voltage regulation, energy distribution, and power loss due to the varying nature of solar output over daytime hours.

Load flow study gives a clear picture of power distribution over the network and voltage level maintenance at different buses. Particular emphasis is placed on assessing to what extent the PV system supports voltage and whether specific parts of the network are confronted with significant deviations from nominal values. Such simulations give a complete analysis of energy transfer efficiency and capability of existing infrastructure for integrating variable renewable generation.

The results from this analysis are that voltage levels throughout the majority of the network are within acceptable limits, and this suggests a well-controlled system by and large. There are tiny anomalies at certain buses, however, which may perhaps need closer inspection considering future innovations or in the introduction of storage possibilities.

Load Flow Analysis – Case 0

The unbalanced load flow results for Case 0 give a notion of phase-wise voltage magnitudes, active/reactive power, and power factor at the essential buses. Bus 1, being near the principal utility source, has a balanced three-phase voltage of 100% magnitude, and generates 1.68 MW. The delivered power at downstream nodes has a high-power factor in all the phases, representing nearly purely active power flow with insignificant capacitive nature as per Table 1.

Table 1

Load flow results for Case 0

BUS	VOLTAGE (KV)	VOLTAGE MAGN. (%)	GENERATION (MW)	POWER FACTOR (%)
BUS 1	33.000	100.00	1.68	99.9
BUS 39	0.400	102.13	0.000	100

Yet, Bus 39, which is nearest to the PV, has a voltage magnitude of as 102.13%, slightly greater than Bus 1. Although it has no local load or generation, power is received from Bus 38 shows a power factor close to 100%, indicating ideal purely active flow.

This evaluation provides a preliminary overview of the technical operation of the current photovoltaic-integrated system in Arraba. It establishes a baseline for measuring gains made by energy storage systems in the later chapters, especially in terms of grid stability and operational efficiency.

Load Flow Analysis – Case 1

For Case 1, the ESS modes of operation at Bus 39 being considered are charging and discharging. These scenarios reflect how the ESS affects grid power flow, voltage level, and generation in the upstream zone.

Under ESS charging, Bus 1 has increased generation to 2.66 MW, with power going to downstream loads. The voltage remains unchanged at 100%, while power factor is maintained close to 99.7%, indicating highly efficient power transfer. At Bus 39, the voltage is reduced to 99.88%. Although no load or generation is directly allocated to Bus 39 in this mode, power injection to the storage system can be clearly observed.

When it discharges, Bus 1 generation drops to 1.94 MW, reflecting reduced grid demand. Bus 39 voltage rises to 101.65%, and power flows out from the ESS to Bus 38. The system again reflects almost perfect power factor conditions. The results for case 1 are summarized in table 2.

Table 2

Load flow results for Case 1

MODE	BUS	VOLTAGE (KV)	VOLTAGE MAGN. (%)	GENERATION (MW)	POWER FACTOR (%)
CHARGING	Bus 1	33.000	100	2.66	99.7
	Bus 39	0.400	99.88	0.000	100
DISCHARGING	Bus 1	33.000	100	1.94	99.8
	Bus 39	0.400	102.65	0.000	100

Load Flow Analysis – Case 2

In Case 2, the ESS at Bus 39 operates in both charging and discharging modes to subject the system response to more dynamic power transfer conditions. As previously stated, charging in Case 2 is more stringent than in Case 1, Bus 1 sends out 2.66 MW with a power factor of 99.5%, and Bus 39 witnesses a slight rise in voltage to 100.26%.

In this setup, the ESS backfeeds 0.489 MW per phase onto the grid at Bus 39, resulting in a local rise in voltage to 100.63%, the highest to date. Upstream generation at Bus 1 reduces to 1.2 MW, and current passing to Bus 3 reduces in proportion. The power factor at Bus 1 is still good at -99.1% despite such back feeding, whereas system balance is maintained.

This bidirectional operation reflects the function of the ESS in flattening the load profile and supporting grid efficiency. The most critical phase-averaged indicators for both buses under both ESS modes are presented in Table 3.

Table 3

Load flow results for Case 2

MODE	BUS	VOLTAGE (KV)	VOLTAGE MAGN. (%)	GENERATION (MW)	POWER FACTOR (%)
CHARGING	Bus 1	33.000	100	2.66	99.5
	Bus 39	0.400	100.26	0.000	100
DISCHARGING	Bus 1	33.000	100	1.2	99.1
	Bus 39	0.400	100.63	0.000	100

Load Flow Analysis – Case 3

In Case 3, the system is operating in maximum penetration mode with the ESS and PV system fully operational. There are two modes of operation that are considered: charging and discharging, which offers valuable insight into bidirectional power flow and how it affects grid stability.

With ESS charging, there is large power consumption at the low-voltage node Bus 39, with each phase consuming 1.205 MW through Con1, while 1.975 MW per phase is being delivered by the grid through Con2. Voltage at Bus 39 rises to 100.64%, and the system is operating at a near-perfect power factor (±100%).

Meanwhile, Bus 1 contributes only0.359 MW, indicating that most of the demand is being locally met from distributed sources.

In discharge mode, at Bus 1, the power generation drops to negative (−-0.013 MW), meaning that the upstream source is now absorbing power. The power factor at Bus 1 also drops to about 68.6%, reflecting greater reactive exchange — a far cry from the quasi-ideal situation when in charging mode. The key electrical parameters for both modes are provided in Table 4.

Table 4

Load flow results for Case 3

MODE	BUS	VOLTAGE (KV)	VOLTAGE MAGN. (%)	GENERATION (MW)	POWER FACTOR (%)
CHARGING	Bus 1	33.000	100	0.359	89.1
	Bus 39	0.400	100.64	0.000	100
DISCHARGING	Bus 1	33.000	100	-0.013	68.6
	Bus 39	0.400	100.76	0.000	100

To additionally evaluate the behavior of the interaction between the PV system and the main grid, particularly with regards to the potential for reverse power flow, generation values at Bus 1 were analyzed under different operating conditions. The results obtained from the appendices from A to H are shown in Table 5. For Cases 0 to 2 there is no indication of reversing power flow since generation at Bus 1 is always positive. In Case 3, the representative of the 100% maximal PV penetration scenario, a slight power rejection is observed during both the charging and discharging periods, with values of -0.005 MW and -0.014 MW, respectively. These values reflect a small export of power back into the supplying grid, indicating that during high penetration conditions, excess energy could occasionally be injected into the upstream network. Although small in magnitude, this reverse flow points towards the need for effective control schemes to deal with bidirectional power transfer, particularly with more renewable sources coming on grid.

Table 5

Power Flow Evaluation at Bus 1 Under Different Operational Scenarios

Case No.	Mode	Generation @ Bus1	Status
Case 0	-	1.665 MW	No rejection
Case 1	Charging	2.66 MW	No rejection
	Discharging	1.94 MW	No rejection
Case 2	Charging	1.71 MW	No rejection
	Discharging	1.2 MW	No rejection
Case 3	Charging	- 0.005 MW	Minor rejection
	Discharging	- 0.014 MW	Minor rejection

4.3 Harmonic Distortion

Power system harmonics are voltage or current waveforms that are non-sinusoidal in nature, which take place as a result of frequencies that are integer multiples of the fundamental frequency. Distortion is typically created by inverter-based generating equipment and non-linear loads. Harmonics can lead to various complications, such as overheating of equipment, energy losses, malfunctioning of sensitive equipment, and an overall decline in power quality. In order to quantify harmonic distortion and its impact on the grid, the following main measures are taken:

- RMS Voltage: Shows percentage root mean square voltage to nominal in order to verify if any decrease is seen due to the harmonics.
- Total Harmonic Distortion (THD): Provides the relation of total sum of all the harmonic currents and the fundamental component indicating the total amount of distortion percentage.
- Telephone Interference Factor (TIF): A weighted harmonic distortion index for indicating an estimate of communication line interference capability.
- THDG and THDS: These are the generator voltage total harmonic distortion and system voltage total harmonic distortion, respectively, to compare the distortion against the source or system total.

IEEE standard 519-2014 specifies maximum recommended limits of harmonic voltage and current magnitudes of electrical power systems to enhance compatibility and maintain grid stability. For example, the voltage THD at the point of common coupling is typically supposed to be less than 5% for systems rated below 69 kV, while tighter limits apply for higher voltages. These recommendations are essential for grid operators and system planners in order to manage harmonic-related risks effectively while ensuring long-term power quality and reliability [41].

Observation and measurement of such parameters are critical to operational reliability and voltage quality assurance, especially for distribution systems with high power electronic and distributed generation penetration levels. Harmonic distortion is examined in Case 0 to study the effect on focused buses and observe localized harmonic performance at different voltage levels.

Harmonic Distortion Analysis – Case 0

Case 0 harmonic distortion analysis was carried out in order to assess the waveform distortion and voltage quality on crucial buses. At Bus 1, harmonics were minimal, with 0.06% THD and TIF of 2.18, indicating very good power quality and minimal harmonic impact. In comparison, Bus 39 was experiencing quite high harmonic activity, with THD = 2.87%, TIF = 94.63, and THDG and THDS also at 2.87%, which represents visible waveform distortion. Even though all of the values are still well within IEEE 519-2014 recommended limits, Bus 39 is more vulnerable to harmonic impacts and could be a problem in the case of higher nonlinear load penetration or inverter-based generation in the future. Detailed harmonic distortion levels of the two buses are presented in Table 6.

The harmonic spectrum of Appendix I shows the voltage distortion content distribution with orders from 1 to 20. Bus 39 exhibits clearly dominant harmonic content on the 7th, 11th, 13th, 17th, and 19th orders with the 17th very close to a value of nearly 1.9%.

Conversely, Bus 1 and Bus 38 are nearly flat for all orders of harmonics, supporting the observation that high-frequency distortion is highly localized at the lower voltage bus. The evidence sustains the inference that Bus 39 is more prone to harmonic amplification.

Harmonic Distortion Analysis – Case 1

The harmonic distortion levels in Case 1 were measured across the system with particular emphasis on Bus 1 and Bus 39 to ascertain the impact of partial integration of PV and ESS on power quality.

At Bus 1, the harmonic indices are low and consistent with the previous case. The THD is 0.11%, and the TIF is 4.00, both well within IEEE 519-2014 limits. These indices confirm that the upstream medium-voltage side is free from harmonic activity for this partial penetration case.

In contrast, Bus 39 exhibits a high increase of harmonic distortion with THD = 5.68% and TIF = 186.87, which are both higher than normal acceptable levels. The THDG and THDS are also high at 5.68%, indicating severe harmonic presence either due to inverter-based ESS operation or nonlinear devices near the low-voltage side. This confirms that Bus 39 remains the weakest spot in the network from the power quality perspective under distributed energy integration. These figures are presented in Table 6.

The harmonic spectrum in Appendix I also shows the source of the distortion. Bus 39 has dominant harmonic components at orders 7th, 11th, 13th, 17th, and 19th, with the 17th harmonic exceeding 3.0%, the highest among all orders. These frequencies are characteristic of inverter-based sources and switching operations, which are common in PV-ESS converters. On the other hand, Bus 1 and Bus 38 show near zero harmonic contributions of all orders, verifying that harmonic propagation is mostly contained in the low-voltage side and does not back-feed significantly into the upstream medium-voltage system.

Harmonic Distortion Analysis – Case 2

In Case 2, with higher levels of PV and ESS integration, harmonic distortion levels were evaluated again at Bus 1 and Bus 39.

At Bus 1, the THD has increased slightly to 0.33%, and the TIF is 11.79. These values, although higher than in previous cases, are still within acceptable IEEE 519-2014 limits, which indicates that harmonic propagation at the medium-voltage side is still low and manageable.

At Bus 39, however, THD is 2.82% and TIF is 93.75, again showing a heavy harmonic load at the low-voltage level. This is lower than in Case 1 but still close to normal compliance limits, worthy of consideration for power quality control. Both THDG and THDS also both equal the THD at 2.82%, again showing distributed harmonic distortion that might be due to multiple converters or charging sources operating in parallel. The summary of these measures appears in Table 6.

The harmonic spectrum of Appendix I indicates the voltage distortion across harmonic orders at Bus 1, Bus 38, and Bus 39. The dominant components at Bus 39 appear again at the 7th, 11th, 13th, 17th, and 19th orders, with the 17th harmonic being ~1.8%. Surprisingly, harmonic content at Bus 38 and even Bus 1 is slightly more evident than in Case 1, reflecting some upstream propagation of harmonics.

Harmonic Distortion Analysis – Case 3

In Case 3, when the system is under full PV and ESS penetration, the harmonic distortion profile indicates high value throughout the network. THD at Bus 1 is now 0.59%, while TIF is 21.08, showing an increased harmonic impact in the upstream medium-voltage

domain for the very first time. Although still at tolerable values, this trend shows that distortion due to harmonics is no longer merely confined to the lower-voltage domain and has begun to be transmitted upstream.

At Bus 39, THD is 3.22%, and TIF is 107.34, the highest total distortion in all of the cases considered here. THDG and THDS measurements are also high at 3.22%, confirming inverter-based components' high low-frequency harmonic content. All of these measurements are tabulated in Table 6.

Table 6

Harmonic Distortion Metrics for all cases

CASE	BUS	RMS VOLTAGE (%)	THD (%)	TIF	THDG (%)	THDS (%)
CASE 0	Bus 1	100.00	0.06	2.18	0.06	0.06
	Bus 39	96.18	2.87	94.63	2.87	2.87
CASE 1	Bus 1	100.00	0.11	4.00	0.11	0.11
	Bus 39	90.32	5.68	186.87	5.68	5.68
CASE 2	Bus 1	100.00	0.33	11.79	0.33	0.33
	Bus 39	96.35	2.82	93.75	2.82	2.82
CASE 3	Bus 1	100.00	0.59	21.08	0.59	0.59
	Bus 39	95.76	3.22	107.34	3.22	3.22

As Appendix I demonstrates, Bus 39 continues to have the highest most dominant harmonic content, with evident spikes at harmonic orders 7, 11, 13, 17, and 19. The 17th harmonic again reaches its peak as the largest component, although Bus 1 and Bus 38 harmonics are stronger than in the other instances in agreement with the original observation of upward harmonic propagation upon full penetration.

4.4 Short Circuit Analysis

Short circuit analysis is essential for assessing the fault current levels in power systems and ensuring that equipment can safely withstand and interrupt these high currents. According to the IEC 60909 standard, standardized methods are used to calculate short-circuit currents in three-phase AC systems under various fault scenarios. These calculations support system protection coordination, equipment sizing, and grid stability during fault conditions [42].

Short-Circuit Current Analysis – Case 0

A short-circuit simulation was performed on Bus 1 and Bus 39 in Case 0 to analyze the electrical stress under fault conditions. The outcomes, as presented in Table 7 are as follows: At Bus 1, the peak initial short-circuits current (ip) was 22.187 kA and the steady-state fault current (Ik) was 8.765 kA. The existing making (I″k) was 9.063 kA, which is moderate fault levels within the scope of normal protection settings at the medium-voltage level. Bus 39 had a significantly higher fault level.

The maximum current was 29.937 kA initially, and Ik was 14.780 kA, with a I″k of 14.793 kA, showing high short-circuit stress on this LV bus. According to these results, Bus 39 must be given special attention in circuit breaker selection, protection coordination, and fault withstand ratings, especially in the area of future load growth or distributed generation. No routine device capacity violations were present in this instance.

The same harmonic distortion and short-circuit current computation will be carried out for the other cases to study the impacts of increased PV integration and energy storage systems on network performance. The results will be compared with Case 0 to assess improvements or threats in terms of power quality, fault current values, and system reliability under different operation modes.

Short-Circuit Current Analysis – Case 1

A short-circuit simulation test was conducted on Bus 1 and Bus 39 under Case 1 to evaluate fault current performance after the connection of a 1 MW PV system and partial charging of energy storage. The results, as indicated in Table 7 indicate the following: At Bus 1, the maximum ip was 22.187 kA and the Ik was 8.765 kA. The I″k was 9.063 kA, indicating medium fault levels acceptable with typical protection settings at the medium-voltage level. Conversely, Bus 39 possessed an appreciably higher fault level.

The peak current was the first at 29.937 kA, and Ik was 14.780 kA with a I″k of 14.793 kA, the results are identical to those in Case 0 showing high short-circuit stress on this LV bus. Such observations suggest Bus 39 would require special consideration when choosing a circuit breaker, performing protection coordination, and for fault withstand rating requirements, especially because of future expansion in loads or distributed generation schemes. Violation of normal device capacity was not observed here.

Short-Circuit Current Analysis – Case 2

The simulation of 3-phase short-circuit at Bus 1 and Bus 39 was done in Case 2, a case with a 3 MW PV system and energy storage under higher penetration level. The outcomes, as illustrated in Table 7 indicate a significant increase in the level of fault current, particularly on the low-voltage side. At Bus 1, the ip was 22.236 kA, and the fault current at Ik was 8.800 kA. The I″k was 9.098 kA, indicating moderate fault levels manageable by standard protection settings at the medium-voltage level.

On the other hand, Bus 39 experienced much more serious fault levels. Maximum initial current was 159.635 kA and Ik 78.133 kA with I″k = 78.517 kA, indicating high short-circuit stress on this LV bus. This indicates that extra caution may need to be provided in the future for circuit breaker selection, coordination, and fault withstand ratings to Bus 39. This level of short-circuit stress far exceeds normal low-voltage equipment tolerances and warrants prompt attention to breaker size, device withstand levels, and dynamic protection coordination methods at Bus 39.

Short-Circuit Current Analysis – Case 3

A 3-phase short-circuit simulation was performed at Bus 1 and Bus 39 under Case 3, which represents the scenario with maximum PV and ESS penetration (6 MW PV, 100% integration). The resulting short-circuits levels, shown in Table 7 confirm a sharp rise in fault stress, especially at the low-voltage level.

In Bus 1, the ip was 22.309 kA, and Ik was 8.748 kA. I″k was 9.150 kA, which indicated medium levels of faults within the range of standard settings on the medium-voltage level.

In contrast, Bus 39 experienced a significantly higher fault level. The initial peak current was 252.154 kA, and Ik was 116.017 kA, with a I″k of 125.342 kA, reflecting substantial short-circuit stress on this low-voltage bus. These values far exceed standard equipment ratings and clearly indicate device overstress under current configurations.

Given this magnitude, immediate attention is warranted to revise protection coordination, verify circuit breaker withstand ratings, and possibly redesign LV panels and isolation systems to accommodate the substantial increase in available fault current at Bus 39.

Table 7

Short-Circuit Simulation Results for all cases

CASE	BUS ID	VOLTAGE (KV)	IP (KA)	I″K (KA)	IK (KA)
CASE 0	Bus 1	33.000	22.187	8.765	9.063
	Bus 39	0.400	29.937	14.780	14.793
CASE 1	Bus 1	33.000	22.187	8.765	9.063
	Bus 39	0.400	29.937	14.780	14.793
CAZSE 2	Bus 1	33.000	22.236 (+0.22%)	8.800 (+0.4%)	9.098 (+0.39%)
	Bus 39	0.400	159.635 (+433%)	78.133 (+428.6%)	78.517 (+430.7%)
CASE 3	Bus 1	33.000	22.309 (+0.55%)	8.748 (-0.19%)	9.150 (+0.96%)
	Bus 39	0.400	252.154 (+742%)	116.017 (+684.9%)	125.342 (+7473%)

4.5 Battery Sizing

In this section, the battery sizing for the hybrid renewable energy system is recalculated to meet the energy demands of the grid and ensure optimal storage for power generated by the PV system. To determine the appropriate size of the battery for the system, several factors need to be considered, including the energy demand, autonomy, depth of discharge, and efficiency of the battery. The battery will store excess energy generated by the PV system during periods of high solar radiation, which can then be used during periods of low or no generation.

The following assumptions shown in Table 8 were made for the battery sizing calculations:

Table 8

Battery Sizing Assumptions

Assumption	Value
Days of Autonomy	1 day
Depth of Discharge	90%
Efficiency	97.8%
Sunshine Hours	6.7 hours

These assumptions are critical in determining the battery size and ensuring accurate calculations based on realistic operating conditions. As noted in Table 8, the autonomy is set to 1 day, meaning the battery is expected to supply power for a full day without recharging. The DoD is considered as 0.9, meaning 90% of the total capacity of the battery can be utilized. Efficiency is set at 97.8%, which is a typical value for modern lithium-ion batteries.

The required battery size can be determined using the following formula:

$$Battery\ Capacity = \frac{Power\ Required \times Duration\ required}{Efficiecncy\ \times DoD} \ldots\ldots\ldots (1)$$

Where: DoD is Depth of discharge, assumed 0.9 for lithium-ion batteries.

Applying equation 1 to the calculated battery capacities for each case will result in the following:

- Case 1 (1 MW PV): The required battery capacity is 7.61 MWh.
- Case 2 (3 MW PV): The required battery capacity is 22.84 MWh.
- Case 3 (6 MW PV): The required battery capacity is 45.67 MWh.

4.6 Voltage Profiles

This part of the study will discuss the voltage profiles for the Arraba village electrical network under the four scenarios. The voltage profiles at each bus in the network are crucial for evaluating the system's performance, particularly in terms of voltage stability, which is an essential aspect of the overall network reliability. The voltage profile for all cases is shown in Figure 6, providing a comprehensive view of the voltage behavior across the network.

Figure 6

Voltage Profile for Different Cases

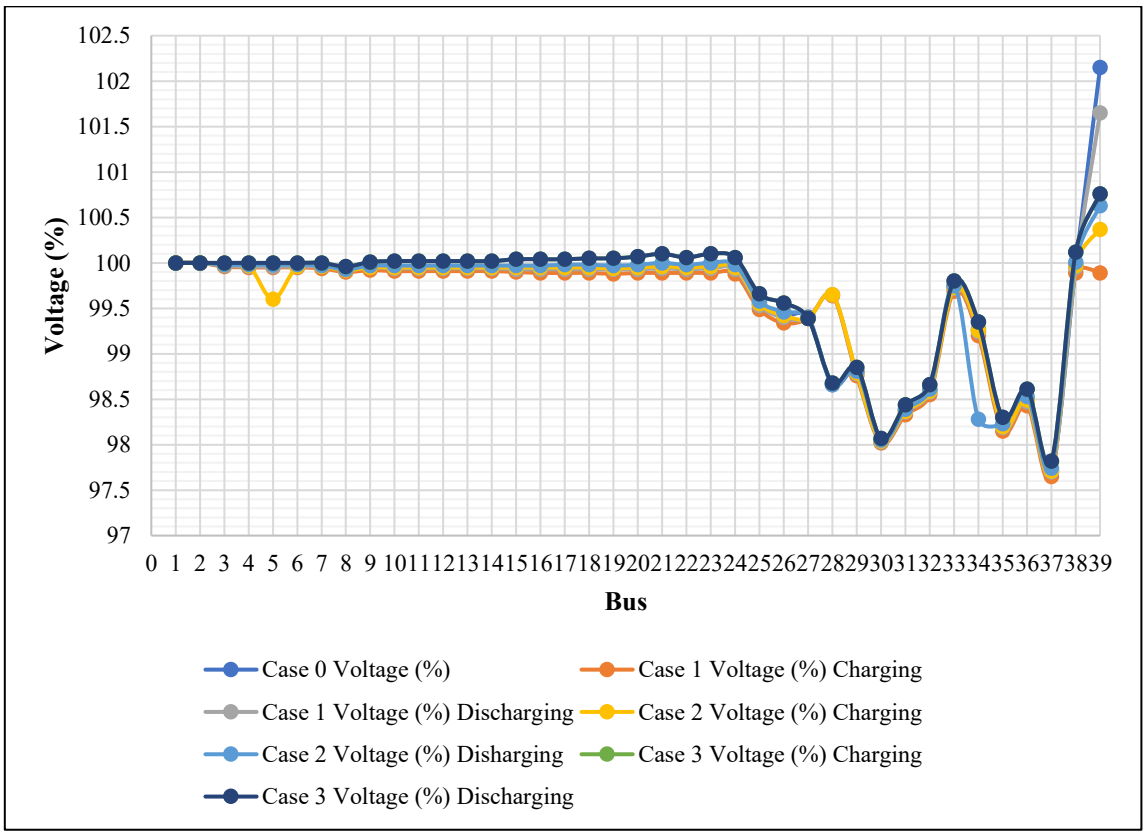

Case 0: Current Network Configuration

As shown in Appendix A, the voltage profiles across the network in Case 0 generally show stable voltage levels, with only minor fluctuations at different buses. For instance, Bus 1 maintains a voltage of 100%, while other buses like Bus 25 and Bus 26 experience slightly lower voltages of 99.549% and 99.418%, respectively. This is expected, as the system is purely reliant on the 1 MW PV generation without any energy storage, making it susceptible to fluctuations caused by varying generation and load conditions. The network experiences small but significant voltage drops at distant buses (e.g., Bus 25 and Bus 26), which could indicate potential voltage instability issues under load or higher generation conditions.

Case 1: 1 MW PV System with 17% P: and ESS

The introduction of the ESS in Case 1 helps to stabilize the voltage profile, especially during charging and discharging cycles of the battery. When charging, the voltage at the buses remains almost unchanged from Case 0, with slight improvements in voltage

stability across most of the network. For example, Bus 1 remains at 100%, and Bus 25 and Bus 26 show minor improvements in voltage (99.49% and 99.34%, respectively), for more detailed information, referring to Appendix B.

As shown in Appendix C during discharging, the voltage levels slightly dip compared to the charging scenario, but the ESS still plays a role in minimizing larger voltage fluctuations. The voltage profile at most of the buses remains above 99%, indicating that the ESS has effectively mitigated fluctuations that could otherwise lead to instability.

Case 2: 3 MW PV System with 50% PL and ESS

With the increased PV capacity in Case 2, voltage profiles presented in Appendix D show relatively high stability across the network, but there are minor variations compared to Case 1. The higher penetration level of renewable energy, paired with the ESS, helps to handle higher PV generation and manage fluctuating demand. Buses closer to the generation point, such as Bus 1 and Bus 2, maintain their voltages at or above 99.97% during both charging and discharging states.

For buses farther from the PV generation point like Bus 25 and Bus 26, the voltages are generally within acceptable limits, though there is a slight reduction during discharging 99.55% and 99.42%, respectively. As shown in Appendix E these slight voltage reductions during discharging are still manageable and indicate that the ESS is helping to smooth out the power flows.

Case 3: 6 MW PV with 100% PL and ESS

In Case 3, the 100% penetration of PV energy leads to near-ideal voltage stability across most of the network. The introduction of ESS is crucial here as it allows for balancing the high generation from the PV system and managing the excess energy during periods of low load or during peak sunlight hours. Voltage levels at key buses as Bus 1, Bus 2, and Bus 9 remain at or above 100%, even during both charging and discharging of the ESS, see Appendix F and Appendix G for more details.

However, some minor voltage fluctuations are observed at distant buses like e.g., Bus 25 and Bus 26, with voltages around 99.66% and 99.56% during charging and discharging. These fluctuations are indicative of the challenges faced when dealing with high penetration of renewable energy but remain within acceptable voltage limits. The

performance at these distant buses suggests that the system can handle the full 6 MW of PV generation effectively, as the voltage drops are small and do not pose significant risks to the network's stability.

The voltage profiles across all cases demonstrate that the integration of an ESS improves the overall voltage stability, particularly during charging and discharging cycles. In all cases, the ESS plays a significant role in mitigating voltage drops and ensuring consistent voltage levels across the network, especially during times of high generation or varying demand. As the PV penetration increases, the network becomes more reliant on the ESS to balance energy flows and maintain voltage stability, with minor voltage drops observed in the more distant buses. Overall, the integration of ESS in Cases 1, 2, and 3 provides clear benefits in maintaining voltage stability and supporting the increasing renewable energy penetration.

4.7 Peak-Shaving Effect

To complement the static analysis, a dynamic time-domain simulation was conducted to evaluate the operational performance of the PV and Energy ESS integration under real-time load variations. This section emphasizes the peak-shaving capabilities of the ESS across all four cases by analyzing the 24-hour power demand profiles and comparing the original grid demand with the net demand observed after PV and ESS deployment.of the electrical system, including both transmission and storage components.

Case 0: Current Network Configuration

In the baseline configuration, where the system includes a 1 MW PV installation without any energy storage, the grid is responsible for supplying the entire load profile. Without the ability to store excess PV energy or shift loads, the network experiences full exposure to peak demand events, particularly during the evening hours between 6:00 PM and 9:00 PM. This results in a pronounced peak in power consumption, placing considerable stress on transformers and distribution infrastructure. Additionally, any midday PV surplus cannot be effectively utilized or stored, leading to wasted generation and a poor load factor. The load profile remains unchanged throughout the day, which highlights the limitations of a PV-only system in terms of peak management.

Case 1: 1 MW PV System with 17% P: and ESS

With the integration of an ESS into the existing 1 MW PV system at a 17% penetration level, noticeable improvements begin to emerge. The simulation results, as illustrated in Figure 7, indicate that the ESS discharges strategically during peak demand hours, particularly in the early evening, resulting in a reduction in peak load from approximately 2,700 kW to around 1,800 kW. This represents a peak shaving of roughly 33%. During early morning hours, the ESS is charged from either the PV surplus or the grid during off-peak times. Although the capacity of the ESS is limited, its operation clearly smooths the load profile and slightly enhances voltage stability. This case demonstrates the initial benefits of ESS integration, where even a modest storage solution can reduce strain on the network and provide economic and technical advantages.

Figure 7

Dynamic Load Profile for Case 1 at 1 MW PV with 17% Penetration and ESS

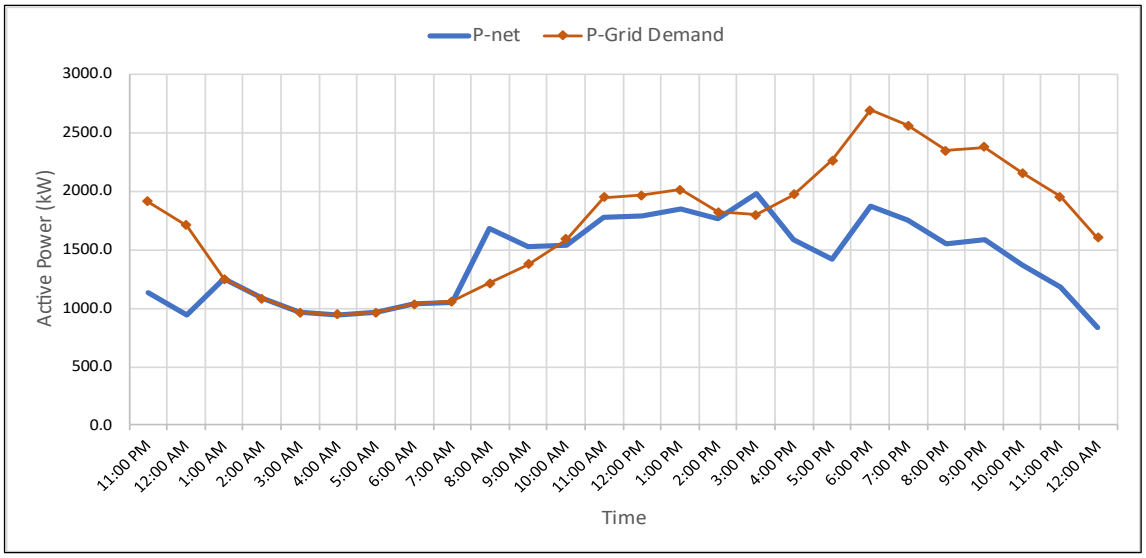

Case 2: 3 MW PV System with 50% PL and ESS

As the PV capacity increases to 3 MW and penetration reaches 50%, the impact of the ESS on the load profile becomes significantly more pronounced. The simulation data, shown in Figure 8, reveal multiple instances of net demand dips throughout the day, particularly between late morning and mid-afternoon, as the ESS is charged during surplus PV generation. These dips are followed by a substantial reduction in peak demand during the evening hours. The peak load is reduced from approximately 2,700 kW to 1,350 kW, yielding a peak-shaving benefit of nearly 51%. Moreover, brief export events

begin to appear as the PV system occasionally generates more energy than both the load and ESS can accommodate. This case illustrates the dual benefit of flattening the load curve and enabling grid exports, signifying an increasingly self-sufficient and efficient energy system.

Figure 8

Dynamic Load Profile for Case 2 – 3 MW PV with 50% Penetration and ESS

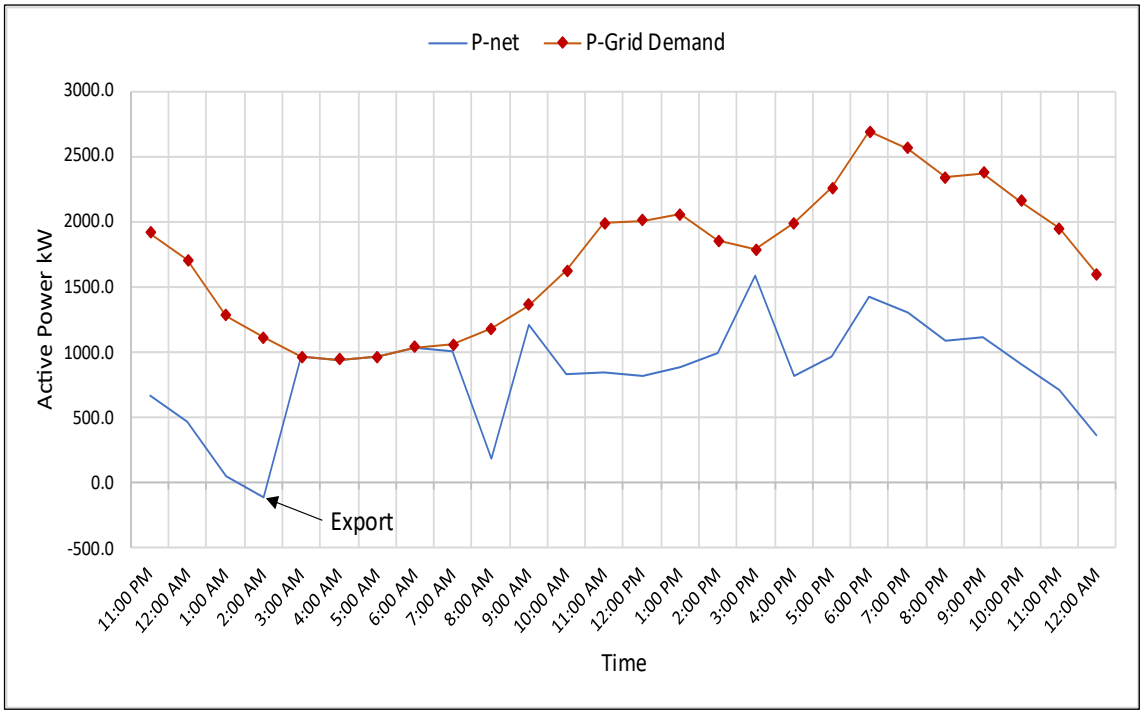

Case 3: 6 MW PV with 100% PL and ESS

In the final and most advanced scenario, the system operates with 6 MW of PV capacity, reaching 100% penetration. The combination of high solar generation and robust energy storage produces the most favorable results. The power profiles, presented in Figure 9, demonstrate that throughout the early morning hours, the net power is consistently negative or near zero, indicating frequent export or battery charging behavior. Between 9:00 AM and 12:00 PM, and again from 3:00 PM to 5:00 PM, large export events are observed due to PV overproduction exceeding local demand and ESS charging capability. Most importantly, the evening peak, typically the most critical period for grid stress, is significantly mitigated. Net demand is reduced from about 2,700 kW to less than 1,000 kW, translating into a 63% reduction. The resulting load profile is smooth, stable, and ideal for both utility-scale operation and customer-side reliability. This case confirms the

technical viability of achieving near-complete peak shaving through high-penetration PV combined with energy storage.

Figure 9

Dynamic Load Profile for Case 3 – 6 MW PV with 100% Penetration and ESS

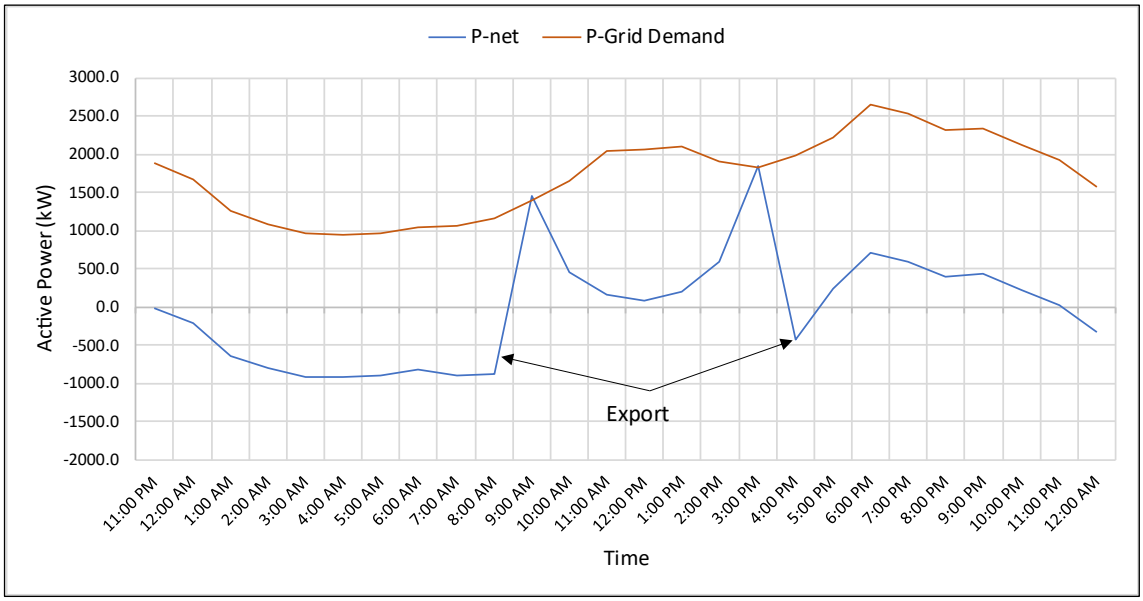

4.8 Loss Analysis

This section evaluates the power losses across the different cases for the Arraba village electrical network. The losses are analyzed during both the charging and discharging phases of ESS in Cases 1, 2, and 3, in addition to the apparent losses in Case 0, which serves as the base case. Power losses are crucial indicators for assessing the efficiency of the electrical system, including both transmission and storage components.

Case 0: Current Network Configuration

In Case 0, the apparent power losses are calculated to be 0.064 MW. These losses primarily result from the transmission and distribution of energy within the network without any energy storage system. The absence of ESS means that there is no additional mechanism to manage the power flow, which could otherwise help to reduce losses. This value represents a baseline for comparison against the other cases that include energy storage systems.

Case 1: 1 MW PV System with 17% P: and ESS

In Case 1, the presence of the ESS during charging reduces the apparent AC losses significantly compared to Case 0. The total AC losses are only 0.016 MW, which is a substantial improvement. However, there are still DC losses of 0.03 MW, which can be attributed to the inefficiencies in the charging process of the ESS. These losses occur as the energy is converted from AC to DC and stored in the battery.

During discharging, the apparent AC losses increase slightly to 0.019 MW compared to the charging phase. However, the DC losses are negligible, indicating that the discharging process is relatively efficient when compared to charging, especially as the ESS facilitates smoother energy release.

Case 2: 3 MW PV System with 50% PL and ESS

In Case 2, the increase in PV system penetration leads to higher apparent AC losses of 0.026 MW during charging. Additionally, the DC losses are recorded at 0.021 MW. The higher power generation from the PV system means that more energy is being converted and stored, leading to slightly higher losses during both AC to DC conversion and storage.

During discharging, the apparent AC losses decreased to 0.017 MW, which is slightly lower than during charging. Additionally, the DC losses are minimal at 0.001 MW, reflecting a more efficient discharge process.

Case 3: 6 MW PV with 100% PL and ESS

In Case 3, the highest penetration of PV energy results in the highest observed losses during charging. The apparent AC losses are 0.059 MW, and the DC losses are significantly higher at 0.077 MW. The increase in DC losses reflects the challenges associated with managing large amounts of energy during the charging phase. These losses, particularly the higher DC losses in Case 3, underscore the inefficiencies in large-scale energy storage systems when handling higher PV generation, but they remain manageable during discharging.

Similar to Case 2, the apparent AC losses during discharging are 0.021 MW, which is a reduction from the charging phase. The DC losses during discharging are minimal at 0.001 MW, demonstrating the relatively high efficiency of the ESS during energy release.

The power loss analysis reveals important insights into the efficiency of the system under different scenarios. In general, the introduction of the ESS in Cases 1, 2, and 3 leads to a reduction in apparent AC losses compared to Case 0. However, DC losses vary depending on the charging and discharging processes, with Case 3 experiencing the highest losses due to the larger amount of energy being stored and managed.

Figure 23 compares the total losses (AC and DC) during both charging and discharging across all cases. As seen in the Figure 10, the losses increase with the penetration level of the PV system, particularly during the charging phase. However, the presence of the ESS generally helps reduce the losses during discharging, with Case 3 showing relatively low discharging losses despite the higher charging losses.

Figure 10

Comparison of AC and DC Power Losses Across Different Cases

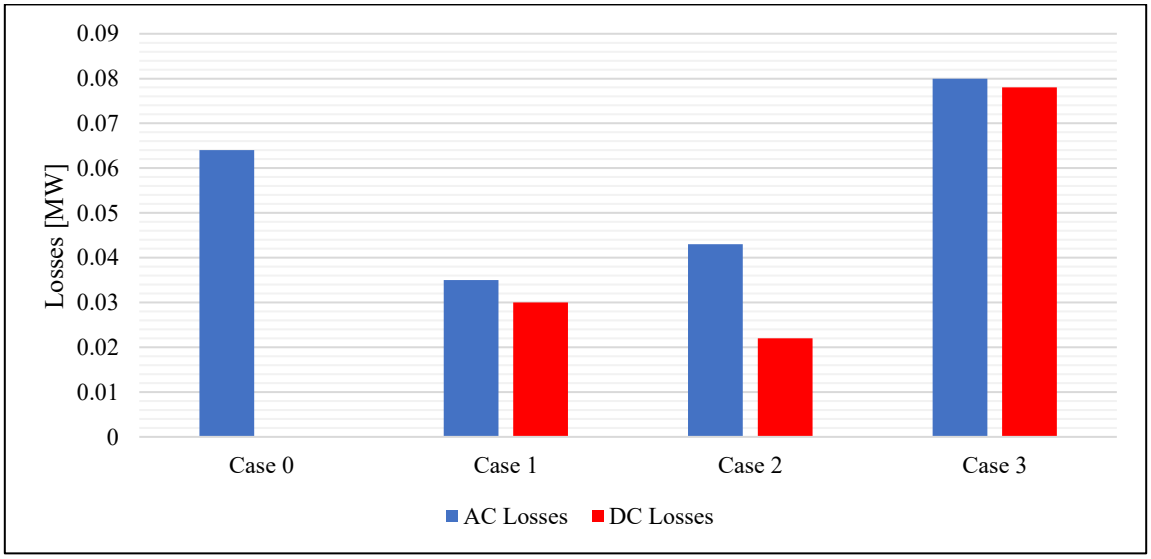

4.9 Economic Analysis

The economic analysis of integrating an ESS with a grid-connected PV system was conducted using the System Advisor Model (SAM) and the Battery Energy Capital Cost table provided. The analysis focuses on evaluating the capital cost, operating costs, payback period, and levelized cost of energy (LCOE) for three cases involving different sizes of PV systems and ESS configurations.

The capital cost of the Li-Ion battery for each case was calculated based on the energy cost per kWh. The cost assumed to be $184/kWh in 2025 according to the ATB [41]. Using the battery capacity for each case, the total battery capital cost was determined.

4.9.1 Inputs for SAM

The economic evaluation conducted using the SAM required several key input parameters related to capital costs for the PV system and ESS. These inputs, which reflect both direct and indirect costs, were used based on ATB to estimate the total investment required for each configuration [41]. Table 9 summarizes the specific input costs used in the model.

Table 9

Capital Cost Inputs for SAM Model

DIRECT CAPITAL COSTS	
Module	0.2$/Wdc
Inverter	0.06$/W
Lithium-Ion Battery (Lib Pack)	184.00$/kWh
Electrical BOS (Includes conduit, wiring, dc cable, etc)	$0.07–$0.14/W
INSTALLATION LABOR	0.01$Wdc
INDIRECT CAPITAL COSTS	
Engineering And Developer Overhead + Grid Interconnection	0.02$/Wdc
Land Costs (Land Prep. & Transmission)	0.01$/Wdc
Sales Tax	16%
ANALYSIS PARAMETERS	
Project Life	25 years
Inflation Rate	2.5%
Real Discount Rate	6.4%
Sales Tax (% of indirect cost basis)	16%

4.9.2 Financial Metrics and Calculation Methods

The financial metrics used to evaluate the systems were derived using SAM's computational framework, which is based on standard equations for renewable energy financial evaluation, as defined by Short et al. (1995) [43].

The Net Present Value (NPV) evaluates the long-term profitability of a project by discounting future savings and costs to present-day values. The NPV can be calculated by Equation 2:

$$NPV = \sum_{n=0}^{N} \frac{F_n}{(1+d)^n} \dots\dots\dots (2)$$

Where:

F_n: Net cash flow in year n

d: Discount rate

n: Analysis period

A positive NPV indicates that investment is economically beneficial over its lifetime. This method is consistent with SAM's internal financial engine and follows the formulation presented in the NREL methodology [43].

The simple payback period is the time it takes for cumulative cash inflows (savings) to recover the initial investment, which can be obtained by applying Equation 3:

$$\sum_{n} \Delta I_n \leq \sum_{n} \Delta S_n \dots\dots\dots (3)$$

Where:

ΔI_n: Nondiscounted incremental investment costs (capital + financing)

ΔS_n: Nondiscounted annual cash flow savings

Payback period is the earliest year n when cumulative savings equals or exceeds the total investment

The Levelized Cost of Energy (LCOE) is a critical financial metric used to compare the cost-effectiveness of different energy systems. It represents the present value of the total life-cycle cost (TLCC) of the system divided by the present value of total energy output over the system's lifetime. LCOE is calculated as:

$$LCOE = \frac{TLCC}{\sum_{n=1}^{N} (\frac{Q_n}{(1+d)^n})} \dots\dots\dots (4)$$

Where:

Q_n: Energy output (or saved) in year n

TLCC: The total life-cycle cost

4.9.3 Results and Observations

Reports presented in Appendix H were exported from the SAM, the economic feasibility of each case was analyzed through the calculation of several key metrics. Total Installed Cost was determined by summing the capital expenditure, which includes the cost of the ESS, PV system, inverters, and other necessary infrastructure. Case 1 exhibited the lowest initial investment, while Case 3, which involved a larger PV system and ESS, required a significantly higher investment.

The annual savings resulting from the implementation of ESS were calculated based on the reduced electricity costs through peak shaving and energy storage. The savings varied across different cases, with Case 3 offering the highest annual savings due to its larger PV generation capacity and ESS storage. However, this higher savings potential came at the cost of a higher initial investment.

To assess the profitability of each configuration over its expected lifetime, the present net value was calculated for each case. While Case 3 provided the highest annual savings, its larger upfront cost led to a longer payback period, making Case 1 the most economically feasible option in terms of return on investment, due to its shorter payback period.

The LCOE was another critical metric used to evaluate the cost-effectiveness of energy generation in each case. Case 1 exhibited the lowest LCOE, indicating that the investment in ESS for this configuration provided the most economical energy production. The LCOE for Case 2 and Case 3 were slightly higher, though the larger systems offered more capacity and higher potential savings.

A sensitivity analysis was conducted to understand how fluctuations in key parameters such as ESS cost, electricity prices, and demand profiles affect the economic feasibility of each case. The analysis showed that Case 1 remains the most cost-effective option across various scenarios, including changes in battery costs and electricity prices. In

contrast, the larger systems (Case 2 and Case 3) were found to be less economically viable due to their high upfront costs, despite offering substantial savings over time.

The comparison of grid performance metrics across the different cases Table 10 highlights the impact of ESS on grid stability, energy efficiency, and power quality, with Case 1 emerging as optimal configuration.

Table 10

Comparison of Grid Performance Metrics Across Different Cases

Metric	Case 0	Case 1	Case 2	Case 3
PV System Capacity	1 MW	1 MW	3 MW	6 MW
ESS	None	7.61 MWh	22.84 MWh	45.67 MWh
Voltage Regulation	Limited	Improved	Improved	Improved
Harmonic Distortion	Moderate	High	Moderate	High
Short-Circuit Levels	Low	Low	Very High	Extremely High
Peak Shaving	N/A	33%	51%	63%
Losses	High	Low	Moderate	High
Nominal LCOE	N/A	17.4 cents/kWh	18.6 cents/kWh	18.8 cents/kWh
Payback Period	N/A	8.2 years	9.8 years	9.9 years
Total Installed Cost	N/A	$1,609,835	$5,953,514	$12,246,799

The comparison of the four cases provides valuable insights into the technical performance vs. economic feasibility trade-offs in grid-connected photovoltaic systems with integrated energy storage. The size of the photovoltaic system increases stepwise from 1 MW in Case 0 and Case 1, to 3 MW in Case 2, and to 6 MW in Case 3. While this scaling up enhances overall energy production and grid supply, it also results in significantly higher system costs in Cases 2 and 3. Compared to Case 1, which is a good balance between system size and performance, Case 1 is the most cost-effective configuration.

In terms of energy storage, Case 1 possesses a 7.61 MWh lithium-ion battery energy storage system that provides efficient charging during overgeneration and discharging during peak demand. The configuration enables dynamic load balancing and voltage fluctuation suppression, with improved power quality and stability performance. While Cases 2 and 3 employ higher ESS capacities to match higher PV output, the increased

capital cost rendered by the same lowers their economic viability. The total net present value (NPV) of Case 1 is $1,609,835, far lower than Case 2 at $5,953,514 and Case 3 at $12,246,799. Furthermore, the LCOE in Case 1 is the lowest at 17.4 cents/kWh, and then 18.6 cents/kWh and 18.8 cents/kWh in Cases 2 and 3, respectively.

Voltage regulation also improves substantially in all the cases. While all cases featuring ESS show voltage stabilization, Case 1 does so economically at minimal cost, whereas incremental voltage increases in Cases 2 and 3 are not justified by their higher investment. Energy loss is also minimized in Case 1, due to balanced energy use by efficient operation of the ESS, and while losses fall further in higher-capacity cases, greater system cost outweighs overall economic efficacy.

From a power quality perspective, harmonic distortion is well controlled in Case 0 and moderately increased in Case 2. It rises, however, in Case 1 and Case 3, particularly in low-voltage buses. Case 1 has a high THD level predominantly at the point of injection of energy, with the need for fundamental filtering actions. In Case 3, THD levels are even worse, perhaps necessitating advanced filtering in order to meet standards.

Short-circuit analysis shows that fault levels are constant and within acceptable limits at Bus 1 in all cases. Fault current increases substantially on the Bus 39 in Cases 2 and 3, Case 3 having very high fault current levels (above 250 kA peak), far beyond those acceptable to traditional equipment. Case 1, on the other hand, has low fault current levels on both medium and low-voltage buses, so coordination is possible and affordable.

Overall, Case 1 is the most economically and technically viable option. It has good voltage regulation, peak load management, and energy storage at the expense of low investment burden and competitive LCOE. It is, hence, the first choice for viable implementation in such village-scale grids that aim to raise the share of renewables without having to pay too expensive a price.

Chapter Five
Conclusions and Recommendations

5.1 Conclusions

Based on the simulation and analysis of various configurations, the following are some of the results:

- The addition of ESS also greatly enhanced voltage stability across the system. Even a relatively small energy storage system, as in Case 1, reduced voltage fluctuations by a great extent. Increased ESS deployment in Cases 2 and 3 further improved voltage profiles; however, incremental improvements did not grow proportionally with their increased costs.
- Implementation of ESS assisted in achieving a sure reduction in power losses, particularly in reactive power losses. Out of all the cases, Case 1 demonstrated the minimum overall losses due to ideal energy balancing demand times and discharging at peak demand hours. Cases 2 and 3 also depicted improvements, but the additional cost of their larger configurations did not yield corresponding gains in loss reduction.
- Of all the major benefits of ESS integration observed in this study, peak shaving was likely the most important. In Case 1, the ESS discharged effectively during peak-demand periods, relieving some of the burden from the central grid and leveling the daily load curve. Not only does this enhance the performance of the grid and reduce strain on the infrastructure but also averts possible outages and delays the need for costly grid upgrades.
- Although Cases 2 and 3 had higher technical performance with higher PV and ESS capacity, their high capital costs reduced their overall economic viability. Case 1, however, achieved a very good balance, achieving huge amounts of system effectiveness and reliability at significantly lower costs.
- Case 1 was the most efficient and feasible integration arrangement for the village supply. It resulted in substantial voltage control, peak reduction, and energy saving improvements at moderate costs, hence an ideal solution for small- and medium-scale schemes where financial limitations are a main issue.

5.2 Recommendations

Following the results of the current research, a few proposals are made for the application of ESS in grid-connected PV systems and some potential research directions:

- Installation of a moderately sized ESS is strongly suggested in the situation of tight-budgeted power grids or power grids with high-energy load fluctuations. Technical-economic ratio of voltage regulation, peak curtailment, and loss minimization is optimally attained by this setup, best suited to rural, small-grid, or developing-grid operations.
- To enhance the performance of ESS in power quality control and energy wastage minimization, future research should aim to integrate advanced grid control strategies. Predictive control methods, machine learning, and real-time monitoring can be implemented to enhance charge and discharge cycles, enhance peak shaving effectiveness, and optimize overall grid response and efficiency.
- As adoption continues to grow from renewable generation sources such as wind and solar energy, ESS will be ever more needed in order to compensate for their variability. On systems with high levels of renewable penetration, ESS can potentially help significantly in mitigating the variance of generation, frequency support, and grid stability. Hybrid ESS systems and integration of those with variable generation sources should be explored further.
- While Case 1 was most economical, bigger-scale ESS configurations depicted in Cases 2 and 3 could be more suitable in the case of bigger peak grids, greater renewable generation capacity, or future scaling requirements. Any scaling has to be accompanied by rigorous cost-benefit thinking for long-term financial sustainability.

Overall, integration of ESS offers enormous benefits in terms of voltage regulation, peak load management, energy loss savings, and utilization of renewable resources. Case 1 is discovered in this study to be the most efficient and viable configuration for instant deployment in village-scale grids. Further optimization of the size, location, and operating practices of ESS will be necessary to propel the sustainable development of next-generation power systems.

5.3 Future Work

Though in this work it was proven how economically and technologically favorable integrating ESS within village-level grids could be, some principal avenues demand investigation as well.

Future studies must investigate the integration of several storage technologies to improve flexibility, efficiency, and response time under different load conditions.

Utilization of predictive algorithms and machine learning for maximizing the charge/discharge cycles on the basis of real-time data and demand forecasting could significantly improve the performance of ESS and the grid flexibility.

Testing the aging and life expectancy of ESS under real operating conditions is essential. This includes assessing the application of second-life batteries from electric vehicles as a cost-reduction measure.

Incorporating ESS into microgrids, especially for remote or unreliable-grid locations, must be explored to advance energy resilience, maximize the utilization of renewables, and enable islanding operation.

References

[1] Moien A. Omar, M. M. (2018). Grid connected PV- home systems in Palestine: A review on technical performance, effects and economic feasibility,. *Renewable and Sustainable Energy Reviews*, 2490-2497.

[2] Khatib, T., Bazyan, A., Assi, H., & Malhis, S. (2021). Palestine Energy Policy for Photovoltaic Generation: Current Status and What Should Be Next? *Sustainability*, 13(5).

[3] Awwad, A. I. (2015). *Techno-Economic Evaluation and Improvement Possibilities of Local Grid Connected Housr-PV Power System.* Palestine: M.Sc Thesis presented to An- Njah Nationak University.

[4] Ibrik, I. (2020). *Micro-Grid Solar Photovoltaic Systems for Rural Development and Sustainable Agriculture in Palestine.* Agronomy 10.

[5] Suyanto, H. a. (2020). Transient Stability Analysis of a Hybrid Grid-Connected Battery-PV in Baubau Power System. *2020 2nd International Conference on Industrial Electrical and Electronics (ICIEE)*, 27-30.

[6] Tran, Q.-T. a. (2018). Integration of PV Systems into Grid: From Impact Analysis to Solutions. *IEEE International Conference on Environment and Electrical Engineering*, 1-6.

[7] Forson Peprah, S. G.-B.-D. (2022). Impact assessment of grid tied rooftop PV systems on LV distribution network. *Scientific African*.

[8] Saif Ur Rehman, S. R. (2018). Feasibility Study of a Grid-Tied Photovoltaic System for Household in Pakistan: Considering an Unreliable Electric Grid. *Wiley Online Library*.

[9] Nallapaneni Manoj Kumar, K. S. (2017). Techno-economic analysis of 1 MWp grid connected solar PV plant in Malaysia. *International*.

[10] Carbone, R. (2009). Grid-connected photovoltaic systems with energy storage. *International Conference on Clean Electrical Power*, (pp. 760-767). Capri, Italy.

[11] Y. Ru, J. K. (2013). Storage Size Determination for Grid-Connected Photovoltaic Systems,. *IEEE Transactions on Sustainable Energy*, 68-81.

[12] Balint D. Olaszi, J. L. (2017). Comparison of different discharge strategies of grid-connected residential PV systems with energy storage in perspective of optimal battery energy storage system sizing. *Renewable and Sustainable Energy Reviews*, 710-718.

[13] V. Rallabandi, O. M. (2019). Incorporating Battery Energy Storage Systems Into Multi-MW Grid Connected PV Systems. *IEEE Transactions on Industry Applications*, 638-647.

[14] A.A. Solomon, D. F. (2012). Appropriate storage for high-penetration grid-connected photovoltaic plants. *Energy Policy*, 335-344.

[15] X. Vallve, A. G. (2007). Micro storage and demand side management in distributed PV grid-connected installations. *9th International Conference on Electrical Power Quality and Utilisation*, (pp. 1-6). Barcelona, Spain.

[16] Maria C. Argyrou, C. C. (2021). Modeling a residential grid-connected PV system with battery–supercapacitor storage: Control design and stability analysis. *Energy Reports*, 4988-5002.

[17] Masoume Shabani, F. W. (2022). Techno-economic assessment of battery storage integrated into a grid-connected and solar-powered residential building under different battery ageing models. *Applied Energy*, Volume 318.

[18] Montaser Mahmoud, M. R. (2020). A review of mechanical energy storage systems combined with wind and solar applications. *Energy Conversion and Management*.

[19] Subhashree, C. (2021). Flywheel energy storage systems: A critical review on technologies, applications, and future prospects. *Wiley*.

[20] A.G. Olabi, T. W. (2020). Compressed air energy storage systems: Components and operating parameters – A review. *Journal of Energy Storage*.

[21] Ahmed Zayed AL Shaqsi, K. S.-H. (2020). Review of energy storage services, applications, limitations, and benefits. *Energy Reports*, 288-306.

[22] Tianmei Chen, Y. J. (2020). Applications of Lithium-Ion Batteries in Grid-Scale Energy Storage Systems. *Transactions of Tianjin University*.

[23] Xing Luo, J. W. (2015). Overview of current development in electrical energy storage technologies and the application potential in power system operation. *Applied Energy*, 511-536.

[24] IEA. (April 15, 2023). Lithium-ion battery demand for electric vehicles (EVs) worldwide from 2016 to 2022, by region (in gigawatt-hours) [Graph]. In Statista. Retrieved December 05, 2023, from https://www.statista.com/statistics/1415641/global-evbattery-demand-by-region/

[25] Wen, G., Hu, G., Hu, J., Shi, X., & Chen, G. (2015). Frequency regulation of sourcegrid-load systems: A compound control strategy. IEEE transactions on industrial informatics, 12(1), 69-78.

[26] Crawford, A. J., Huang, Q., Kintner-Meyer, M. C., Zhang, J. G., Reed, D. M., Sprenkle, V. L., ... & Choi, D. (2018). Lifecycle comparison of selected Li-ion battery chemistries under grid and electric vehicle duty cycle combinations. Journal of Power Sources, 380, 185-193.

[27] Chen, T., Jin, Y., Lv, H., Yang, A., Liu, M., Chen, B., ... & Chen, Q. (2020). Applications of lithium-ion batteries in grid-scale energy storage systems. Transactions of Tianjin University, 26(3), 208-217.

[28] Purvins, A., & Sumner, M. (2013). Optimal management of stationary lithium-ion battery system in electricity distribution grids. Journal of Power Sources, 242, 742-755.

[29] Andrea, D. (2010). Battery management systems for large lithium-ion battery packs. Artech house.

[30] Liu, X., Yuan, Y., Liu, J., Liu, B., Chen, X., Ding, J., ... & Hu, W. (2019). Utilizing solar energy to improve the oxygen evolution reaction kinetics in zinc–air battery. Nature communications, 10(1), 4767.

[31] Uddin, K., Gough, R., Radcliffe, J., Marco, J., & Jennings, P. (2017). Techno-economic analysis of the viability of residential photovoltaic systems using lithium-ion batteries for energy storage in the United Kingdom. Applied Energy, 206, 12-21.

[32] Hesse, H. C., Schimpe, M., Kucevic, D., & Jossen, A. (2017). Lithium-ion battery storage for the grid—A review of stationary battery storage system design tailored for applications in modern power grids. Energies, 10(12), 2107.

[33] Ananda-Rao, K., Ali, R., & Taniselass, S. (2017). Battery energy storage system assessment in a designed battery controller for load leveling and peak shaving applications. Journal of Renewable and Sustainable Energy, 9(4).

[34] Child, M., Kemfert, C., Bogdanov, D., & Breyer, C. (2019). Flexible electricity generation, grid exchange and storage for the transition to a 100% renewable energy system in Europe. Renewable energy, 139, 80-101.

[35] Ram, M., Child, M., Aghahosseini, A., Bogdanov, D., Lohrmann, A., & Breyer, C. (2018). A comparative analysis of electricity generation costs from renewable, fossil fuel and nuclear sources in G20 countries for the period 2015-2030. Journal of cleaner production, 199, 687-704.

[36] Crabtree, G., Kócs, E., & Trahey, L. (2015). The energy-storage frontier: Lithium-ion batteries and beyond. Mrs Bulletin, 40(12), 1067-1078.

[37] A.G. Olabi, T. W. (2020). Compressed air energy storage systems: Components and operating parameters – A review. *Journal of Energy Storage*.

[38] Ashleigh Townsend, R. G. (2022). A Comparative Review of Lead-Acid, Lithium-Ion and Ultra-Capacitor Technologies and Their Degradation Mechanisms. *Energies*, 15(13).

[39] Qudra Renewable Energy Solutions. (2024). Project portfolio: Arraba 1 MW Ground Mount. Qudra Renewable Energy Solutions. https://qudra.ps/projects/

[40] United Nations Development Programme (UNDP). (2021). Towards a resilient energy sector in the State of Palestine. UNDP. https://www.undp.org/

[41] Shelar, S., Bankar, D. S., & Bakre, S. (2024). Review of revisions of IEEE 519 Standard on Power System Harmonics (1981 to 2022). 415–420. https://doi.org/10.1109/ichqp61174.2024.10768696

[42] Kasikci, I. (2018). *Short circuits in power systems: A practical guide to IEC 60909-0*. John Wiley & Sons.

[43] Short, W., Packey, D. J., & Holt, T. (1995). *A manual for the economic evaluation of energy efficiency and renewable energy technologies* (No. NREL/TP-462-5173). National Renewable Energy Lab.(NREL), Golden, CO (United States).

Appendices

Appendix A

Case 0: Single Line Diagram and Load Flow Report

One-Line Diagram - TDLF With PV (Time Domain Load Flow)

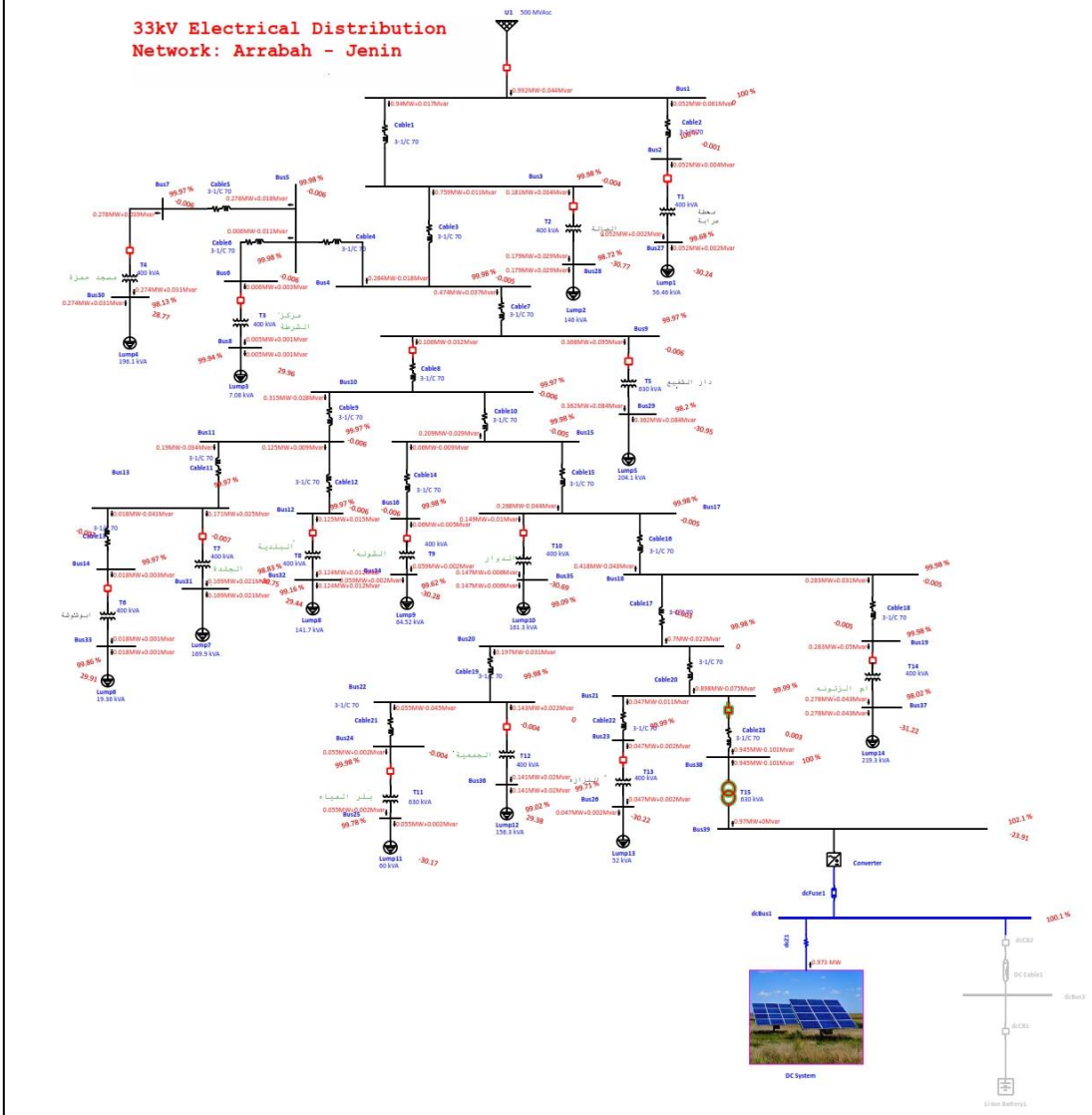

page 1 17:03:40 Oct 17, 2024 Project File: Arraba

LOAD FLOW REPORT

Bus		Voltage		Generation		Load		Load Flow					XFMR
ID	kV	% Mag.	Ang.	MW	Mvar	MW	Mvar	ID	MW	Mvar	Amp	%PF	%Tap
* Bus1	33.000	100.000	0.0	1.665	-0.152	0.000	0.000	Bus3	1.570	-0.096	27.5	-99.8	
								Bus2	0.095	-0.057	1.9	-86.0	
Bus2	33.000	99.997	0.0	0.000	0.000	0.000	0.000	Bus1	-0.095	-0.008	1.7	99.6	
								Bus27	0.095	0.008	1.7	99.6	
Bus3	33.000	99.975	0.0	0.000	0.000	0.000	0.000	Bus1	-1.570	0.068	27.5	-99.9	
								Bus4	1.353	-0.083	23.7	-99.8	
								Bus28	0.217	0.015	3.8	99.8	
Bus4	33.000	99.970	0.0	0.000	0.000	0.000	0.000	Bus3	-1.353	0.075	23.7	-99.8	
								Bus5	0.325	-0.038	5.7	-99.3	
								Bus9	1.027	-0.038	18.0	-99.9	
Bus5	33.000	99.965	0.0	0.000	0.000	0.000	0.000	Bus4	-0.325	0.013	5.7	-99.9	
								Bus7	0.318	0.000	5.6	100.0	
								Bus6	0.007	-0.013	0.3	-48.2	
Bus6	33.000	99.965	0.0	0.000	0.000	0.000	0.000	Bus5	-0.007	0.000	0.1	99.9	
								Bus8	0.007	0.000	0.1	99.9	
Bus7	33.000	99.961	0.0	0.000	0.000	0.000	0.000	Bus5	-0.318	-0.022	5.6	99.8	
								Bus30	0.318	0.022	5.6	99.8	
Bus8	0.400	99.936	-0.1	0.000	0.000	0.007	0.000	Bus6	-0.007	0.000	10.4	99.9	
Bus9	33.000	99.954	0.0	0.000	0.000	0.000	0.000	Bus4	-1.027	0.011	18.0	100.0	
								Bus10	0.706	-0.018	12.4	-100.0	
								Bus29	0.321	0.007	5.6	100.0	
Bus10	33.000	99.950	0.0	0.000	0.000	0.000	0.000	Bus9	-0.706	0.008	12.4	100.0	
								Bus11	0.510	-0.031	8.9	-99.8	
								Bus15	0.196	0.024	3.5	99.3	
Bus11	33.000	99.949	0.0	0.000	0.000	0.000	0.000	Bus10	-0.510	0.029	8.9	-99.8	
								Bus13	0.290	-0.040	5.1	-99.0	
								Bus12	0.220	0.012	3.9	99.9	
Bus12	33.000	99.949	0.0	0.000	0.000	0.000	0.000	Bus11	-0.220	-0.018	3.9	99.7	
								Bus32	0.220	0.018	3.9	99.7	
Bus13	33.000	99.946	0.0	0.000	0.000	0.000	0.000	Bus11	-0.290	0.022	5.1	-99.7	
								Bus14	0.033	-0.041	0.9	-62.4	

Bus		Voltage		Generation		Load		Load Flow					XFMR
ID	kV	% Mag.	Ang.	MW	Mvar	MW	Mvar	ID	MW	Mvar	Amp	%PF	%Tap
Bus29	0.400	98.799	-1.0	0.000	0.000	0.318	0.002	Bus9	-0.318	-0.002	464.3	100.0	
Bus30	0.400	98.049	-1.5	0.000	0.000	0.312	0.013	Bus7	-0.312	-0.013	460.3	99.9	
Bus31	0.400	98.380	-1.2	0.000	0.000	0.254	0.014	Bus13	-0.254	-0.014	372.6	99.9	
Bus32	0.400	98.598	-1.0	0.000	0.000	0.217	0.014	Bus12	-0.217	-0.014	318.3	99.8	
Bus33	0.400	99.743	-0.2	0.000	0.000	0.032	0.003	Bus14	-0.032	-0.003	47.1	99.7	
Bus34	0.400	99.266	-0.5	0.000	0.000	0.108	0.009	Bus16	-0.108	-0.009	157.8	99.7	
Bus35	0.400	98.213	-1.3	0.000	0.000	0.270	0.022	Bus17	-0.270	-0.022	398.7	99.7	
Bus36	0.400	98.492	-1.1	0.000	0.000	0.228	0.018	Bus22	-0.228	-0.018	335.4	99.7	
Bus37	0.400	97.713	-1.8	0.000	0.000	0.371	0.009	Bus19	-0.371	-0.009	547.9	100.0	
Bus38	33.000	99.970	0.0	0.000	0.000	0.000	0.000	Bus21	0.985	-0.110	17.3	-99.4	
								Bus39	-0.985	0.110	17.3	-99.4	
Bus39	0.400	102.149	6.3	1.012	0.000	0.000	0.000	Bus38	1.012	0.000	1430.5	100.0	

* Indicates a voltage regulated bus (voltage controlled or swing type machine connected to it)

# Indicates a bus with a load mismatch of more than 0.1 MVA

SUMMARY OF TOTAL GENERATION, LOADING & DEMAND

	MW	Mvar	MVA	% PF
Source (Swing Buses):	1.665	-0.152	1.672	99.58 Leading
Source (Non-Swing Buses):	1.012	0.000	1.012	100.00 Lagging
Total Demand:	2.678	-0.152	2.682	99.84 Leading
Total Motor Load:	2.614	0.136	2.617	99.86 Lagging
Total Static Load:	0.000	0.000	0.000	
Total Constant I Load:	0.000	0.000	0.000	
Total Generic Load:	0.000	0.000	0.000	
Apparent Losses:	0.064	-0.289		
System Mismatch:	0.000	0.000		

Number of Iterations: 5

Appendix B

Case 1: Single Line Diagram and Load Flow Report in Charging Mode

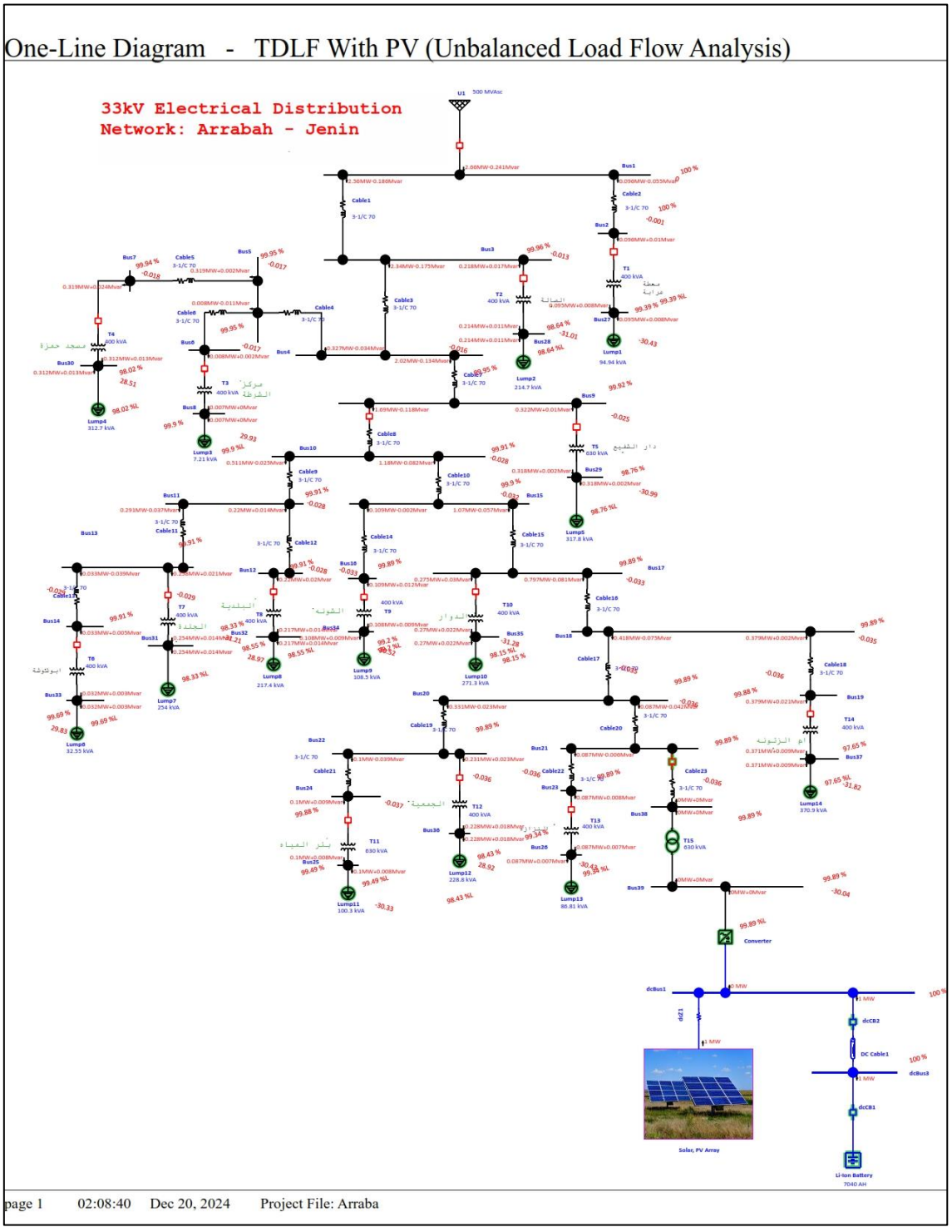

AC Unbalanced Load Flow Report

Bus			Voltage		Generation		Load		Load Flow							XFMR
ID	kV	Phase	% Mag.	Ang.	MW	Mvar	MW	Mvar	ID	Phase	MW	Mvar	Amp	Ang.	% PF	% Tap
* Bus1	33.000	A	100.00	0.0	0.886	-0.080	0.000	0.000	Bus3	A	0.854	-0.062	44.9	4.2	-99.7	
		B	100.00	-120.0	0.886	-0.080	0.000	0.000		B	0.854	-0.062	44.9	-115.8	-99.7	
		C	100.00	120.0	0.886	-0.080	0.000	0.000		C	0.854	-0.062	44.9	124.2	-99.7	
										N			0.0			
									Bus2	A	0.032	-0.018	1.9	29.7	-86.9	
										B	0.032	-0.018	1.9	-90.3	-86.9	
										C	0.032	-0.018	1.9	149.7	-86.9	
										N			0.0			
Bus2	33.000	A	100.00	0.0	0.000	0.000	0.000	0.000	Bus1	A	-0.032	-0.003	1.7	173.9	99.4	
		B	100.00	-120.0	0.000	0.000	0.000	0.000		B	-0.032	-0.003	1.7	53.9	99.4	
		C	100.00	120.0	0.000	0.000	0.000	0.000		C	-0.032	-0.003	1.7	-66.1	99.4	
										N			0.0			
									Bus27	A	0.032	0.003	1.7	-6.1	99.4	
										B	0.032	0.003	1.7	-126.1	99.4	
										C	0.032	0.003	1.7	113.9	99.4	
										N			0.0			
Bus3	33.000	A	99.96	0.0	0.000	0.000	0.000	0.000	Bus1	A	-0.853	0.053	44.9	-176.5	-99.8	
		B	99.96	-120.0	0.000	0.000	0.000	0.000		B	-0.853	0.053	44.9	63.5	-99.8	
		C	99.96	120.0	0.000	0.000	0.000	0.000		C	-0.853	0.053	44.9	-56.5	-99.8	
										N			0.0			
									Bus4	A	0.781	-0.058	41.1	4.3	-99.7	
										B	0.781	-0.058	41.1	-115.7	-99.7	
										C	0.781	-0.058	41.1	124.3	-99.7	
										N			0.0			
									Bus28	A	0.073	0.006	3.8	-4.5	99.7	
										B	0.073	0.006	3.8	-124.5	99.7	
										C	0.073	0.006	3.8	115.5	99.7	
										N			0.0			
Bus4	33.000	A	99.95	0.0	0.000	0.000	0.000	0.000	Bus3	A	-0.781	0.056	41.1	-175.9	-99.7	
		B	99.95	-120.0	0.000	0.000	0.000	0.000		B	-0.781	0.056	41.1	64.1	-99.7	
		C	99.95	120.0	0.000	0.000	0.000	0.000		C	-0.781	0.056	41.1	-55.9	-99.7	
										N			0.0			

Bus			Voltage		Generation		Load		Load Flow							XFMR
ID	kV	Phase	% Mag.	Ang.	MW	Mvar	MW	Mvar	ID	Phase	MW	Mvar	Amp	Ang.	% PF	% Tap
Bus37	0.400	A	97.65	-31.8	0.000	0.000	0.124	0.003	Bus19	A	-0.124	-0.003	548.2	146.8	100.0	
		B	97.65	-151.8	0.000	0.000	0.124	0.003		B	-0.124	-0.003	548.2	26.8	100.0	
		C	97.65	88.2	0.000	0.000	0.124	0.003		C	-0.124	-0.003	548.2	-93.2	100.0	
										N			0.0			
Bus38	33.000	A	99.89	0.0	0.000	0.000	0.000	0.000	Bus21	A	0.000	0.000	0.0	-0.1	100.0	
		B	99.89	-120.0	0.000	0.000	0.000	0.000		B	0.000	0.000	0.0	-120.1	100.0	
		C	99.89	120.0	0.000	0.000	0.000	0.000		C	0.000	0.000	0.0	119.9	100.0	
										N			0.0			
									Bus39	A	0.000	0.000	0.0	179.9	100.0	
										B	0.000	0.000	0.0	59.9	100.0	
										C	0.000	0.000	0.0	-60.1	100.0	
										N			0.0			
Bus39	0.400	A	99.89	-30.0	0.000	0.000	0.000	0.000	Bus38	A	0.000	0.000	0.2	-30.0	-100.0	
		B	99.89	-150.0	0.000	0.000	0.000	0.000		B	0.000	0.000	0.2	-150.0	100.0	
		C	99.89	90.0	0.000	0.000	0.000	0.000		C	0.000	0.000	0.2	90.0	100.0	
										N			0.0			
									Converter	A	0.000	0.000	0.2	150.0	-100.0	
										B	0.000	0.000	0.2	30.0	100.0	
										C	0.000	0.000	0.2	-90.0	100.0	
										N			0.0			

* Indicates a voltage regulated bus (voltage controlled or swing type machine connected to it)

# Indicates a bus with a load mismatch of more than 0.1 MVA

+ The power flows across center-tap transformers correspond to the phases of the From side.

Appendix C

Case 1: Single Line Diagram and Load Flow Report in Discharging Mode

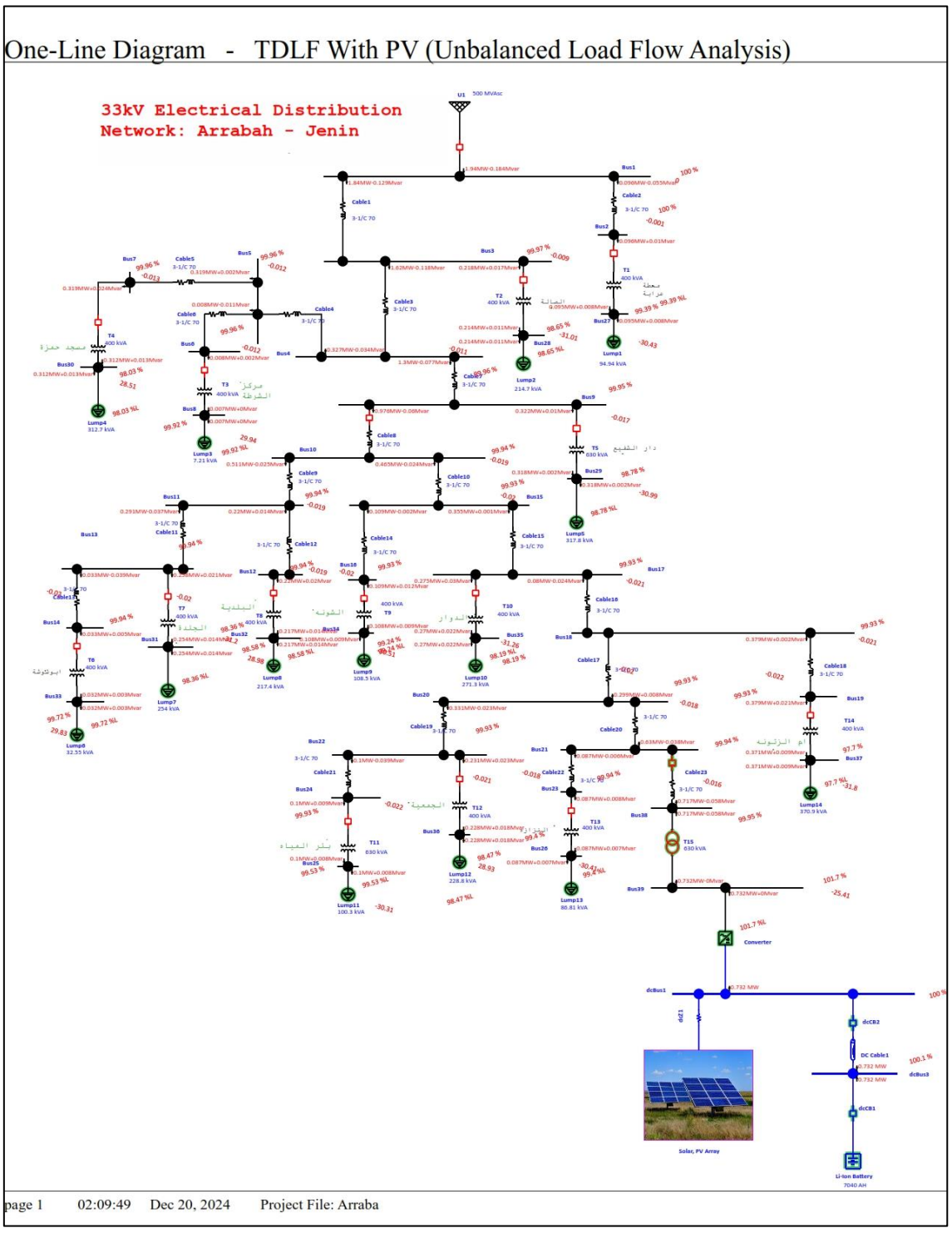

AC Unbalanced Load Flow Report

Bus			Voltage		Generation		Load		Load Flow							XFMR
ID	kV	Phase	% Mag.	Ang.	MW	Mvar	MW	Mvar	ID	Phase	MW	Mvar	Amp	Ang.	% PF	% Tap
* Bus1	33.000	A	100.00	0.0	0.646	-0.061	0.000	0.000	Bus3	A	0.614	-0.043	32.3	4.0	-99.8	
		B	100.00	-120.0	0.646	-0.061	0.000	0.000		B	0.614	-0.043	32.3	-116.0	-99.8	
		C	100.00	120.0	0.646	-0.061	0.000	0.000		C	0.614	-0.043	32.3	124.0	-99.8	
										N			0.0			
									Bus2	A	0.032	-0.018	1.9	29.7	-86.9	
										B	0.032	-0.018	1.9	-90.3	-86.9	
										C	0.032	-0.018	1.9	149.7	-86.9	
										N			0.0			
Bus2	33.000	A	100.00	0.0	0.000	0.000	0.000	0.000	Bus1	A	-0.032	-0.003	1.7	173.9	99.4	
		B	100.00	-120.0	0.000	0.000	0.000	0.000		B	-0.032	-0.003	1.7	53.9	99.4	
		C	100.00	120.0	0.000	0.000	0.000	0.000		C	-0.032	-0.003	1.7	-66.1	99.4	
										N			0.0			
									Bus27	A	0.032	0.003	1.7	-6.1	99.4	
										B	0.032	0.003	1.7	-126.1	99.4	
										C	0.032	0.003	1.7	113.9	99.4	
										N			0.0			
Bus3	33.000	A	99.97	0.0	0.000	0.000	0.000	0.000	Bus1	A	-0.614	0.034	32.3	-176.9	-99.9	
		B	99.97	-120.0	0.000	0.000	0.000	0.000		B	-0.614	0.034	32.3	63.1	-99.9	
		C	99.97	120.0	0.000	0.000	0.000	0.000		C	-0.614	0.034	32.3	-56.9	-99.9	
										N			0.0			
									Bus4	A	0.542	-0.039	28.5	4.1	-99.7	
										B	0.542	-0.039	28.5	-115.9	-99.7	
										C	0.542	-0.039	28.5	124.1	-99.7	
										N			0.0			
									Bus28	A	0.073	0.006	3.8	-4.5	99.7	
										B	0.073	0.006	3.8	-124.5	99.7	
										C	0.073	0.006	3.8	115.5	99.7	
										N			0.0			
Bus4	33.000	A	99.96	0.0	0.000	0.000	0.000	0.000	Bus3	A	-0.542	0.037	28.5	-176.1	-99.8	
		B	99.96	-120.0	0.000	0.000	0.000	0.000		B	-0.542	0.037	28.5	63.9	-99.8	
		C	99.96	120.0	0.000	0.000	0.000	0.000		C	-0.542	0.037	28.5	-56.1	-99.8	
										N			0.0			

Bus			Voltage		Generation		Load		Load Flow							XFMR
ID	kV	Phase	% Mag.	Ang.	MW	Mvar	MW	Mvar	ID	Phase	MW	Mvar	Amp	Ang.	% PF	% Tap
Bus37	0.400	A	97.70	-31.8	0.000	0.000	0.124	0.003	Bus19	A	-0.124	-0.003	548.0	146.8	100.0	
		B	97.70	-151.8	0.000	0.000	0.124	0.003		B	-0.124	-0.003	548.0	26.8	100.0	
		C	97.70	88.2	0.000	0.000	0.124	0.003		C	-0.124	-0.003	548.0	-93.2	100.0	
										N			0.0			
Bus38	33.000	A	99.95	0.0	0.000	0.000	0.000	0.000	Bus21	A	0.239	-0.019	12.6	4.6	-99.7	
		B	99.95	-120.0	0.000	0.000	0.000	0.000		B	0.239	-0.019	12.6	-115.4	-99.7	
		C	99.95	120.0	0.000	0.000	0.000	0.000		C	0.239	-0.019	12.6	124.6	-99.7	
										N			0.0			
									Bus39	A	-0.239	0.019	12.6	-175.4	-99.7	
										B	-0.239	0.019	12.6	64.6	-99.7	
										C	-0.239	0.019	12.6	-55.4	-99.7	
										N			0.0			
Bus39	0.400	A	101.65	-25.4	0.000	0.000	-0.244	0.000	Bus38	A	0.244	0.000	1039.3	-25.4	-100.0	
		B	101.65	-145.4	0.000	0.000	-0.244	0.000		B	0.244	0.000	1039.3	-145.4	-100.0	
		C	101.65	94.6	0.000	0.000	-0.244	0.000		C	0.244	0.000	1039.3	94.6	100.0	
										N			0.0			
									Converter	A	-0.244	0.000	1039.3	154.6	-100.0	
										B	-0.244	0.000	1039.3	34.6	100.0	
										C	-0.244	0.000	1039.3	-85.4	100.0	
										N			0.0			

* Indicates a voltage regulated bus (voltage controlled or swing type machine connected to it)
# Indicates a bus with a load mismatch of more than 0.1 MVA
+ The power flows across center-tap transformers correspond to the phases of the From side.

SUMMARY OF TOTAL GENERATION , LOADING & DEMAND

	Phase	MW	Mvar	MVA	% PF
Source (Swing Buses):	A	0.646	-0.061	0.649	99.55 Leading
	B	0.646	-0.061	0.649	99.55 Leading
	C	0.646	-0.061	0.649	99.55 Leading
Source (Non-Swing Buses):	A	0.000	0.000	0.000	100.00 Leading
	B	0.000	0.000	0.000	100.00 Leading
	C	0.000	0.000	0.000	
Battery Source:		0.732			
Total AC Demand:	A	0.627	0.045	0.629	99.74 Lagging
	B	0.627	0.045	0.629	99.74 Lagging
	C	0.627	0.045	0.629	99.74 Lagging
Total DC Demand:		0.000			
Apparent AC Losses:	A	0.019	-0.107		
	B	0.019	-0.107		
	C	0.019	-0.107		
Total DC Losses:		0.000			
System Mismatch:		0.000	0.000		

Number of Iterations: 7

Appendix D

Case 2: Single Line Diagram and Load Flow Report in Charging Mode

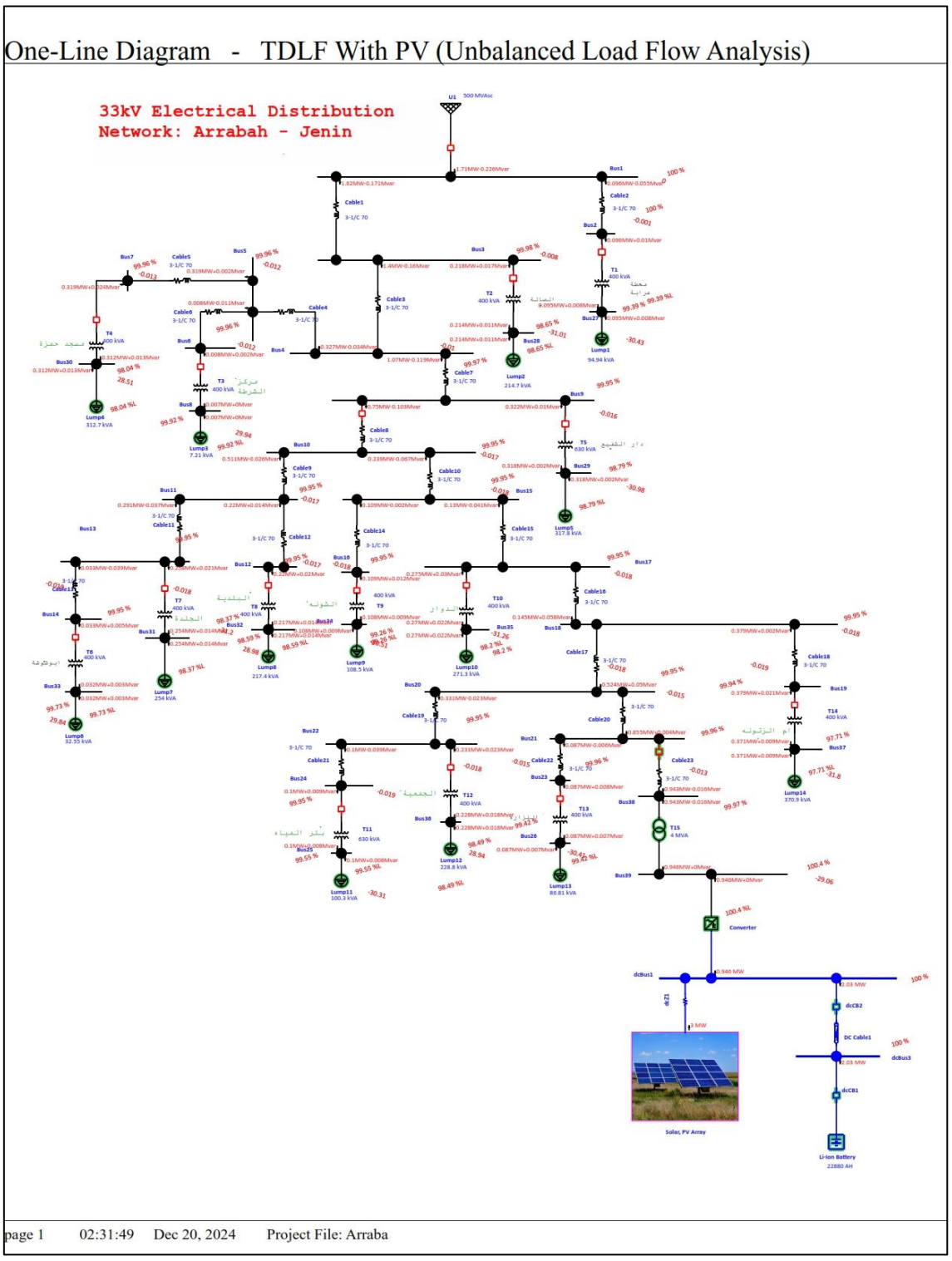

AC Unbalanced Load Flow Report

Bus			Voltage		Generation		Load		Load Flow							XFMR
ID	kV	Phase	% Mag.	Ang.	MW	Mvar	MW	Mvar	ID	Phase	MW	Mvar	Amp	Ang.	% PF	% Tap
* Bus1	33.000	A	100.00	0.0	0.571	-0.075	0.000	0.000	Bus3	A	0.539	-0.057	28.5	6.1	-99.4	
		B	100.00	-120.0	0.571	-0.075	0.000	0.000		B	0.539	-0.057	28.5	-113.9	-99.4	
		C	100.00	120.0	0.571	-0.075	0.000	0.000		C	0.539	-0.057	28.5	126.1	-99.4	
										N			0.0			
									Bus2	A	0.032	-0.018	1.9	29.7	-86.9	
										B	0.032	-0.018	1.9	-90.3	-86.9	
										C	0.032	-0.018	1.9	149.7	-86.9	
										N			0.0			
Bus2	33.000	A	100.00	0.0	0.000	0.000	0.000	0.000	Bus1	A	-0.032	-0.003	1.7	173.9	99.4	
		B	100.00	-120.0	0.000	0.000	0.000	0.000		B	-0.032	-0.003	1.7	53.9	99.4	
		C	100.00	120.0	0.000	0.000	0.000	0.000		C	-0.032	-0.003	1.7	-66.1	99.4	
										N			0.0			
									Bus27	A	0.032	0.003	1.7	-6.1	99.4	
										B	0.032	0.003	1.7	-126.1	99.4	
										C	0.032	0.003	1.7	113.9	99.4	
										N			0.0			
Bus3	33.000	A	99.98	0.0	0.000	0.000	0.000	0.000	Bus1	A	-0.539	0.048	28.4	-174.9	-99.6	
		B	99.98	-120.0	0.000	0.000	0.000	0.000		B	-0.539	0.048	28.4	65.1	-99.6	
		C	99.98	120.0	0.000	0.000	0.000	0.000		C	-0.539	0.048	28.4	-54.9	-99.6	
										N			0.0			
									Bus4	A	0.467	-0.053	24.7	6.5	-99.4	
										B	0.467	-0.053	24.7	-113.5	-99.4	
										C	0.467	-0.053	24.7	126.5	-99.4	
										N			0.0			
									Bus28	A	0.073	0.006	3.8	-4.5	99.7	
										B	0.073	0.006	3.8	-124.5	99.7	
										C	0.073	0.006	3.8	115.5	99.7	
										N			0.0			
Bus4	33.000	A	99.97	0.0	0.000	0.000	0.000	0.000	Bus3	A	-0.466	0.051	24.6	-173.8	-99.4	
		B	99.97	-120.0	0.000	0.000	0.000	0.000		B	-0.466	0.051	24.6	66.2	-99.4	
		C	99.97	120.0	0.000	0.000	0.000	0.000		C	-0.466	0.051	24.6	-53.8	-99.4	
										N			0.0			

Bus			Voltage		Generation		Load		Load Flow							XFMR
ID	kV	Phase	% Mag.	Ang.	MW	Mvar	MW	Mvar	ID	Phase	MW	Mvar	Amp	Ang.	% PF	% Tap
Bus37	0.400	A	97.71	-31.8	0.000	0.000	0.124	0.003	Bus19	A	-0.124	-0.003	547.9	146.8	100.0	
		B	97.71	-151.8	0.000	0.000	0.124	0.003		B	-0.124	-0.003	547.9	26.8	100.0	
		C	97.71	88.2	0.000	0.000	0.124	0.003		C	-0.124	-0.003	547.9	-93.2	100.0	
										N			0.0			
Bus38	33.000	A	99.97	0.0	0.000	0.000	0.000	0.000	Bus21	A	0.314	-0.005	16.5	0.9	-100.0	
		B	99.97	-120.0	0.000	0.000	0.000	0.000		B	0.314	-0.005	16.5	-119.1	-100.0	
		C	99.97	120.0	0.000	0.000	0.000	0.000		C	0.314	-0.005	16.5	120.9	-100.0	
										N			0.0			
									Bus39	A	-0.314	0.005	16.5	-179.1	-100.0	
										B	-0.314	0.005	16.5	60.9	-100.0	
										C	-0.314	0.005	16.5	-59.1	-100.0	
										N			0.0			
Bus39	0.400	A	100.37	-29.1	0.000	0.000	-0.315	0.000	Bus38	A	0.315	0.000	1361.0	-29.1	-100.0	
		B	100.37	-149.1	0.000	0.000	-0.315	0.000		B	0.315	0.000	1361.0	-149.1	100.0	
		C	100.37	90.9	0.000	0.000	-0.315	0.000		C	0.315	0.000	1361.0	90.9	100.0	
										N			0.0			
									Converter	A	-0.315	0.000	1361.0	150.9	-100.0	
										B	-0.315	0.000	1361.0	30.9	100.0	
										C	-0.315	0.000	1361.0	-89.1	100.0	
										N			0.0			

* Indicates a voltage regulated bus (voltage controlled or swing type machine connected to it)

\# Indicates a bus with a load mismatch of more than 0.1 MVA

+ The power flows across center-tap transformers correspond to the phases of the From side.

SUMMARY OF TOTAL GENERATION , LOADING & DEMAND

	Phase	MW	Mvar	MVA	% PF
Source (Swing Buses):	A	0.571	-0.075	0.576	99.14 Leading
	B	0.571	-0.075	0.576	99.14 Leading
	C	0.571	-0.075	0.576	99.14 Leading
Source (Non-Swing Buses):	A	0.011	0.000	0.011	100.00 Leading
	B	0.011	0.000	0.011	100.00 Leading
	C	0.000	0.000	0.000	
Battery Source:		0.968			
Total AC Demand:	A	0.556	0.045	0.558	99.67 Lagging
	B	0.556	0.045	0.558	99.67 Lagging
	C	0.556	0.045	0.558	99.67 Lagging
Total DC Demand:		0.000			
Apparent AC Losses:	A	0.026	-0.121		
	B	0.026	-0.121		
	C	0.015	-0.121		
Total DC Losses:		0.021			
System Mismatch:		0.000	0.000		

Number of Iterations: 14

Appendix E

Case 2: Single Line diagram and Load Flow Report in Discharging Mode

One-Line Diagram - TDLF With PV (Unbalanced Load Flow Analysis)

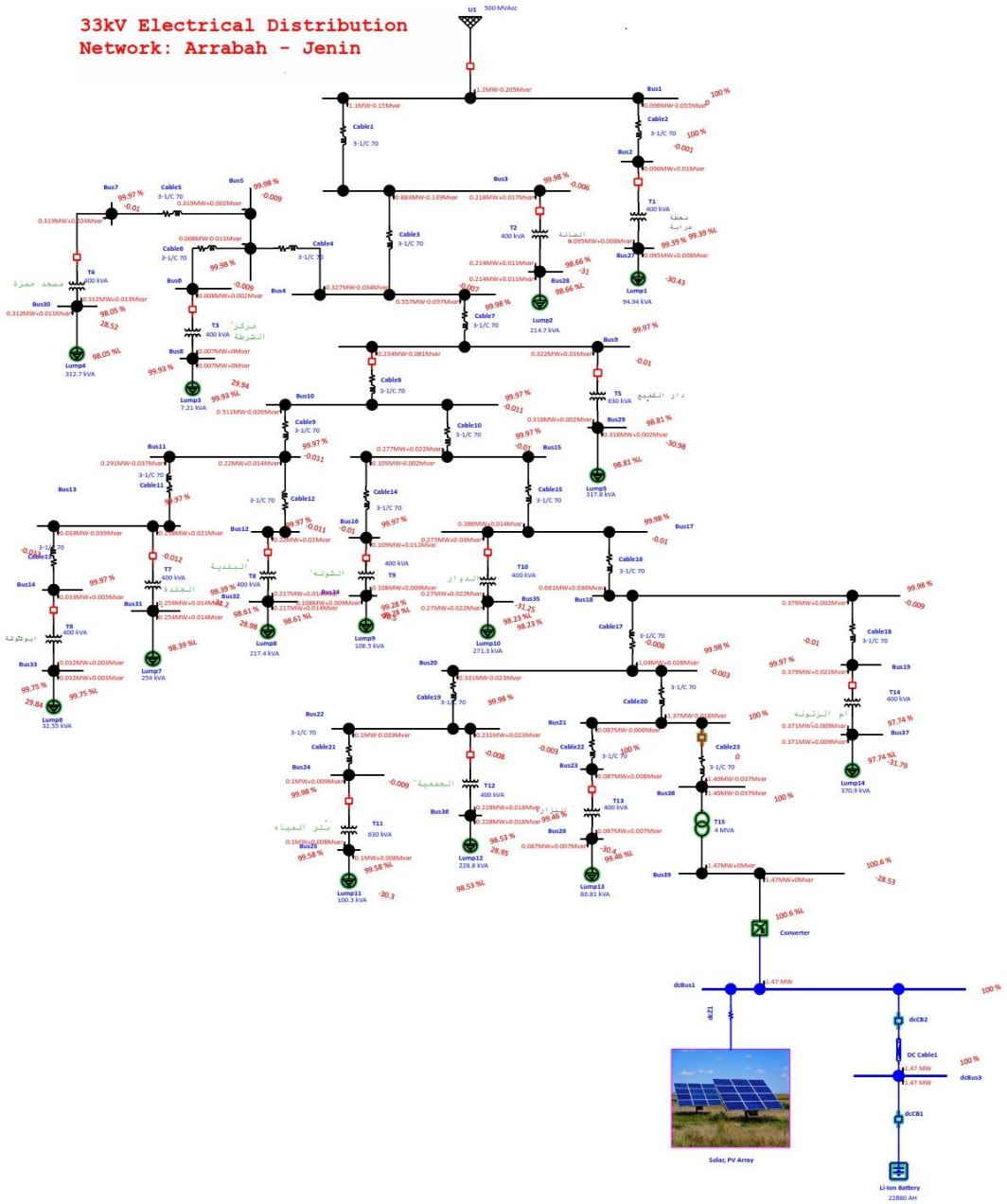

page 1 02:34:34 Dec 20, 2024 Project File: Arraba

AC Unbalanced Load Flow Report

Bus			Voltage		Generation		Load		Load Flow							XFMR
ID	kV	Phase	% Mag.	Ang.	MW	Mvar	MW	Mvar	ID	Phase	MW	Mvar	Amp	Ang.	% PF	% Tap
* Bus1	33.000	A	100.00	0.0	0.399	-0.068	0.000	0.000	Bus3	A	0.367	-0.050	19.4	7.8	-99.1	
		B	100.00	-120.0	0.399	-0.068	0.000	0.000		B	0.367	-0.050	19.4	-112.2	-99.1	
		C	100.00	120.0	0.399	-0.068	0.000	0.000		C	0.367	-0.050	19.4	127.8	-99.1	
										N			0.0			
									Bus2	A	0.032	-0.018	1.9	29.7	-86.9	
										B	0.032	-0.018	1.9	-90.3	-86.9	
										C	0.032	-0.018	1.9	149.7	-86.9	
										N			0.0			
Bus2	33.000	A	100.00	0.0	0.000	0.000	0.000	0.000	Bus1	A	-0.032	-0.003	1.7	173.9	99.4	
		B	100.00	-120.0	0.000	0.000	0.000	0.000		B	-0.032	-0.003	1.7	53.9	99.4	
		C	100.00	120.0	0.000	0.000	0.000	0.000		C	-0.032	-0.003	1.7	-66.1	99.4	
										N			0.0			
									Bus27	A	0.032	0.003	1.7	-6.1	99.4	
										B	0.032	0.003	1.7	-126.1	99.4	
										C	0.032	0.003	1.7	113.9	99.4	
										N			0.0			
Bus3	33.000	A	99.98	0.0	0.000	0.000	0.000	0.000	Bus1	A	-0.367	0.041	19.4	-173.7	-99.4	
		B	99.98	-120.0	0.000	0.000	0.000	0.000		B	-0.367	0.041	19.4	66.3	-99.4	
		C	99.98	120.0	0.000	0.000	0.000	0.000		C	-0.367	0.041	19.4	-53.7	-99.4	
										N			0.0			
									Bus4	A	0.294	-0.046	15.6	8.9	-98.8	
										B	0.294	-0.046	15.6	-111.1	-98.8	
										C	0.294	-0.046	15.6	128.9	-98.8	
										N			0.0			
									Bus28	A	0.073	0.006	3.8	-4.5	99.7	
										B	0.073	0.006	3.8	-124.5	99.7	
										C	0.073	0.006	3.8	115.5	99.7	
										N			0.0			
Bus4	33.000	A	99.98	0.0	0.000	0.000	0.000	0.000	Bus3	A	-0.294	0.044	15.6	-171.5	-98.9	
		B	99.98	-120.0	0.000	0.000	0.000	0.000		B	-0.294	0.044	15.6	68.5	-98.9	
		C	99.98	120.0	0.000	0.000	0.000	0.000		C	-0.294	0.044	15.6	-51.5	-98.9	
										N			0.0			

SUMMARY OF TOTAL GENERATION , LOADING & DEMAND

	Phase	MW	Mvar	MVA	% PF
Source (Swing Buses):	A	0.399	-0.068	0.405	98.57 Leading
	B	0.399	-0.068	0.405	98.57 Leading
	C	0.399	-0.068	0.405	98.57 Leading
Source (Non-Swing Buses):	A	0.000	0.000	0.000	100.00 Leading
	B	0.000	0.000	0.000	100.00 Leading
	C	0.000	0.000	0.000	
Battery Source:		1.469			
Total AC Demand:	A	0.382	0.045	0.384	99.30 Lagging
	B	0.382	0.045	0.384	99.30 Lagging
	C	0.382	0.045	0.384	99.30 Lagging
Total DC Demand:		0.000			
Apparent AC Losses:	A	0.017	-0.114		
	B	0.017	-0.114		
	C	0.017	-0.114		
Total DC Losses:		0.001			
System Mismatch:		0.000	0.000		

Number of Iterations: 6

Bus			Voltage		Generation		Load		Load Flow							XFMR
ID	kV	Phase	% Mag.	Ang.	MW	Mvar	MW	Mvar	ID	Phase	MW	Mvar	Amp	Ang.	% PF	% Tap
Bus37	0.400	A	97.74	-31.8	0.000	0.000	0.124	0.003	Bus19	A	-0.124	-0.003	547.7	146.8	100.0	
		B	97.74	-151.8	0.000	0.000	0.124	0.003		B	-0.124	-0.003	547.7	26.8	100.0	
		C	97.74	88.2	0.000	0.000	0.124	0.003		C	-0.124	-0.003	547.7	-93.2	100.0	
										N			0.0			
Bus38	33.000	A	100.01	0.0	0.000	0.000	0.000	0.000	Bus21	A	0.486	-0.012	25.5	1.5	-100.0	
		B	100.01	-120.0	0.000	0.000	0.000	0.000		B	0.486	-0.012	25.5	-118.5	-100.0	
		C	100.01	120.0	0.000	0.000	0.000	0.000		C	0.486	-0.012	25.5	121.5	-100.0	
										N			0.0			
									Bus39	A	-0.486	0.012	25.5	-178.5	-100.0	
										B	-0.486	0.012	25.5	61.5	-100.0	
										C	-0.486	0.012	25.5	-58.5	-100.0	
										N			0.0			
Bus39	0.400	A	100.63	-28.5	0.000	0.000	-0.489	0.000	Bus38	A	0.489	0.000	2105.9	-28.5	100.0	
		B	100.63	-148.5	0.000	0.000	-0.489	0.000		B	0.489	0.000	2105.9	-148.5	100.0	
		C	100.63	91.5	0.000	0.000	-0.489	0.000		C	0.489	0.000	2105.9	91.5	100.0	
										N			0.0			
									Converter	A	-0.489	0.000	2105.9	151.5	-100.0	
										B	-0.489	0.000	2105.9	31.5	100.0	
										C	-0.489	0.000	2105.9	-88.5	100.0	
										N			0.0			

* Indicates a voltage regulated bus (voltage controlled or swing type machine connected to it)

\# Indicates a bus with a load mismatch of more than 0.1 MVA

+ The power flows across center-tap transformers correspond to the phases of the From side.

Appendix E

Case 3: Single Line diagram and Load Flow Report in Charging Mode

One-Line Diagram - TDLF With PV (Unbalanced Load Flow Analysis)

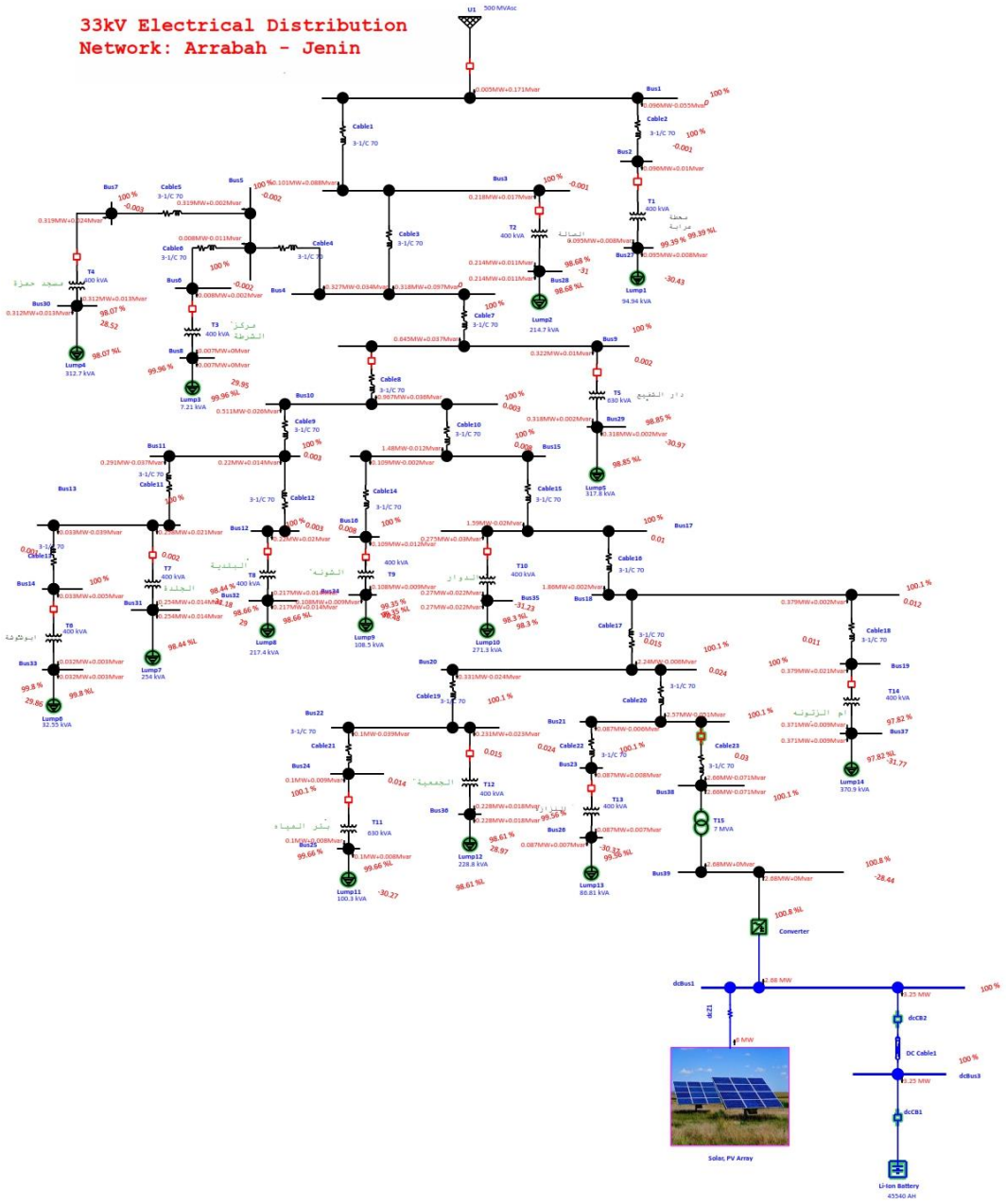

page 1 02:43:44 Dec 20, 2024 Project File: Arraba

AC Unbalanced Load Flow Report

Bus			Voltage		Generation		Load		Load Flow							XFMR
ID	kV	Phase	% Mag.	Ang.	MW	Mvar	MW	Mvar	ID	Phase	MW	Mvar	Amp	Ang.	% PF	% Tap
* Bus1	33.000	A	100.00	0.0	-0.002	-0.057	0.000	0.000	Bus3	A	-0.034	-0.039	2.7	130.9	65.5	
		B	100.00	-120.0	-0.002	-0.057	0.000	0.000		B	-0.034	-0.039	2.7	10.9	65.5	
		C	100.00	120.0	-0.002	-0.057	0.000	0.000		C	-0.034	-0.039	2.7	-109.1	65.5	
										N			0.0			
									Bus2	A	0.032	-0.018	1.9	29.7	-86.9	
										B	0.032	-0.018	1.9	-90.3	-86.9	
										C	0.032	-0.018	1.9	149.7	-86.9	
										N			0.0			
Bus2	33.000	A	100.00	0.0	0.000	0.000	0.000	0.000	Bus1	A	-0.032	-0.003	1.7	173.9	99.4	
		B	100.00	-120.0	0.000	0.000	0.000	0.000		B	-0.032	-0.003	1.7	53.9	99.4	
		C	100.00	120.0	0.000	0.000	0.000	0.000		C	-0.032	-0.003	1.7	-66.1	99.4	
										N			0.0			
									Bus27	A	0.032	0.003	1.7	-6.1	99.4	
										B	0.032	0.003	1.7	-126.1	99.4	
										C	0.032	0.003	1.7	113.9	99.4	
										N			0.0			
Bus3	33.000	A	100.00	0.0	0.000	0.000	0.000	0.000	Bus1	A	0.034	0.029	2.3	-41.1	75.4	
		B	100.00	-120.0	0.000	0.000	0.000	0.000		B	0.034	0.029	2.3	-161.1	75.4	
		C	100.00	120.0	0.000	0.000	0.000	0.000		C	0.034	0.029	2.3	78.9	75.4	
										N			0.0			
									Bus4	A	-0.106	-0.035	5.9	161.8	95.0	
										B	-0.106	-0.035	5.9	41.8	95.0	
										C	-0.106	-0.035	5.9	-78.2	95.0	
										N			0.0			
									Bus28	A	0.073	0.006	3.8	-4.5	99.7	
										B	0.073	0.006	3.8	-124.5	99.7	
										C	0.073	0.006	3.8	115.5	99.7	
										N			0.0			
Bus4	33.000	A	100.00	0.0	0.000	0.000	0.000	0.000	Bus3	A	0.106	0.032	5.8	-17.0	95.6	
		B	100.00	-120.0	0.000	0.000	0.000	0.000		B	0.106	0.032	5.8	-137.0	95.6	
		C	100.00	120.0	0.000	0.000	0.000	0.000		C	0.106	0.032	5.8	103.0	95.6	
										N			0.0			

Bus			Voltage		Generation		Load		Load Flow							XFMR
ID	kV	Phase	% Mag.	Ang.	MW	Mvar	MW	Mvar	ID	Phase	MW	Mvar	Amp	Ang.	% PF	% Tap
Bus37	0.400	A	97.82	-31.8	0.000	0.000	0.124	0.003	Bus19	A	-0.124	-0.003	547.3	146.8	100.0	
		B	97.82	-151.8	0.000	0.000	0.124	0.003		B	-0.124	-0.003	547.3	26.8	100.0	
		C	97.82	88.2	0.000	0.000	0.124	0.003		C	-0.124	-0.003	547.3	-93.2	100.0	
										N			0.0			
Bus38	33.000	A	100.12	0.0	0.000	0.000	0.000	0.000	Bus21	A	0.887	-0.024	46.5	1.6	-100.0	
		B	100.12	-120.0	0.000	0.000	0.000	0.000		B	0.887	-0.024	46.5	-118.4	-100.0	
		C	100.12	120.0	0.000	0.000	0.000	0.000		C	0.887	-0.024	46.5	121.6	-100.0	
										N			0.0			
									Bus39	A	-0.887	0.024	46.5	-178.4	-100.0	
										B	-0.887	0.024	46.5	61.6	-100.0	
										C	-0.887	0.024	46.5	-58.4	-100.0	
										N			0.0			
Bus39	0.400	A	100.76	-28.4	0.000	0.000	-0.893	0.000	Bus38	A	0.893	0.000	3839.0	-28.4	-100.0	
		B	100.76	-148.4	0.000	0.000	-0.893	0.000		B	0.893	0.000	3839.0	-148.4	100.0	
		C	100.76	91.6	0.000	0.000	-0.893	0.000		C	0.893	0.000	3839.0	91.6	100.0	
										N			0.0			
									Converter	A	-0.893	0.000	3839.0	151.6	-100.0	
										B	-0.893	0.000	3839.0	31.6	100.0	
										C	-0.893	0.000	3839.0	-88.4	100.0	
										N			0.0			

* Indicates a voltage regulated bus (voltage controlled or swing type machine connected to it)
# Indicates a bus with a load mismatch of more than 0.1 MVA
+ The power flows across center-tap transformers correspond to the phases of the From side.

SUMMARY OF TOTAL GENERATION , LOADING & DEMAND

	Phase	MW	Mvar	MVA	% PF
Source (Swing Buses):	A	-0.002	-0.057	0.057	-2.87 Leading
	B	-0.002	-0.057	0.057	-2.87 Leading
	C	-0.002	-0.057	0.057	-2.87 Leading
Source (Non-Swing Buses):	A	0.039	0.000	0.039	100.00 Leading
	B	0.039	0.000	0.039	100.00 Leading
	C	0.000	0.000	0.000	
Battery Source:		2.757			
Total AC Demand:	A	-0.022	0.045	0.051	-43.80 Lagging
	B	-0.022	0.045	0.051	-43.80 Lagging
	C	-0.022	0.045	0.051	-43.80 Lagging
Total DC Demand:		0.000			
Apparent AC Losses:	A	0.059	-0.102		
	B	0.059	-0.102		
	C	0.020	-0.102		
Total DC Losses:		0.077			
System Mismatch:		0.000	0.000		

Number of Iterations: 18

Appendix G

Case 3: Single Line diagram and Load Flow Report in Discharging Mode

One-Line Diagram - TDLF With PV (Unbalanced Load Flow Analysis)

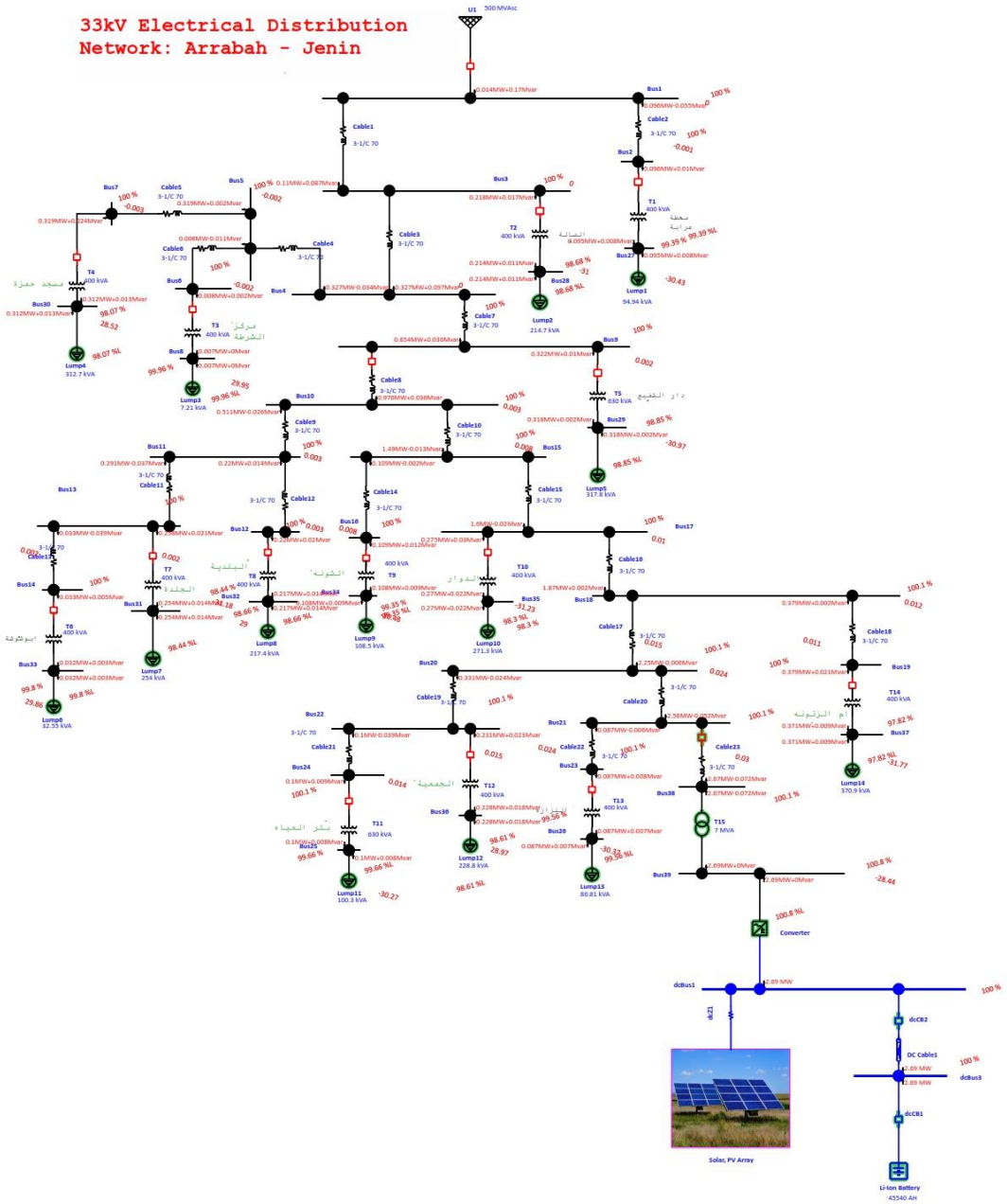

page 1 02:44:22 Dec 20, 2024 Project File: Arraba

AC Unbalanced Load Flow Report

Bus			Voltage		Generation		Load		Load Flow							XFMR
ID	kV	Phase	% Mag.	Ang.	MW	Mvar	MW	Mvar	ID	Phase	MW	Mvar	Amp	Ang.	% PF	% Tap
* Bus1	33.000	A	100.00	0.0	-0.005	-0.057	0.000	0.000	Bus3	A	-0.037	-0.039	2.8	133.5	68.9	
		B	100.00	-120.0	-0.005	-0.057	0.000	0.000		B	-0.037	-0.039	2.8	13.5	68.9	
		C	100.00	120.0	-0.005	-0.057	0.000	0.000		C	-0.037	-0.039	2.8	-106.5	68.9	
										N			0.0			
									Bus2	A	0.032	-0.018	1.9	29.7	-86.9	
										B	0.032	-0.018	1.9	-90.3	-86.9	
										C	0.032	-0.018	1.9	149.7	-86.9	
										N			0.0			
Bus2	33.000	A	100.00	0.0	0.000	0.000	0.000	0.000	Bus1	A	-0.032	-0.003	1.7	173.9	99.4	
		B	100.00	-120.0	0.000	0.000	0.000	0.000		B	-0.032	-0.003	1.7	53.9	99.4	
		C	100.00	120.0	0.000	0.000	0.000	0.000		C	-0.032	-0.003	1.7	-66.1	99.4	
										N			0.0			
									Bus27	A	0.032	0.003	1.7	-6.1	99.4	
										B	0.032	0.003	1.7	-126.1	99.4	
										C	0.032	0.003	1.7	113.9	99.4	
										N			0.0			
Bus3	33.000	A	100.00	0.0	0.000	0.000	0.000	0.000	Bus1	A	0.037	0.029	2.5	-38.5	78.3	
		B	100.00	-120.0	0.000	0.000	0.000	0.000		B	0.037	0.029	2.5	-158.5	78.3	
		C	100.00	120.0	0.000	0.000	0.000	0.000		C	0.037	0.029	2.5	81.5	78.3	
										N			0.0			
									Bus4	A	-0.109	-0.035	6.0	162.3	95.3	
										B	-0.109	-0.035	6.0	42.3	95.3	
										C	-0.109	-0.035	6.0	-77.7	95.3	
										N			0.0			
									Bus28	A	0.073	0.006	3.8	-4.5	99.7	
										B	0.073	0.006	3.8	-124.5	99.7	
										C	0.073	0.006	3.8	115.5	99.7	
										N			0.0			
Bus4	33.000	A	100.00	0.0	0.000	0.000	0.000	0.000	Bus3	A	0.109	0.032	6.0	-16.5	95.9	
		B	100.00	-120.0	0.000	0.000	0.000	0.000		B	0.109	0.032	6.0	-136.5	95.9	
		C	100.00	120.0	0.000	0.000	0.000	0.000		C	0.109	0.032	6.0	103.5	95.9	
										N			0.0			

Bus			Voltage		Generation		Load		Load Flow							XFMR
ID	kV	Phase	% Mag.	Ang.	MW	Mvar	MW	Mvar	ID	Phase	MW	Mvar	Amp	Ang.	% PF	% Tap
Bus37	0.400	A	97.82	-31.8	0.000	0.000	0.124	0.003	Bus19	A	-0.124	-0.003	547.3	146.8	100.0	
		B	97.82	-151.8	0.000	0.000	0.124	0.003		B	-0.124	-0.003	547.3	26.8	100.0	
		C	97.82	88.2	0.000	0.000	0.124	0.003		C	-0.124	-0.003	547.3	-93.2	100.0	
										N			0.0			
Bus38	33.000	A	100.12	0.0	0.000	0.000	0.000	0.000	Bus21	A	0.890	-0.024	46.7	1.6	-100.0	
		B	100.12	-120.0	0.000	0.000	0.000	0.000		B	0.890	-0.024	46.7	-118.4	-100.0	
		C	100.12	120.0	0.000	0.000	0.000	0.000		C	0.890	-0.024	46.7	121.6	-100.0	
										N			0.0			
									Bus39	A	-0.890	0.024	46.7	-178.4	-100.0	
										B	-0.890	0.024	46.7	61.6	-100.0	
										C	-0.890	0.024	46.7	-58.4	-100.0	
										N			0.0			
Bus39	0.400	A	100.76	-28.4	0.000	0.000	-0.896	0.000	Bus38	A	0.896	0.000	3852.4	-28.4	100.0	
		B	100.76	-148.4	0.000	0.000	-0.896	0.000		B	0.896	0.000	3852.4	-148.4	100.0	
		C	100.76	91.6	0.000	0.000	-0.896	0.000		C	0.896	0.000	3852.4	91.6	100.0	
										N			0.0			
									Converter	A	-0.896	0.000	3852.4	151.6	-100.0	
										B	-0.896	0.000	3852.4	31.6	100.0	
										C	-0.896	0.000	3852.4	-88.4	100.0	
										N			0.0			

* Indicates a voltage regulated bus (voltage controlled or swing type machine connected to it)
\# Indicates a bus with a load mismatch of more than 0.1 MVA
+ The power flows across center-tap transformers correspond to the phases of the From side.

SUMMARY OF TOTAL GENERATION , LOADING & DEMAND

	Phase	MW	Mvar	MVA	% PF
Source (Swing Buses):	A	-0.005	-0.057	0.057	-8.29 Leading
	B	-0.005	-0.057	0.057	-8.29 Leading
	C	-0.005	-0.057	0.057	-8.29 Leading
Source (Non-Swing Buses):	A	0.001	0.000	0.001	100.00 Leading
	B	0.001	0.000	0.001	100.00 Leading
	C	0.000	0.000	0.000	
Battery Source:		2.690			
Total AC Demand:	A	-0.025	0.045	0.052	-48.61 Lagging
	B	-0.025	0.045	0.052	-48.61 Lagging
	C	-0.025	0.045	0.052	-48.61 Lagging
Total DC Demand:		0.000			
Apparent AC Losses:	A	0.021	-0.102		
	B	0.021	-0.102		
	C	0.021	-0.102		
Total DC Losses:		0.001			
System Mismatch:		0.000	0.000		

Number of Iterations: 6

SUMMARY OF TOTAL GENERATION , LOADING & DEMAND

	Phase	MW	Mvar	MVA	% PF
Source (Swing Buses):	A	0.886	-0.080	0.889	99.59 Leading
	B	0.886	-0.080	0.889	99.59 Leading
	C	0.886	-0.080	0.889	99.59 Leading
Source (Non-Swing Buses):	A	0.002	0.000	0.002	100.00 Leading
	B	0.002	0.000	0.002	100.00 Leading
	C	0.000	0.000	0.000	
Battery Source:		0.003			
Total AC Demand:	A	0.871	0.045	0.872	99.86 Lagging
	B	0.871	0.045	0.872	99.86 Lagging
	C	0.871	0.045	0.872	99.86 Lagging
Total DC Demand:		0.000			
Apparent AC Losses:	A	0.016	-0.126		
	B	0.016	-0.126		
	C	0.015	-0.126		
Total DC Losses:		0.003			
System Mismatch:		0.000	0.000		

Number of Iterations: 10

System Advisor Model Report

PVWatts - Battery | 1.0 DC MW Nameplate | 32.41, 35.22 UTC +2
Commercial | $1.58/W Installed Cost | NSRDB

PV System Specifications	
System nameplate size	1,020.41 kW
Module type	0
DC to AC ratio	1
Rated inverter size	1,020.41 kW
Inverter efficiency	96 %
Array type	fixed open rack
Array tilt	25 degrees
Array azimuth	180 degrees
Ground coverage ratio	N/A
Total system losses	14.08 %
Shading	no

Performance Adjustments	
DC avail./curtail.	n/a
AC avail./curtail.	none
Degradation	none
Hourly or custom losses	none

Results	Solar Radiation	AC Energy
	(kWh/m2/day)	(kWh)
Jan	3.45	75,514
Feb	4.19	86,944
Mar	5.54	126,389
Apr	6.67	143,787
May	7.32	161,533
Jun	7.75	170,290
Jul	7.71	166,364
Aug	7.68	160,148
Sep	7.23	148,925
Oct	5.6	120,215
Nov	4.12	88,652
Dec	3.55	73,669
Year	5.9	1,522,435

Battery Specifications	
Battery capacity	7,040 kW
Battery chemistry	1
Battery dispatch option	Peak shaving

Battery Performance	
Roundtrip eff. (%)	90.65
Cycle conversion eff. (%)	90.65
Average cycle DoD	38.03
Number of cycles	402
Year 1 energy charged	1,246,255.16 kWh
Year 1 charged from PV	482,122.5 kWh
Year 1 charged from grid	764,132.67 kWh
Year 1 energy discharged	1,129,676.42 kWh

PVWatts - Battery | 1.0 DC MW Nameplate | 32.41, 35.22
Commercial | $1.58/W Installed Cost | UTC +2

Year 1 Monthly Generation and Load Summary

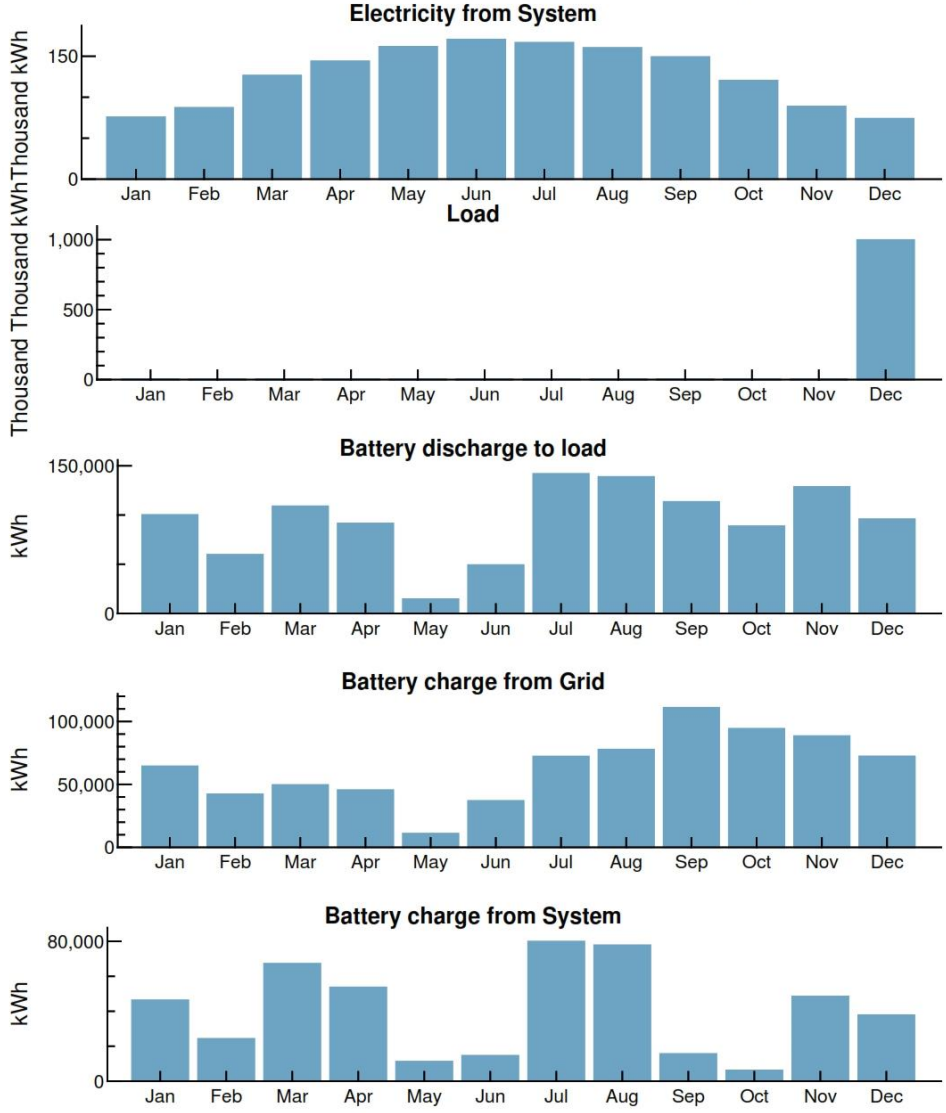

PVWatts - Battery	1.0 DC MW Nameplate	32.41, 35.22
Commercial	$1.58/W Installed Cost	UTC +2

Year 1 Monthly Electric Bill and Savings ($)

Month	Without System	With System	Savings
Jan	163,009	150,927	12,082
Feb	178,711	164,800	13,911
Mar	223,124	202,902	20,222
Apr	233,696	210,689	23,006
May	220,761	194,915	25,845
Jun	173,085	145,839	27,246
Jul	168,626	142,007	26,618
Aug	180,287	154,663	25,623
Sep	196,333	172,505	23,828
Oct	213,515	194,281	19,234
Nov	162,506	148,322	14,184
Dec	159,533	147,746	11,787
Annual	2,273,191	2,029,602	243,589

NPV Approximation using Annuities

Annuities, Capital Recovery Factor (CRF) = 0.1023		
Investment	$-164,600	Sum:
Expenses	$-74,400	$47,200
Savings	$0	NPV = Sum / CRF:
Energy value	$286,400	$462,000

Investment = Installed Cost - Debt Principal - IBI - CBI
Expenses = Operating Costs + Debt Payments
Savings = Tax Deductions + PBI
Energy value = Tax Adjusted Net Savings
Nominal discount rate = 9.06%

Payback Cash Flow (Payback Period = 8.2 years)

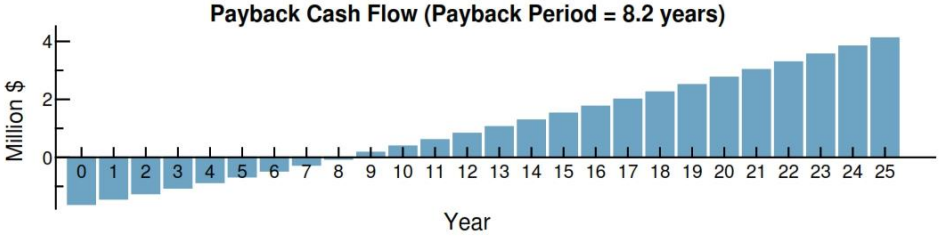

PVWatts - Battery	1.0 DC MW Nameplate	32.41, 35.22
Commercial	$1.58/W Installed Cost	UTC +2

Financial Model

Project Costs	
Total installed cost	$1,609,835
Salvage value	$0

Analysis Parameters	
Project life	25 years
Inflation rate	2.5%
Real discount rate	6.4%

Project Debt Parameters	
Debt fraction	0%
Amount	$0
Term	0 years
Rate	0%

Tax and Insurance Rates	
Federal income tax	0 %/year
State income tax	0 %/year
Sales tax (% of indirect cost basis)	16%
Insurance (% of installed cost)	0 %/year
Property tax (% of assessed val.)	0 %/year

Incentives
None

Electricity Demand and Rate Summary
Annual peak demand 3,164.4 kW
Annual total demand 14,207,224 kWh
Generic Commercial
Fixed charge: $3/month
Monthly excess with kWh rollover
Tiered TOU energy rates: 4 periods, 1 tier

Results	
Nominal LCOE	17.4 cents/kWh
Net present value	$462,200
Payback period	8.2 years

PVWatts - Battery	1.0 DC MW Nameplate	32.41, 35.22
Commercial	$1.58/W Installed Cost	UTC +2

This performance model does not specify any loss diagram items.
Current case name is PV 1MW- Battery?? ???

Appendix H

SAM Reports

System Advisor Model Report

PVWatts - Battery | 3.0 DC MW Nameplate | 32.41, 35.22 UTC +2
Commercial | $1.97/W Installed Cost | NSRDB

PV System Specifications	
System nameplate size	3,024.55 kW
Module type	0
DC to AC ratio	1
Rated inverter size	3,024.55 kW
Inverter efficiency	96 %
Array type	fixed open rack
Array tilt	25 degrees
Array azimuth	180 degrees
Ground coverage ratio	N/A
Total system losses	14.08 %
Shading	no

Performance Adjustments	
DC avail./curtail.	n/a
AC avail./curtail.	none
Degradation	none
Hourly or custom losses	none

Battery Specifications	
Battery capacity	22,880 kW
Battery chemistry	1
Battery dispatch option	Peak shaving

Battery Performance	
Roundtrip eff. (%)	91.06
Cycle conversion eff. (%)	91.06
Average cycle DoD	20.31
Number of cycles	442
Year 1 energy charged	2,411,075.22 kWh
Year 1 charged from PV	2,033,823.44 kWh
Year 1 charged from grid	377,251.78 kWh
Year 1 energy discharged	2,195,638.26 kWh

Results	Solar Radiation	AC Energy
	(kWh/m2/day)	(kWh)
Jan	3.45	234,210
Feb	4.19	268,681
Mar	5.54	384,454
Apr	6.67	437,142
May	7.32	483,840
Jun	7.75	501,188
Jul	7.71	503,574
Aug	7.68	508,782
Sep	7.23	445,088
Oct	5.6	363,927
Nov	4.12	270,827
Dec	3.55	240,902
Year	5.9	4,642,620

Commercial | PVWatts | Sandia Inverter | Lead Acid Battery

System Advisor Model Standard Report generated by SAM 2024.12.12 on Mon Jan 27 21:54:01 2025 1 / 5

PVWatts - Battery | 3.0 DC MW Nameplate | 32.41, 35.22
Commercial | $1.97/W Installed Cost | UTC +2

Year 1 Monthly Generation and Load Summary

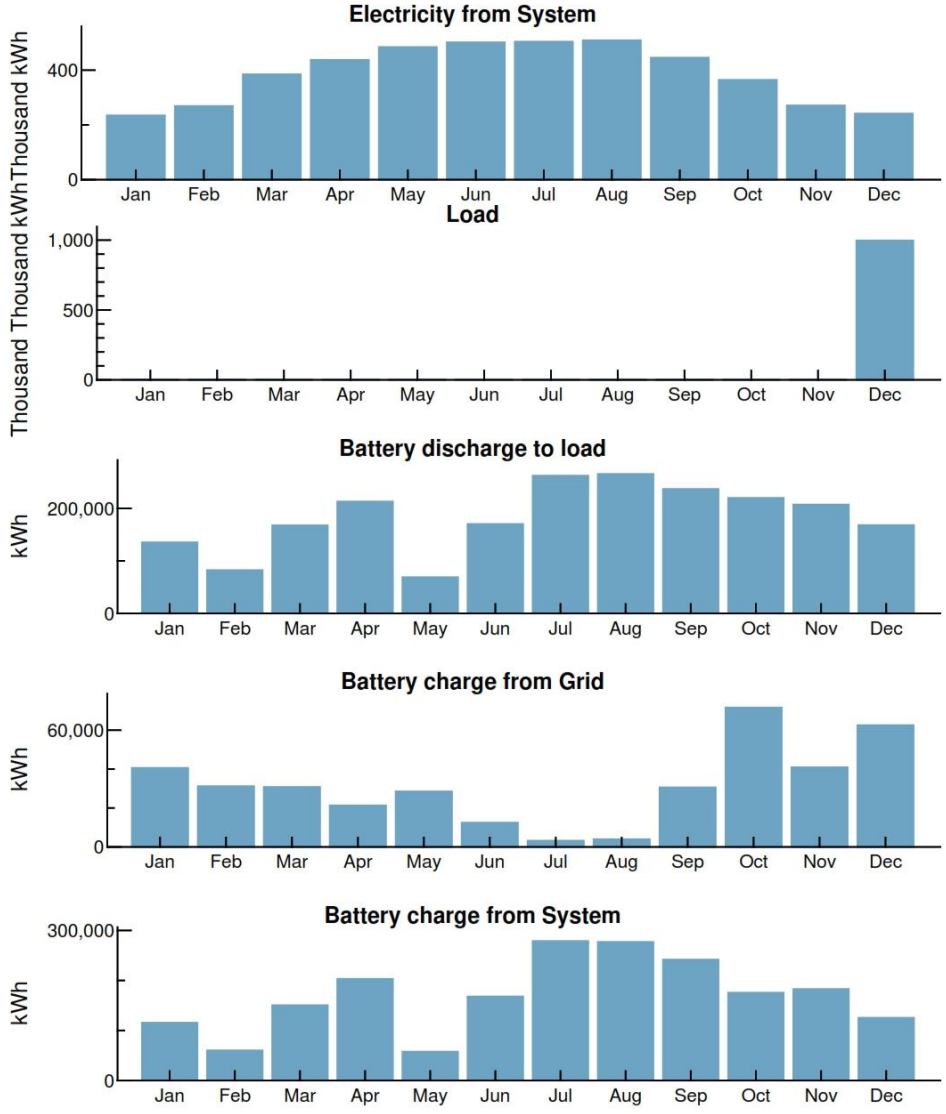

PVWatts - Battery	3.0 DC MW Nameplate	32.41, 35.22
Commercial	$1.97/W Installed Cost	UTC +2

Year 1 Monthly Electric Bill and Savings ($)

Month	Without System	With System	Savings
Jan	163,009	125,535	37,473
Feb	178,711	135,722	42,988
Mar	223,124	161,611	61,512
Apr	233,696	163,753	69,942
May	220,761	143,346	77,414
Jun	173,085	92,895	80,190
Jul	168,626	88,054	80,571
Aug	180,287	98,881	81,405
Sep	196,333	125,119	71,214
Oct	213,515	155,287	58,228
Nov	162,506	119,174	43,332
Dec	159,533	120,989	38,544
Annual	2,273,191	1,530,372	742,819

NPV Approximation using Annuities

Annuities, Capital Recovery Factor (CRF) = 0.1023		
Investment	$-609,000	Sum:
Expenses	$-220,600	$43,700
Savings	$0	NPV = Sum / CRF:
Energy value	$873,400	$427,000

Investment = Installed Cost - Debt Principal - IBI - CBI
Expenses = Operating Costs + Debt Payments
Savings = Tax Deductions + PBI
Energy value = Tax Adjusted Net Savings
Nominal discount rate = 9.06%

Payback Cash Flow (Payback Period = 9.8 years)

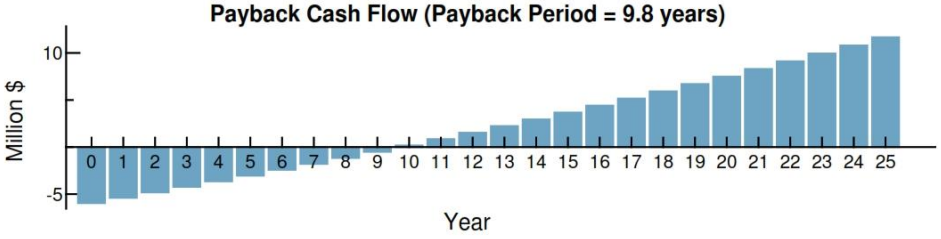

PVWatts - Battery	3.0 DC MW Nameplate	32.41, 35.22
Commercial	$1.97/W Installed Cost	UTC +2

Financial Model

Project Costs	
Total installed cost	$5,953,514
Salvage value	$0

Analysis Parameters	
Project life	25 years
Inflation rate	2.5%
Real discount rate	6.4%

Project Debt Parameters	
Debt fraction	0%
Amount	$0
Term	0 years
Rate	0%

Tax and Insurance Rates	
Federal income tax	0 %/year
State income tax	0 %/year
Sales tax (% of indirect cost basis)	16%
Insurance (% of installed cost)	0 %/year
Property tax (% of assessed val.)	0 %/year

Incentives
None

Electricity Demand and Rate Summary
Annual peak demand 3,164.4 kW
Annual total demand 14,207,224 kWh
Generic Commercial
Fixed charge: $3/month
Monthly excess with kWh rollover
Tiered TOU energy rates: 4 periods, 1 tier

Results	
Nominal LCOE	18.6 cents/kWh
Net present value	$427,200
Payback period	9.8 years

PVWatts - Battery	3.0 DC MW Nameplate	32.41, 35.22
Commercial	$1.97/W Installed Cost	UTC +2

This performance model does not specify any loss diagram items.
Current case name is PV 3MW- Battery ?? ???

System Advisor Model Report

PVWatts - Battery | 6.0 DC MW Nameplate | 32.41, 35.22 UTC +2
Commercial | $2.02/W Installed Cost | NSRDB

PV System Specifications	
System nameplate size	6,049.11 kW
Module type	0
DC to AC ratio	1
Rated inverter size	6,049.11 kW
Inverter efficiency	96 %
Array type	fixed open rack
Array tilt	25 degrees
Array azimuth	180 degrees
Ground coverage ratio	N/A
Total system losses	14.08 %
Shading	no

Performance Adjustments	
DC avail./curtail.	n/a
AC avail./curtail.	none
Degradation	none
Hourly or custom losses	none

Results	Solar Radiation	AC Energy
	(kWh/m2/day)	(kWh)
Jan	3.45	477,320
Feb	4.19	540,398
Mar	5.54	774,467
Apr	6.67	869,780
May	7.32	978,484
Jun	7.75	995,822
Jul	7.71	1,004,578
Aug	7.68	1,004,741
Sep	7.23	920,357
Oct	5.6	739,097
Nov	4.12	553,093
Dec	3.55	495,214
Year	5.9	9,353,357

Battery Specifications	
Battery capacity	45,540 kW
Battery chemistry	1
Battery dispatch option	Peak shaving

Battery Performance	
Roundtrip eff. (%)	91.14
Cycle conversion eff. (%)	91.14
Average cycle DoD	18.43
Number of cycles	412
Year 1 energy charged	4,092,503.58 kWh
Year 1 charged from PV	3,915,677.93 kWh
Year 1 charged from grid	176,825.65 kWh
Year 1 energy discharged	3,729,814.51 kWh

PVWatts - Battery | 6.0 DC MW Nameplate | 32.41, 35.22
Commercial | $2.02/W Installed Cost | UTC +2

Year 1 Monthly Generation and Load Summary

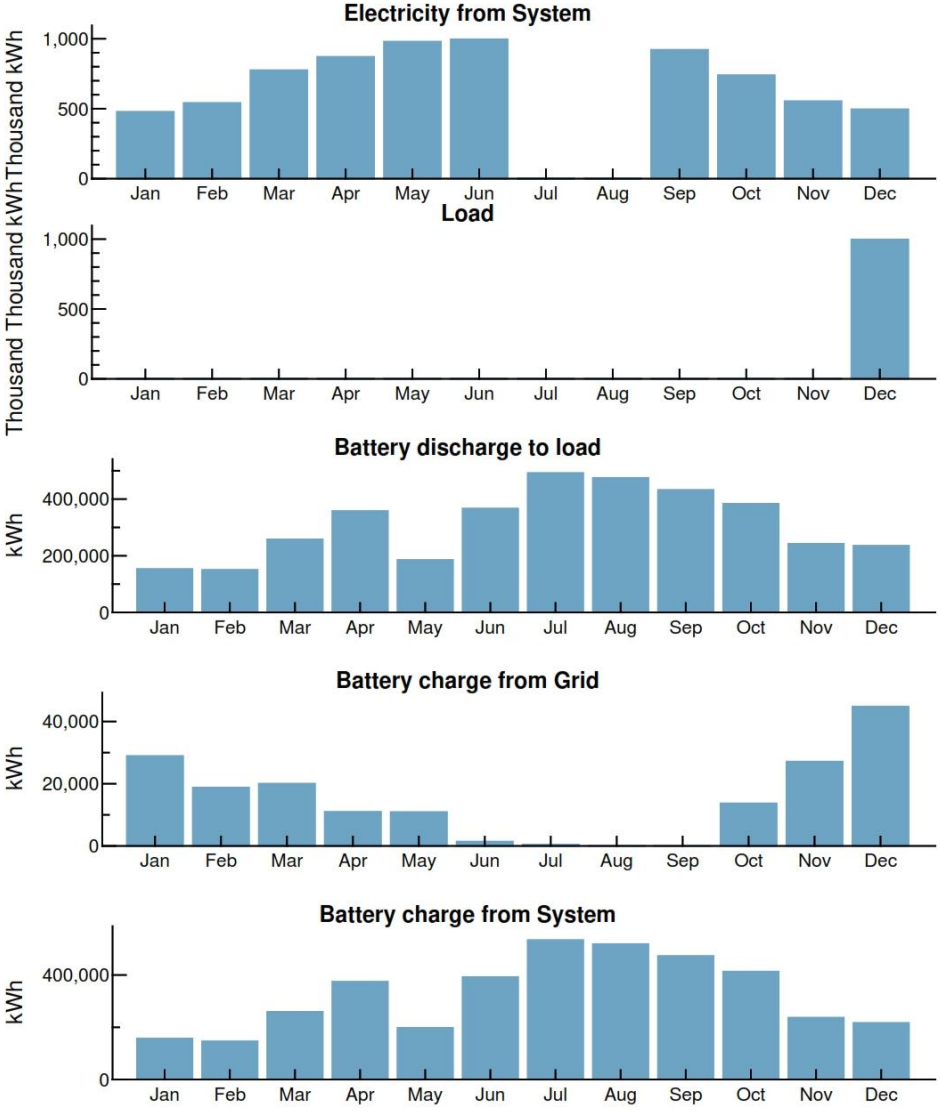

PVWatts - Battery	6.0 DC MW Nameplate	32.41, 35.22
Commercial	$2.02/W Installed Cost	UTC +2

Year 1 Monthly Electric Bill and Savings ($)

Month	Without System	With System	Savings
Jan	163,009	86,638	76,371
Feb	178,711	92,247	86,463
Mar	223,124	99,209	123,914
Apr	233,696	94,531	139,164
May	220,761	64,203	156,557
Jun	173,085	13,754	159,331
Jul	168,626	8,218	160,407
Aug	180,287	19,203	161,083
Sep	196,333	49,076	147,257
Oct	213,515	95,260	118,255
Nov	162,506	74,011	88,494
Dec	159,533	80,299	79,234
Annual	2,273,191	776,654	1,496,537

NPV Approximation using Annuities

Annuities, Capital Recovery Factor (CRF) = 0.1023		
Investment	$-1,252,800	Sum:
Expenses	$-441,300	$65,400
Savings	$0	NPV = Sum / CRF:
Energy value	$1,759,700	$640,000

Investment = Installed Cost - Debt Principal - IBI - CBI
Expenses = Operating Costs + Debt Payments
Savings = Tax Deductions + PBI
Energy value = Tax Adjusted Net Savings
Nominal discount rate = 9.06%

Payback Cash Flow (Payback Period = 9.9 years)

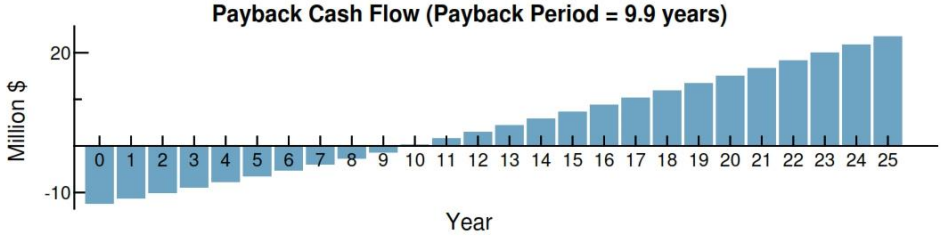

PVWatts - Battery	6.0 DC MW Nameplate	32.41, 35.22
Commercial	$2.02/W Installed Cost	UTC +2

Financial Model

Project Costs	
Total installed cost	$12,246,799
Salvage value	$0

Analysis Parameters	
Project life	25 years
Inflation rate	2.5%
Real discount rate	6.4%

Project Debt Parameters	
Debt fraction	0%
Amount	$0
Term	0 years
Rate	0%

Tax and Insurance Rates	
Federal income tax	0 %/year
State income tax	0 %/year
Sales tax (% of indirect cost basis)	16%
Insurance (% of installed cost)	0 %/year
Property tax (% of assessed val.)	0 %/year

Incentives
None

Electricity Demand and Rate Summary
Annual peak demand 3,164.4 kW
Annual total demand 14,207,224 kWh
Generic Commercial
Fixed charge: $3/month
Monthly excess with kWh rollover
Tiered TOU energy rates: 4 periods, 1 tier

Results	
Nominal LCOE	18.8 cents/kWh
Net present value	$640,000
Payback period	9.9 years

PVWatts - Battery	6.0 DC MW Nameplate	32.41, 35.22
Commercial	$2.02/W Installed Cost	UTC +2

This performance model does not specify any loss diagram items.
Current case name is PV 6MW- Battery ?? ???

Appendix I

Voltage Harmonic Spectrum of Bus 1, Bus 38, and Buis 39 for all Cases

Case 0

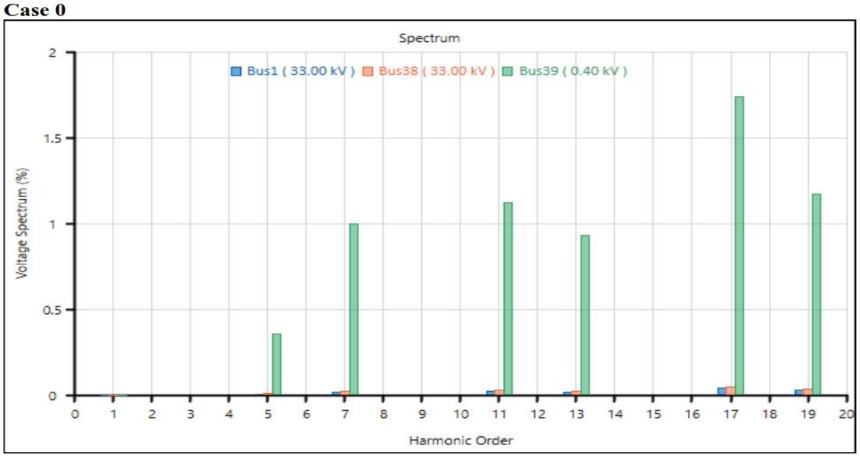

Case 1

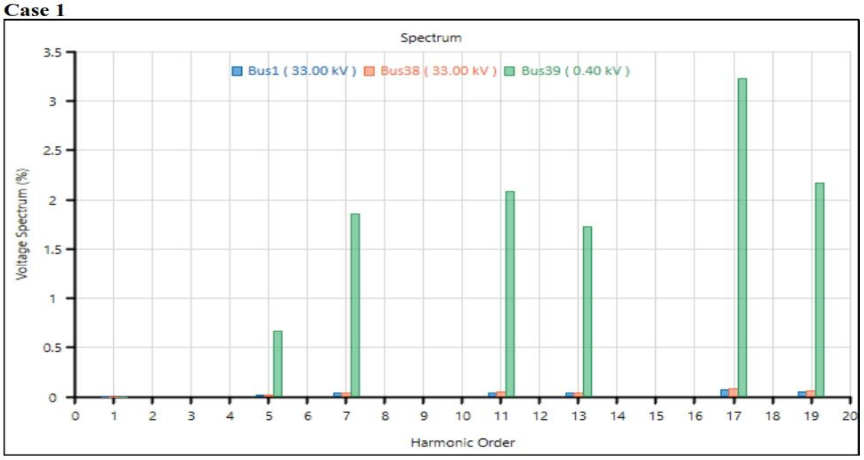

121

Case 2

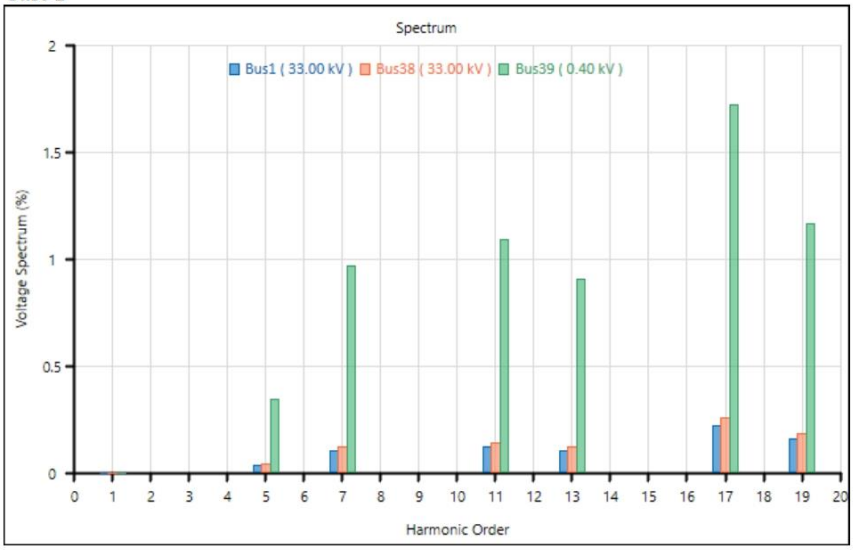

Case 3

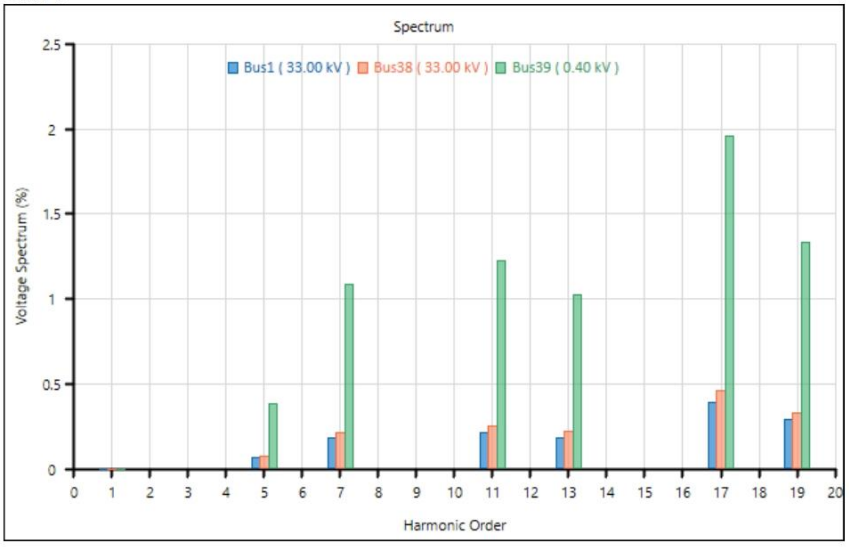

122

جـامعـــة النجاح الوطنية
كليـــة الدراســـات العليـــا

تقييم الجدوى الفنية والاقتصادية لدمج أنظمة تخزين الطاقة في أنظمة الطاقة الفوطوضوئية المتصلة بالشبكة – دراسة حالة

إعداد
رامي حسام محمد يعقوب

إشراف
د. أيسر ياسين

قدمت هذه الرسالة استكمالا لمتطلبات الحصول على درجة الماجستير في هندسة الطاقة النظيفة وترشيد الاستهلاك، من كلية الدراسات العليا، في جامعة النجاح الوطنية، نابلس– فلسطين.

2025

تقييم الجدوى الفنية والاقتصادية لدمج أنظمة تخزين الطاقة في أنظمة الطاقة الفوطوضوئية المتصلة بالشبكة – دراسة حالة

إعداد

رامي حسام محمد يعقوب

إشراف

د. أيسر ياسين

الملخص

تبحث هذه الدراسة في التأثيرات الفنية والاقتصادية لدمج أنظمة تخزين الطاقة في الأنظمة الكهروضوئية المتصلة بالشبكة الكهربائية، وذلك باستخدام شبكة الكهرباء في قرية عرابة الواقعة في محافظة جنين كحالة دراسية. تمت مقارنة أربع تكوينات مختلفة من أنظمة الطاقة الشمسية الكهروضوئية وأحجام متنوعة من أنظمة تخزين الطاقة لتقييم تأثيرها على أهم مؤشرات أداء الشبكة، مثل تنظيم الجهد الكهربائي، وتقليل فاقد الطاقة، والتحكم الديناميكي في الأحمال. ومن خلال استخدام برنامج ETAP للمحاكاة، تم تحليل سلوك الشبكة تحت ظروف تشغيل واقعية، بما في ذلك التشوهات التوافقية الناتجة عن محولات التيار في النظام الكهروضوئي، والتي لوحظت بوضوح في الحالة الأولى والثالثة عند نقاط الجهد المنخفض، حيث تتطلب معالجة هذه التشوهات تدابير إضافية لضمان جودة الطاقة. كما تم تحليل تدفق الطاقة العكسي الذي قد يحدث في حالات الاختراق العالي للطاقة الشمسية. وقد تم رصد تدفق طاقة عكسي في الحالة الثالثة، حيث لوحظ تصدير طفيف للطاقة نحو الشبكة الرئيسية، مما يسلط الضوء على أهمية وجود آليات تحكم فعالة عند مستويات الاختراق العالية.

من الناحية الاقتصادية، تم تقييم كفاءة الأنظمة باستخدام برنامجSystem Advisor Model ، مع التركيز على مؤشرات رئيسية مثل فترة استرداد رأس المال، والقيمة الحالية الصافية، وتكلفة الطاقة المستوية. ومن بين الحالات الأربع المدروسة، أظهرت الحالة الأولى أعلى كفاءة من حيث تقليل التكاليف، حيث حققت أقل

تكلفة طاقة مستوية بلغت 17.4 سنتًا لكل كيلوواط ساعة، وفترة استرداد تبلغ 8.2 سنوات. وعلى الرغم من أن الحالتين الثانية والثالثة أظهرتا أداءً فنيًا أعلى، إلا أن ارتفاع تكاليف الاستثمار فيهما قلل من جدواهما الاقتصادية.

وتستنتج الدراسة أن الحالة الأولى تمثل الخيار الأمثل من حيث التوازن بين الكفاءة الفنية والجدوى الاقتصادية، حيث تجمع بين تنظيم الجهد الجيد، وتحسين إدارة الأحمال، وجودة الطاقة المقبولة رغم التشوهات التوافقية، وذلك بأقل عبء استثماري وأفضل تكلفة للطاقة. مما يجعلها حلاً مناسبًا لتحقيق استقرار الشبكة الكهربائية وتقليل أحمال الذروة في التطبيقات الصغيرة والمتوسطة الحجم. وتوصي الدراسة بإجراء أبحاث مستقبلية طويلة الأمد تتناول تقنيات التخزين الهجينة، وتطوير خوارزميات تحكم تنبؤية، بالإضافة إلى دراسة موثوقية أداء أنظمة التخزين في ظل ظروف تشغيل مختلفة ومتغيرة للشبكات الكهربائية.

الكلمات المفتاحية: نظام تخزين الطاقة، نظام الطاقة الكهروضوئية المتصل بالشبكة، الجدوى الفنية، الفوائد الاقتصادية، تنظيم الجهد.